Modulation of the MJO-Related Teleconnections by the QBO and the Prediction Skill of the NAO in Subseasonal-to-Seasonal Models

Pei-Ning Feng

Department of Atmospheric and Oceanic Sciences

McGill University

Montreal, Quebec, Canada

August 2020

A thesis submitted to McGill University in partial fulfillment of the requirements for the degree of Doctor of Philosophy

Abstract

The weather and climate in the extratropics are profoundly influenced by the dominant climate variabilities occurring over a wide range of time scales from days to weeks, months, years and even longer. At the same time, the teleconnection, which is often referred to as the large-scale modes of the low-frequency variability and sometimes driven by the tropical convection, also play an important role in weather and climate forecasts. The prominent mode of climate variability over the North Atlantic basin, the North Atlantic Oscillation (NAO), has long been investigated and regarded as an important factor for subseasonal predictions.

Throughout the thesis, we analyze the observational data to clarify how tropical convection and stratospheric climate variability influence the NAO, and then assess the prediction skill and representation of the NAO in the operational models of the World Climate/Weather Research Program's (WCRP/WWRP) Subseasonal-to-Seasonal (S2S) prediction project.

The Madden-Julian Oscillation (MJO) is the prominent mode of intraseasonal variability in the tropics. Certain phases of the MJO were observed to have evident connections with the NAO at a lag of about 10 days. In the observations, we find that in the extended boreal winter season, the NAO responses after the occurrences of the MJO differ in the two phases of the quasi-biennial oscillation (QBO). Both the positive phase of the NAO after the occurrences of the MJO phase 3 and the negative phase of the NAO after the occurrences of the MJO phase 7 during the westerly phase of the QBO (WQBO) are significantly stronger than during the easterly phase of the QBO (EQBO). The modulation of the QBO on the MJO-related teleconnections might be through the modification on the extratropical basic state. During the WQBO, the anomalous westerlies in the North Pacific enhance the subtropical westerly jet and

thus might be preferentially favorable for the propagation of Rossby waves from the tropics to the extratropics compared with EQBO. At the same time, the anomalous westerly wind over the polar region that is associated with a stronger polar vortex might also help the troposphere-stratosphere coupling to influence the NAO. However, the observed modulation of the MJO-NAO teleconnection by the QBO is not fully represented by the S2S models. Most S2S models capture the enhancement of the positive NAO after the occurrence of the MJO phase 3 during the WQBO, while the enhancement of the negative NAO after the occurrence of the MJO phase 7 is not well represented. During the EQBO, the representation of a significant negative NAO after the occurrence of the MJO phase 7 can be simulated by a few models, but the positive NAO after the occurrence of the MJO phase 3 is almost not seen in most models.

We also assess the prediction skill of the NAO in the S2S models. In particular, we look at the forecasts initiated with various initial conditions during the reforecast period of each model: 1) the positive and negative phases of the NAO, 2) the two phases of the QBO, and 3) the amplitude and the phases of the MJO. The forecasts initiated with a negative NAO tend to have a higher NAO forecast skill than those starting from a positive NAO. On the other hand, NAO forecasts did not show a significant difference in skill depending on which of the two phases of the QBO of the winter season it was initiated. Similarly, the prediction skills of the NAO also did not depend on whether it was initiated during an active or inactive MJO event when the phase of the MJO is not taken into account. However, among the eight phases, the MJO phases 3-5 and phases 7-1 lead to a better prediction skill of the NAO than other phases and the inactive MJO-initiated forecasts. From the assessments, we also find that most operational models with relatively higher model top represent a higher sensitivity to the selected initial conditions in general than the models with a lower model top.

Résumé

La météo et le climat des régions extratropicales sont profondément influencés par les variabilités climatiques dominantes se produisant sur une large gamme d'échelles allant de quotidienne à hebdomadaire, mensuelle, annuelle et au-delà. De plus, la téléconnexion, par laquelle on réfère souvent aux modes de variabilités à grande échelle de la variabilité basse fréquence et qui est parfois le produit de la convection tropicale, joue aussi un rôle important pour les prédictions météorologiques et climatiques. Le principal mode de variabilité climatique sur le bassin de l'Atlantique Nord, l'Oscillation nord-atlantique (NAO), est depuis longtemps l'objet de recherches et considéré comme un élément influençant les prédictions intra-saisonnières de manière importante.

Au courant de cette thèse, nous analyserons les données d'observations afin de clarifier la manière dont la convection tropicale et la variabilité climatique stratosphérique influence la NAO. Ensuite, nous évaluerons la capacité du projet de prédiction intra-saisonnière à saisonnière (S2S) du Programme mondial de recherches sur le climat/la météo (WCRP/WWRP) à prédire et représenter la NAO dans ses modèles opérationnels.

L'Oscillation Madden-Julian (MJO) est le principal mode de variabilité intra-saisonnière de la région tropicale. Il a été observé que certaines phases de la MJO ont des liens avec la NAO pour un décalage temporel d'environ 10 jours. En analysant les observations, nous avons trouvé que les réponses de la NAO suivant les MJO étaient différentes pour les deux phases de l'Oscillation quasi biennale (QBO) durant l'hiver boréal élargi. Autant la phase positive de la NAO suivant une MJO phase 2 que la phase négative de la NAO suivant une MJO phase 7 sont plus intenses durant la phase de la QBO aux vents d'ouest (WQBO) que pendant la phase de la QBO aux vents alizés (EQBO). La modulation par la QBO des téléconnexions liées à la MJO

semble se produire par la modification de l'état normal des régions extratropicales. Pendant la WQBO, les vents d'ouest inhabituels du Pacifique Nord intensifient le courant-jet subtropical venant d'ouest et ils pourraient ainsi être un terrain plus favorable, en comparaison avec la EQBO, à la propagation des ondes de Rossby à partir des tropiques vers les régions extratropicales. Concurremment, les vents d'ouest anormaux au-dessus des régions polaires, associés à un vortex polaire plus intense, pourraient aussi influencer la NAO à travers une amplification du couplage troposphère-stratosphère. Toutefois, la modulation observée de la téléconnexion MJO-NAO à travers la QBO n'est pas bien représentée par les modèles S2S. La plupart de ces modèles démontrent une amplification de la phase positive de la NAO après une MJO phase 3 se produisant pendant une WQBO, mais ils ne démontrent pas l'amplification de la phase négative de la NAO après une MJO phase 7. Pendant une EQBO, la phase significativement négative de la NAO suivant une MJO phase 7 est simulée par quelques modèles, mais presque aucun des modèles ne simule la phase positive de la NAO suivant une MJO phase 3.

Nous évaluons aussi la capacité des modèles S2S à prédire la NAO. En particulier, nous considérons les prédictions avec différentes conditions initiales durant la période de validation de chaque modèle: 1) durant les phases positives et négatives de la NAO, 2) durant les deux phases de la QBO et 3) selon l'amplitude et la phase de la MJO. Les prédictions initialisées lors d'une phase négative de la NAO sont généralement meilleures que celles initialisées avec une NAO positive. En revanche, la phase de la QBO lors de l'initialisation n'a pas d'impact significatif sur la prédiction de la NAO par les modèles. De même, que la MJO soit active ou inactive n'influence pas la qualité des prévisions de la NAO si on ne prend pas en compte la phase de la MJO. Toutefois, parmi les huit phases de la MJO, une initialisation pendant les phases 3-5 et les phases 7-1 produit de meilleures prédictions de la NAO que pendant les autres phases ou en l'absence de la MJO. Nous concluons que la plupart des modèles opérationnels

ayant un sommet relativement plus élevé sont en général plus sensibles aux conditions initiales que ceux qui ont un sommet plus bas.

Contributions of Authors

I performed all the research work and wrote this thesis, under the supervision of Prof. Hai Lin, Prof. Jacques Derome, and Prof. Timothy M. Merlis.

Chapter 2 is in the form of a published article in Journal of Geophysical Research, co-authored by Prof. Lin, who provided the supervision of the research works and edited the manuscript. I also acknowledge Prof. Derome and Prof. Merlis for the editorial work and the helpful suggestions and discussions.

Chapter 3 has been submitted to Journal of Climate and is now under review, co-authored by Prof. Lin, Prof. Derome, and Prof. Merlis. The original idea arose from the discussion with all the co-authors given the results from Chapter 2. Chapter 4 is also the extension of Chapter 2 as well. For Chapter 3 and Chapter 4, Prof. Lin primarily supervised the research work and did the editorial work with Prof. Derome and Prof. Merlis. The contents are the consequences from our numerous discussions.

Statement of Originality

The original contributions to knowledge of this thesis are summarized as follows:

- The investigation of the observations in Chapter 2 provides a new discovery of how the extratropics responds to the occurrences of the Madden-Julian Oscillation (MJO) under the two phases of the quasi-biennial oscillation (QBO) that modifies both the properties of the MJO and the basic state.

- As an extension of Chapter 2, the prediction skill of the North Atlantic Oscillation (NAO) of the latest operational models of WCRP/WWRP Subseasonal-to-Seasonal (S2S) prediction project is analyzed since the conditional NAO prediction skill of the S2S models had not been previously assessed. Thus, in Chapter 3, in order to first examine the influence of the climate variabilities investigated in Chapter 2, we assess the prediction skill of the NAO from the reforecasts initiated 1) with an NAO event, 2) during the two phases of the QBO, and 3) an MJO event, respectively. Then in Chapter 4, we analyze the representation of the MJO-NAO teleconnection under the modulation of QBO in the S2S models.

Acknowledgements

I would like to express my sincere gratitude to my supervisors, Professor Hai Lin, Professor Jacques Derome, and Professor Timothy M. Merlis. First and foremost, I must offer my heartfelt thanks to Professor Hai Lin for this great opportunity that I could take my Ph.D. program here in McGill University. I do appreciate his guidance, patience and support. It is hard to describe with words for how much I learn from him and my gratitude to him. I would like to thank Professor Jacques Derome, for his instruction and encouragement. He always inspires me with his wisdom and knowledge and gives me kind helps. I have to thank Professor Timothy M. Merlis, for giving me the direction and advice. His positive attitude encourages me much on the academic career. It is very precious for me to work with them, and their attitude and passion for academics form the role model to me. I am also grateful to all the staff who are always ready to help and all the wonderful people of Department of the Atmospheric and Oceanic Sciences.

I am deeply grateful to my dearest family in Taiwan, my parents and my brother, for your unconditional love and support. Without you I can never get to where I am today.

謝謝我在臺灣的家人，我的父母和弟弟。謝謝你們總是包容我的各種任性，沒有你們的支持我不可能走到這裡，非常感謝。

Contents

List of Tables

List of Figures

Chapter 1

Introduction

1.1 Climate variabilities and teleconnections

Climate variability, according to the definition of the World Meteorological Organization (WMO), is the variability in the mean state and other statistics of the climate on all temporal and spatial scales beyond individual weather events (Houghton et al. 1990). The anomaly over a given period of time could determine the pattern of temperature, rainfall, and other variables in various time scales. Climate variability comprises both internal variability, which is generated from the natural internal processes of the climate system, and the external variability, which is due to external factors such as anthropogenic activities.

A teleconnection is the term for a significant correlation between temporal fluctuations of a field at widely separated points (American Meteorological Society 2020) and usually associated with a planetary wave (Wallace and Gutzler 1981). A teleconnection is often applied to the linkage of the atmospheric variability between distant regions (Lin et al. 2019), and the name suggests the propagation of the information in different locations through the atmosphere (American Meteorological Society 2020). Both spatially and temporally, teleconnections influence the atmospheric circulation profoundly due to their recurring and persistent character. The pattern of the teleconnections may last at least for weeks and span various time scales (Feldstein and Franzke 2017). Hence, the simulation of teleconnections is now regarded as an important metric for a model's forecast on the subseasonal time scale, which is challenging

even for state-of-art models (Lin et al. 2019).

Climate variabilities have profound linkage to weather and climate. The interaction between the tropics and the extratropics is often through teleconnections. The heating source over the tropics may generate Rossby waves propagating eastward and poleward to the mid-latitudes (Hoskins and Karoly 1981; Hoskins and Ambrizzi 1993; Jin and Hoskins 1995) and hence to form teleconnection patterns (Lin et al. 2019). In addition, the extratropics can also influence the tropics through the equatorward-propagating waves (Liebmann and Hartmann 1984). A global view of climate variability on the intraseasonal time scale was proposed (Hsu 1996). However, the fluctuation of climate variability may occur on multiple time scales and connect with the other climate variabilities. To further understand the dynamics of the climate variabilities and the underlying mechanisms that drive the teleconnections in various time scales would help to construct a more complete picture of the global climate and improve the forecasts in different time ranges.

1.1.1 North Atlantic Oscillation

In the extratropics, the North Atlantic Oscillation (NAO) is the prominent mode of climate variability in the atmosphere over the North Atlantic basin (e.g., Walker and Bliss 1932; Wallace and Gutzler 1981). The NAO is composed of a zonally symmetric seesaw pattern in sea level pressure (SLP), which also has an equivalent barotropic vertical structure. The positive phase of the NAO draws a pattern with a negative anomaly center located over southern Greenland, and a positive anomaly along the middle-latitude North Atlantic. The negative phase of the NAO depicts the same meridional dipole structure as the positive phase with opposite signs (e.g., Wallace and Gultzer 1981). For the time scale, the NAO variability

has a broad temporal range that spans from days to decades (e.g., Hurrell and van Loon 1997; Feldstein 2000). The boreal winter is when the NAO being most active, and the amplitude usually reaches the maximum during this season. The profound influences of the NAO on weather and climate across the North Atlantic Ocean basin, Europe, and North America have been long investigated (e.g., Hurrell 1995; Hurrell et al. 2003). Although the NAO has been considered to be the regional manifestation of the Northern Annular Mode (NAM; Thompson and Wallace 1998, Hurrell et al. 2003) or the Arctic Oscillation (AO), the NAO remains the dominant mode of the climate variability for the study of the weather and climate over the Atlantic basin.

The underlying dynamics of the NAO are generally interpreted as resulting from the momentum fluxes exchange associated with the baroclinic eddies (Vallis et al. 2004) and the wave breaking of synoptic-scale waves (e.g., Benedict et al. 2004; Woollings et al. 2008). However, many factors impact the waves associated with the NAO over the extratropics. Woollings et al. (2008) suggested that the variabilities of the tropical Pacific and stratosphere are the possible precursors in advance of the wave breaking. Feldstein (2003) found that both the high-frequency and low-frequency transient eddy fluxes drive the growth of the NAO, and the life cycle of the NAO was around two weeks. Later, Rennert and Wallace (2009) discovered a wider crossing-frequency variability of the NAO, including the high frequency as one week to the low frequency longer than one month. The persistence on approximately biweekly scale was illustrated to be associated with the meridional shift of the Atlantic jet by Barnes and Hartmann (2010). Linked to the slower change of the sea surface temperature (SST) and the sea ice, the oceanic forcings that drive the seasonal variability of the NAO have also been reported (e.g., Rodwell et al. 1999; Bader et al. 2011). The previous studies have shown the complexity of the NAO that is associated with multiple time scales, and also implied the challenge of the predictability of the NAO. Since the wave activity is profoundly associated

with the NAO, the time scale of wave interactions might limit the prediction skill with a lead time longer than the wave interactions at the subseasonal time scale.

Although the complexity of the mechanisms of the NAO and the limitation of the models might impact the prediction skill of the NAO, various attempts have been made in order to improve the predictability. The predictability of the NAO on various time scales has been investigated in many studies. For example, Johansson (2007) investigates the daily to seasonal predictability of the NAO in the ECMWF and NCEP operational dynamic models. On the daily scale, the simulated NAO could maintain an anomaly correlation of 0.5 around 10 days and an anomaly correlation of 0.3 up to around 15 days. Extreme events take a longer time to return to the mean state and thus lead to a lingering forecast skill. On the intraseasonal time scales, the NAO skill was expected to be improved through the stratospheric connections (Ambaum et al. 2001) and the atmosphere-ocean coupling (e.g., Czaja et al. 2003). Up to the monthly and seasonal scale, the NAO had weak predictability with the signal amplitude comparable to the noise (Johansson 2007). Wang et al. (2017) obtained longer persistence of seasonal prediction from an empirical model than the dynamical models by using the multiple linear regression techniques combined with the condition of autumn sea ice, stratospheric circulation, and the SST. O'Reilly et al. (2019) investigate the importance of the stratospheric impact on the winter season forecast of the NAO. The result indicated that although the stratospheric influence might be weak, the additional NAO skill from the stratospheric modification exists, which also gives a further explanation for the long timescale anomaly correlation found by Johansson (2007). Later, Scaife et al. (2014) demonstrated that the prediction of the NAO months ahead might be possible and discussed that the resource of the predictability might be from the slow-varying variabilities from ocean and teleconnections. In the experiment of Scaife et al. (2014), the result indicated the extratropical responses corresponding to the tropical heating, sea surface temperature, sea ice, and the quasi-biennial oscillation were represented in the models, while

the amplitude was rather smaller when compared with observations. Over the regions covered by the NAO pattern, the predictability can vary greatly from point to point (Scaife et al. 2014). Thus, when the NAO index that depends on the spatial distributions is applied for the assessment of predictability, the result might be impacted.

As the prediction skill on the subseasonal-to-seasonal (S2S) time scale is assessed, the fluctuations of the teleconnection at this time scale can provide an approach to assess the prediction skills of model simulations. Some operational models could predict the NAO with an anomaly correlation of 0.5 up to around two weeks (Johansson 2007; Ferranti et al. 2015). Ferranti et al. (2015) assessed the predictability of the flow patterns over the Euro-Atlantic region in the ECMWF operational models and found that the negative phase of the NAO has a better prediction skill than the positive phase. Similar results were obtained for the NAM/AO (Lin 2019). Lin (2019) interpreted the possible mechanism as the longer time for the negative NAM/AO to return to the normal state than the positive phase, and the anomalous geopotential height of the negative NAM/AO was also more persistent.

1.1.2 Madden-Julian Oscillation

Many important climate variabilities take place in the tropics at various time scales. For the well-known ENSO related to the change of the sea surface temperature, the time scale is around 2-7 years, while in the higher frequency, the Madden-Julian Oscillation (MJO) is the dominant mode of atmospheric variability on the intraseasonal time scale in the tropics first documented by Madden and Julian (1971, 1972). The MJO was observed for its convective feature. With its onset originating from the tropical western Indian Ocean, the convection system grows and propagates eastward at a speed of about 5 m/s across the Indian Ocean, the Maritime Continent, and the western Pacific and then the convection weakens in central Pacific.

The life cycle takes approximately 30-90 days (Madden and Julian 1971; 1972).

According to the observed features of the MJO, the zonal winds reverse the direction at the upper and lower troposphere around 200 and 850 hPa (e.g., Zhang 2005). Wheeler and Hendon (2004) combined the zonal winds at 200 and 850 hPa and the outgoing longwave radiation (OLR) for the empirical orthogonal function (EOF) calculation and designed the Real-Time Multivariate MJO Index (RMM Index). The first two modes of the principal components are taken as RMM1 and RMM2. The vector space describes the phase and amplitude of the MJO. The MJO progression corresponding to the longitudinal locations of the tropical convection is categorized into eight different phases. The phase 8 and 1 indicate the onset of the MJO in the western Indian Ocean. The dipole structure of the phase 2 and 3 depict an enhanced convection over the Indian Ocean and a suppressed convection over the western Pacific. When the convections across the Maritime Continent, it is defined as the phase 4 and 5. The phases 6 and 7 share a similar dipole structure as phases 2 and 3 with opposite signs. The amplitude of the MJO is defined as the magnitude of the vector formed by RMM1 and RMM2 $\sqrt[2]{(RMM1)^2 + (RMM2)^2}$, and an active MJO event refers to the amplitude that exceeds unity (Wheeler and Hendon 2004).

1.1.3 MJO-NAO Teleconnection

On the subseasonal time scale, the connection between the MJO and the NAO has been investigated in several studies (Cassou 2008; Lin et al. 2009). Certain phases of the MJO have been shown to be associated with the extratropical atmospheric circulation anomalies through teleconnections: phases 2 and 3 of the MJO leads the positive NAO, and the phases 6 and 7 of the MJO leads the negative NAO by around two weeks (Cassou 2008; Lin et al. 2009). The MJO-related NAO events can last around 30 days (Jiang et al. 2017). The phases of the MJO

composed with the zonal dipole structures of the OLR on the flank of the Maritime Continent, i.e., phases 2 and 3 and phases 6 and 7, are shown to have the most influence on the extratropics (Lin et al. 2009). The numerical experiment of Lin et al. (2010) further illustrated that along the equator, certain locations of the tropical heating could provoke the strongest extratropical response. The result is consistent with the locations of the convection of the dipole-structure phases of the MJO.

How the MJO drives the NAO teleconnection might be explained by atmospheric wave dynamics (Hoskins and Karoly, 1981; Karoly, 1983; Hoskins and Ambrizzi, 1993). Lin et al. (2009) interpreted the NAO teleconnection as a Rossby wave train in the 500-hPa geopotential height anomaly field. The MJO, with its diabatic tropical heating, induces the extratropical Rossby wave that propagates northeastward and impacts the formation of the NAO. The evolution of the extratropical atmospheric responses to the tropical dipole heating of the MJO was simulated and reproduced in numerical models (e.g., Lin and Brunet, 2018). The importance of the extratropical zonal westerly flow for Rossby wave propagation has been shown in previous studies (e.g., Hoskins and Ambrizzi 1993; Garfinkel and Hartmann 2010; Lin and Brunet 2018). The importance of the middle-latitude mean flow for the Rossby wave propagation was further illustrated in Lin and Brunet (2018). In their numerical experiments, it was found that both the eastward extension and the southward shift of the subtropical westerly jet are favorable for the Rossby wave propagation that leads to stronger extratropical response associated with the MJO. In addition, the MJO-NAO teleconnection has a documented association with stratospheric processes. The MJO-induced poleward and vertical propagating Rossby waves could modify the stratospheric polar vortex and then impact both the stratospheric and tropospheric NAM/AO with a longer time than through the wave activities in the troposphere (Garfinkel et al. 2012; Jiang et al. 2017).

The MJO-related extratropical teleconnections could be modified by the ENSO induced

circulation anomalies as well (Roundy et al. 2010; Henderson and Maloney 2018). During the warm phase of ENSO as El Niño, the MJO-related extratropical response over the Atlantic basin is more similar with the NAO pattern and significant than during the cold phase as La Nina. The eastward extended Asian jet during El Niño was suggested as an important factor that leads to a higher wavenumber in the east Pacific and thus provides a preferable environment for the waves propagating to the Atlantic basin. Also, the frequency of the occurrence of the negative NAO after the MJO phase 7 increases during El Niño (Henderson and Maloney 2018).

1.1.4 Quasi-Biennial Oscillation

Beyond the troposphere, the connection between the tropics and extratropics through the stratosphere and the modulation on the troposphere has been investigated in many studies (e.g., Baldwin and Dunkerton 1999; Marshall and Scaife 2009; Jiang et al. 2017; Son et al. 2017). In the stratosphere, the leading mode of interannual variability in the tropics is the quasi-biennial oscillation (QBO). The easterly phase (EQBO) and westerly phase (WQBO) of the QBO are defined by the zonal wind anomalies near the equator and alter over a period of around 28 months. Both phases are found to propagate downward to the troposphere (Baldwin et al. 2001). The mechanism that drives the QBO is explained by the momentum transfer of the upward propagating planetary-scale equatorial waves from the troposphere and interactions with the zonal flow (Lindzen and Holton 1968; Holton and Lindzen 1972).

1.1.5 QBO and Its Connection with Extratropical Circulation

The influences of the QBO over the Northern Hemisphere have been long investigated. Holton and Tan (1980; 1982) found the impact of QBO on the high-latitude troposphere through the polar vortex. During the WQBO, the anomalous low geopotential height in the polar region forms a stronger polar night jet that corresponds to a colder polar vortex, which is weaker during the EQBO. The Holton-Tan effect refers to this connection between the QBO and the polar vortex. The possible mechanism is explained by the QBO modification of the waveguide that leads the stratospheric planetary waves through the shifting subtropical critical line during the boreal winters (Holton and Tan 1980). Later, the observational data from longer temporal coverage and model simulations revealed some different possible mechanisms for the connection between the QBO and polar vortex (e.g., Naoe and Shibata 2010; Garfinkel et al. 2012). Different from the previous explanation, Garfinkel et al. (2012) suggested that the modification on the wave propagation might be caused by changes in the meridional circulation of the QBO instead of the subtropical critical line. Besides, the change of the Eliassen-Palm flux (EPF) caused by the QBO is also an important modification in the lower stratosphere that further influences the polar vortex (Garfinkel et al. 2012).

The polar vortex forms the anomalous pressure in the polar region, which is highly associated with the NAM. The weak polar vortex is preferable for the anomalous high of the geopotential height in the polar region, which is associated with the negative phase of the NAM. When the strong vortex occurs, it is more often related to the positive phase of the NAM. The NAO and the NAM share the same sign of the phase at the same time. Thus, the modification of the QBO on the NAM also influences the NAO.

As mentioned in the previous subsection, the main phase of the QBO propagates downward to the troposphere (Baldwin et al. 2001). From the observational vertical profile of

the anomalous zonal wind field, the wind direction of the main phase of the QBO in the tropical stratosphere is opposite to the tropical troposphere, while the zonal wind in the tropospheric subtropics corresponds to the main phase of the QBO (Crooks and Gray 2005; Haigh et al. 2005). Over the subtropics, the jet is a key factor for the propagation of Rossby waves. A stronger Asian jet in the upper troposphere could provide a preferable environment for Rossby waves to propagate from the tropics to the extratropics than a weaker jet via changes in the refractive index (Henderson and Maloney 2018). Lin and Brunet (2018) also reported that the dependence of the extratropical responses through the wave train triggered by MJO on the westerly jet over the Pacific basin. Thus, the subtropical anomalous zonal wind that corresponds to the main phase of the QBO might also have modulations to the tropical-extratropical interactions.

1.1.6 The QBO Modulation on the MJO

During the boreal winter season from December to February, the QBO has a stronger modification to the MJO than ENSO, and around 30-40% interannual variation of the amplitude of the MJO can be explained by the QBO (Son et al. 2017). Under the EQBO, the OLR anomaly is generally stronger than under the WQBO, and this difference is even more robust and significant for the active MJO events. The difference is not sensitive to the existence of ENSO. The life cycle of the MJO takes around 50 days under the EQBO, which is about 10 days longer than under the WQBO (Nishimoto and Yoden 2017; Son et al. 2017). However, Zhang and Zhang (2018) argued that the stronger MJO activity under the EQBO meant more MJO days instead of the stronger amplitude of individual MJO cases. The primary explanation is that the MJO could propagate further east under the EQBO because the circulation weakened the barrier of the Maritime Continent, and thus there were more MJO days than during the

WQBO phase. At the same time, Hendon and Abhik (2018) found that the vertical temperature structure of the MJO was also more in-phase under the EQBO and this maintains the strength of the MJO for the more eastward propagation into the western Pacific than during the WQBO phase. Although the interpretations vary, the investigations of the previous studies indicate that the MJO is more active under the EQBO. Hence, the stratospheric mean state is expected to influence the predictability of the MJO and the MJO-related teleconnections.

The forecast of the MJO is able to maintain a bivariate correlation of the RMM1 and RMM2 higher than 0.5 up to around 25-30 days in various models (e.g., Vitart 2017). It takes longer for the bivariate correlation to drop to 0.5 in the boreal winters from December to February under the EQBO conditions than the WQBO conditions (Marshall et al. 2017; Lim et al. 2019). Although the simulations represented the better MJO skill under the EQBO than the WQBO, the investigation suggested that the stronger amplitude of the MJO under EQBO in the S2S models might not be the direct factor because the skill was not sensitive to the initial amplitude of the MJO (Lim et al. 2019).

1.1.7 Subseasonal-to-Seasonal Predictions

Since the weather systems and climate variabilities involve multiple time scales, various types of forecast are developed for practical needs. Recently, the predictions on the S2S time scale, which covers from two weeks to two months, receive increasing interest and attention for connecting weather and climate forecasts. In the past, the forecast of this temporal coverage was less discussed than on other time scales since the daily prediction and the seasonal forecast have been applied and studied for long (Vitart et al. 2012). Due to the increasing needs from applications of both the science to improve the forecasts between the weather and seasonal predictions and the society as to lower the damage from natural risks, the Subseasonal to

Seasonal (S2S) Prediction Project of the World Weather Research Programme (WWRP) / World Climate Research Programme (WCRP) of the WMO was launched to fill the gap of this time scale in the forecasts and the dataset of the S2S models from 11 research centers was released (Vitart et al. 2017).

As stated in Vitart et al. (2012), the sources of S2S predictability could be from the MJO and MJO-related extratropical responses or the stratosphere-troposphere interactions through NAM, or other processes in the atmosphere, ocean, and land. Many extreme events that might have severe impacts are formed with a strong character at the S2S time scale, which is an objective that this S2S research project aims to understand and improve the predictions. The representation of the climate variabilities in the S2S model simulations is then important for the future applications.

1.2 Structure of the Thesis

1.2.1 Research Questions and Objective

The climate variabilities have been long term investigated for their dynamical characters, and the teleconnection relations between the climate variabilities are also always of interest. However, the broad spatial coverage and the multiple time scales of the teleconnections increase the complexity of the research task. Many studies attempt to complete the puzzles of how the teleconnections interact for the further understanding of weather and climate.

As the MJO-associated extratropical responses (Lin et al. 2009) and the modulations of the MJO by the QBO (Son et al. 2017) were investigated, the question the question arises as to whether the modification of the QBO to the MJO would also modulate the extratropical responses induced by the MJO, directly or indirectly. Besides the observations, we examine

whether the latest S2S models could capture the teleconnections and provide a better understanding of the teleconnection dynamics and serve future prediction applications as well.

Thus, the goal of this thesis is to investigate the evolution of the NAO in the subseasonal time scale associated with the occurrences of the MJO through the modulation of the QBO in both observations and the model simulations and further to assess the predictability of the NAO under certain conditions, which have been identified as modifying the NAO in the observations.

1.2.2 Dissertation Outline

The structure of the remaining portions of the dissertation is as follows:

Chapter 2: Modulation of the MJO-Related Teleconnections by the QBO

In Chapter 2, the extratropical responses over the Atlantic basin after the occurrence of the MJO events under the two phases of the QBO during the extended boreal winter is analyzed with a 35-year observational data. Based on the previous discoveries of the teleconnections between the MJO and the NAO and the modulation of the QBO on the MJO, how the QBO phase leads the difference of the tropospheric tropical-extratropical teleconnections is investigated. At the same time, the anomalous circulation patterns in the two phases of the QBO are compared in order to clarify the possible mechanisms. The convection patterns of the MJO and corresponding extratropical responses with a lag of 10-15 days are also addressed.

Chapter 3: The Predictability of the NAO in the S2S Subseasonal Reforecasts in Boreal Winter

In Chapter 3, the simulated evolution of the NAO with the given initial conditions is assessed and compared with the observations. Based on the study of previous chapter, the initial conditions of S2S reforecasts are selected for the occurrence of the NAO events, QBO events,

and MJO events. The MJO part includes both the comparisons of the amplitude and phases of the MJO. The conditional predictability of the NAO is assessed in S2S models.

Chapter 4: Modulation of the MJO-Related Teleconnections by the QBO in the S2S Subseasonal Reforecasts.

Chapter 4 extends the study of Chapter 2 to assess the evolution of the NAO in the reforecasts initiated with an MJO event of certain phases during the QBO years of the S2S models since the NAO prediction skill of the reforecasts with the MJO and the QBO as the initial conditions has been investigated respectively in Chapter 3. The MJO-associated NAO during the QBO years generated from the ensemble members, and the ensemble mean of each model is assessed and compared with observations.

Chapter 5: Summary and future work

Chapter 5 summarizes the dissertation's main contributions and describes future research.

Chapter 2

Modulation of the MJO-Related Teleconnections by the QBO

This chapter investigates the Madden-Julian Oscillation (MJO)-related extratropical teleconnection under the two phases, easterly and westerly, of the quasi-biennial oscillation (QBO). In order to further understand if the QBO modulation on the characters of the MJO would also modify the extratropical responses induced by the MJO, we analyze the change of the geopotential height in the extratropics after the occurrences of the MJO and the basic state under the two phases of the QBO.

This chapter consists of a paper published in the Journal of Geophysical Research: Feng, P.-N., & Lin, H. (2019), Modulation of the MJO-related teleconnections by the QBO*, Journal of Geophysical Research: Atmospheres*, 124, 12022–12033, doi:10.1029/2019JD030878

Modulation of the MJO-Related Teleconnections by the QBO

Pei-Ning Feng1 and Hai Lin2*

1Department of Atmospheric and Oceanic Sciences, McGill University

2Recherche en prévision numérique atmosphérique, Environment and Climate Change Canada

March 2019

Key Points:

- The MJO-NAO connection is found to be stronger when the QBO is in the westerly than the easterly phase.
- An SVD analysis of tropical OLR and the 2-pentad lagged 500 hPa geopotential height reveals different dominant patterns under EQBO and WQBO.
- The QBO modulation of the MJO-NAO connection can likely be explained by differences in the extratropical mean flow.

---

*Corresponding author address:

Pei-Ning Feng, Department of Atmospheric and Oceanic Sciences, McGill University, Burnside Hall, 805 Sherbrooke Street West, Montreal, Quebec, H3A 0B9. Email: pei-ning.feng@mail.mcgill.ca

Abstract

Previous studies have provided observational evidence for a correlation between certain phases of the Madden-Julian Oscillation (MJO) and the North Atlantic Oscillation (NAO), at a lag of about 10 days. Such a relation implies that the tropical convection of the MJO may provide sources of skill for subseasonal predictions in the extratropical regions. In this study, we show that the MJO-NAO connection is influenced by the phase of the quasi-biennial oscillation (QBO). During the westerly phase of QBO (WQBO), a stronger and longer lasting MJO-NAO teleconnection is observed. About 10 days after the MJO phase 3 (7), which corresponds to enhanced (suppressed) diabatic heating anomaly in the tropical Indian Ocean and reduced (enhanced) convection in the western Pacific, a positive (negative) NAO tends to occur. On the other hand, under the easterly phase of QBO (EQBO), the MJO-NAO teleconnection is also observed, but weaker and with less statistical significance. The QBO possibly influences the MJO related teleconnection by modulating the extratropical basic state. During WQBO years, there is subtropical anomalous westerly wind in the North Pacific, and as a result, the enhanced subtropical westerly jet provides a favorable environment for the MJO induced extratropical Rossby wave to propagate. The anomalous high-latitude North Atlantic westerly is also favorable for troposphere-stratosphere coupling and for the NAO to develop.

2.1 Introduction

The Madden-Julian Oscillation (MJO) is the dominant mode of atmospheric variability on the intraseasonal time scale in the tropics, and it can be described as an eastward propagating convection system (Madden and Julian, 1971, 1972). The convection starts to develop in the western Indian Ocean, moves eastward at a speed of about 5 m/s across the Indian Ocean, the Maritime continent and the western Pacific, and it then weakens when the system approaches the Central Pacific Ocean. To describe the MJO, Wheeler and Hendon (2004) designed the Real-Time Multivariate MJO Index (RMM Index) which allows to categorize the MJO progression into eight different phases that correspond to different longitudinal locations of the tropical convection. For example, the MJO convection is located in the Indian Ocean at phases 2 and 3, whereas at phases 6 and 7 the convection is moved to the western Pacific. On the sub-seasonal to seasonal (S2S) time scale, the tropical-extratropical connections driven by the MJO are regarded as a potential source of predictability (Lin et al., 2009; Vitart et al., 2017).

The North Atlantic Oscillation (NAO) is the prominent mode of climate variability in the atmosphere over the North Atlantic basin and takes the form of a dipole pattern in sea level pressure (SLP), with an equivalent barotropic vertical structure (Wallace and Gutzler, 1981). The NAO usually reaches its maximum amplitude during the boreal winter. In its positive phase the NAO shows a negative pressure anomaly center located over southern Greenland, and a positive pressure anomaly along the middle-latitude North Atlantic. The structure of the negative phase of the NAO is the same as the positive phase, but with the opposite sign. The NAO variability has significant influence on the weather and climate in the Northern Hemisphere, especially in northeast North America and Europe (e.g., Hurrell 1995, Hurrell et al. 2003).

Certain phases of the MJO have been shown to be associated with the extratropical atmospheric circulation anomalies through teleconnections, and the phases with the dipole convection structures (phases 2-3 and 7-8) were shown to have the most influence on the extratropics (Lin et al., 2009; Lin et al., 2010). Phases 2 and 3 of the MJO describe a dipole structure of the outgoing longwave radiation (OLR) anomalies, with negative (enhanced convection) and positive OLR anomalies (suppressed convection) in the Indian Ocean and the Maritime Continent-Western Pacific Ocean, respectively, while phases 6 and 7 represent the same dipole feature, but with opposite signs. The positive phase of the NAO tends to develop about 10 days after the occurrence of phase 3 of the MJO, while the negative phase of the NAO follows phase 7 of the MJO (Lin et al. 2009). Similar results were also reported in Cassou (2008).

The MJO-NAO teleconnection pattern can be explained by atmospheric wave dynamics (Hoskins and Karoly, 1981; Karoly, 1983; Hoskins and Ambrizzi, 1993). Lin et al. (2009) also demonstrated that the linkage between the MJO and the NAO is through a Rossby wave train in the 500-hPa geopotential height anomaly field. In the tropics, the deep convection of the MJO induces extratropical Rossby waves propagating northeastward and influencing the formation of the NAO. During this process, the location of the East Asian jet was found to influence the Rossby wave propagation in model simulation and observations (e.g., Lin and Brunet, 2018).

In the stratosphere, the leading mode of interannual variability in the tropics is the quasi-biennial oscillation (QBO). The QBO has two phases, alternating over a period of around 28 months, and both propagate downward (Baldwin et al. 2001). The two phases of QBO are defined by the mean zonal wind direction: the easterly QBO (EQBO) and the westerly QBO (WQBO). The QBO has long been investigated for its impact on the extratropical circulations. Holton and Tan (1980, 1982) discovered that the equatorial QBO may impact the extratropical

circulations through the planetary waves and showed the influences of the QBO on the polar night jet in the boreal winter. Afterwards, the model simulations of Marshall and Scaife (2009) represented the statistically significant strengthened (weakened) polar vortex during WQBO (EQBO) as observations. In the same study, they also discovered the differences of the polar geopotential height anomaly between the two phases of the QBO is characteristic of AO. The association of the QBO and the Northern Annual Mode (NAM) or the Arctic Oscillation (AO) was also reported in different aspects (e.g., Coughlin and Tung, 2001; Ruzmaikin et al., 2005; Marshall and Scaife, 2009). In previous studies, the mechanisms between the QBO and the tropospheric extratropical and polar regions was shown to be related to the planetary wave activity (Ruzmaikin et al., 2005; Chen and Li, 2007).

The stratosphere recently gained more attention for its role with respect to weather and climate in the troposphere, and its influence on the MJO was also investigated (e.g., Liu et al., 2014; Marshall et al., 2017; Nishimoto and Yoden, 2017; Densmore et al.,2019; Wang et al., 2018; Zhang and Zhang 2018). For example, Son et al. (2017) showed that the QBO has the largest impact on the MJO during boreal winters [December-February (DJF)] when the structure and the amplitude of the MJO have significant differences under the 2 phases of the QBO. During the EQBO, the MJO tends to have stronger amplitude and be able to propagate further eastward (Son et al., 2017), and the vertical thermal structure in the tropics supports the growth of the convection of MJO (Hendon and Abhik, 2018). From another aspect, Zhang and Zhang (2018) tracked individual MJO events and discovered the longer life cycle of the MJO under EQBO conditions, which is regarded as the more active MJO days instead of the significant stronger MJO amplitude from previous thought. Through this property, the better prediction skill of the MJO under the EQBO is also discovered (Marshall et al., 2017). However, although the observed MJO manifests some significant features under the two phases of the QBO, how the QBO mediates the teleconnections between tropics and extratropics seems more

complicated given such connections occur through direct and indirect pathways (Garfinkel and Hartmann, 2010; Liu el al, 2014).

Son et al. (2017) analyzed the MJO related teleconnection in the North Pacific and found that during EQBO winters the teleconnection is stronger than during WQBO winters. They attributed this to the direct influences of the MJO itself since the MJO tends to have stronger amplitude and to last longer during the EQBO winters. This strengthened convection of the MJO during DJF of EQBO is regarded as the primary reason for the enhanced MJO teleconnection. At the same time, the responses of geopotential height field over arctic and North America at 100 hPa after the occurrences of the MJO phase 3 are discovered to be stronger in WQBO winters (Liu et al., 2014). The patterns correspond to the different types of the stratospheric sudden warming and the MJO-associated wave activity fluxes under the two phases of the QBO also indicate the different propagation pathways. This difference of the wave activity flux propagation might be associated with the shift of the tropical jet stream modulated by the QBO (Liu et al., 2014). Hence, if the MJO-NAO teleconnections are also influenced by the QBO is of interest.

Here we focus on the MJO related teleconnection in the North Atlantic, i.e., the MJO-NAO connection, and investigate how this connection is influenced by the phase of the QBO. This paper is structured as follows. First, we introduce the data and methods used in section 2.2, then we compare the MJO-NAO teleconnections during the two phases of the QBO in section 2.3. In section 2.4 we then present a discussion of the results and a possible explanation for them, and the conclusion follows as section 2.5.

2.2 Data and Methods

This study is based on reanalysis data and observations covering of the period of 1979-2013. The wind field and geopotential height data are from the National Centers for Environmental Prediction-National Center for Atmospheric Research (NCEP-NCAR) Reanalysis 1 (Kalnay et al., 1996), and the interpolated outgoing longwave radiation (OLR) data from the National Oceanic and Atmospheric Administration (NOAA) (Liebmann and Smith, 1996) are used to represent tropical convection. All variables have daily temporal resolution and spatial resolution of 2.5-degree latitude by 2.5-degree longitude on global grids.

To obtain the daily anomaly of a variable, the seasonal cycle at each grid point is first removed, and then the 180-day mean (181-day mean of leap year) of each winter is removed to eliminate the interannual variability. The seasonal cycle here is the annual mean and the first 3 harmonics of the daily climatology for the 34 years considered. The pentad data for the extended winter corresponds to 5-day averages of the anomalies for a given variable from November to April. The first pentad corresponds to 2-6 November and the last one as 26-30 April. During leap years, the 24th pentad is a 6-day average inclusive of 29 February. The extended winters examined are those from 1979/80 to 2012/13. In this study, winter indicates the extended winter if not specifically noted.

To define the El Niño-Southern Oscillation (ENSO) events, the NOAA monthly Nino 3.4 sea surface temperature (SST) (https://www.esrl.noaa.gov/psd/gcos_wgsp/Timeseries/Data/nino34.long.anom.data) index is used. The index is calculated as the average SST anomaly (with the mean of 1981-2010 removed) for the area comprised of 5°S-5°N and 170-120°W.We define years of strong El Niño (La Nina) when the index is greater (less) than 1 (−1) standard deviation. In the study of Garfinkel and Hartmann (2010), they discovered that the propagation of Rossby wave produced by ENSO on the seasonal time scale could be affected by the change of the mean flow induced

by the QBO. Since our study focuses on the subseasonal time scale MJO teleconnection and the QBO influence, the ENSO influence is excluded by the removal of the strong ENSO years.

For the MJO, we use the daily RMM index of Wheeler and Hendon (2004) which is downloaded from http://www.bom.gov.au/climate/mjo/graphics/rmm.74toRealtime.txt. The RMM index comes from an empirical orthogonal function (EOF) analysis, in which the meridionally averaged zonal wind at 850 and 200 hPa, and the OLR anomalies between 15°S and 15°N are combined. RMM1 and RMM2 are the first two principal components. The MJO amplitude is defined as the magnitude of the vector formed by RMM1 and RMM2 $\sqrt[2]{(RMM1)^2 + (RMM2)^2}$, and an active MJO event is defined when the amplitude exceeds unity.

In this study, the EQBO and WQBO are classified with the winter average of zonal wind between 10°S and 10°N at 50hPa. When the average from November to April is greater (less) than 0.5 (-0.5) standard deviation, then it is defined as a WQBO (EQBO) year. During the 1979-2013 period, there are 11 EQBO years and 12 WQBO years according to this method. If we remove the years when strong ENSO events occurred, 9 EQBO and 8 WQBO years remain (Table 2.1). In these QBO years, the teleconnections between MJO and extratropics are assessed. Son et al., (2017) mentioned that during 1979-2013 the QBO primarily changes its phase during springs, while there is only one EQBO year (2011/12) changed the phase into westerly in March in our selected years. However, in the 11 pentads during March and April of 2012, there is also only one pentad with active MJO event in phase 3 selected and the existence of this pentad does not affect the robustness of our results. Also, if we shorten the winter season as only DJF, the same list of these years is obtained. In the selected winters of each phase of QBO, the numbers and the mean amplitude of active MJO events in pentad data are shown in Table 2.2. The mean amplitude of all active MJO events in WQBO (1.75) is slightly larger than in EQBO (1.73), however, this difference is not statistically significant. Besides, when we

compare the mean amplitude of the active MJO events in DJF, the mean amplitude is stronger in EQBO phase, which agrees with the previous studies (e.g., Son et al., 2017). Thus, the degree of freedom of the student-t test applied in this study is the number minus one. When it reaches 2-pentad lag, the degree of freedom of the lagged composites of the MJO phase 3 in EQBO is 21, 26 for MJO phase 7. For WQBO, the degree of freedom with respect to the MJO phase 3 is 23 and 22 for the MJO phase 7 because some pentads in the end of April cannot be selected.

To calculate the composite NAO index, we compute the projection of pentad Z500 anomaly onto the NAO spatial pattern, which is defined as the second rotated EOF mode of monthly mean Z500 anomaly over the Northern Hemisphere (Lin et al., 2009 Fig. 1).

To identify the dominant co-varying patterns of tropical convection and the Northern Hemisphere circulation, a singular value decomposition (SVD) analysis (Bretherton et al., 1992; Wallace et al., 1992) is performed on the pentad anomaly data of OLR and Z500 which lags the OLR by 2 pentads. The two variables are normalized by their own spatially averaged temporal standard deviation respectively. The spatial coverage of the OLR data is from 20°S to 20°N, and the domain of the geopotential height field covers 20-90°N. The covariance matrix of the anomalies is taken for the SVD calculation.

2.3 MJO-NAO Teleconnection under WQBO and EQBO

In this section, the lagged composites of the NAO index and the geopotential height at 500 hPa after the occurrences of the MJO phase 3 and 7 in both EQBO and WQBO winters are presented.

2.3.1 Evolution of the extratropical response

Figure 2.1 shows the lagged composite of geopotential height anomaly at 500 hPa (Z500) in the extratropics from 0 to 2 pentads after the occurrence of the MJO phase 3 for both the EQBO winters (Fig. 2.1a-c) and the WQBO (Fig. 2.1d-f). A Student t-test is used in order to identify the areas where the composite anomaly is different from zero, at the 95% significance level. The composite NAO index is shown in the parenthesis of each panel in Figure 2.1.

Simultaneously with the occurrence of the MJO phase 3, there is a positive anomaly in the North Pacific (Fig. 2.1a and d) which agrees with previous studies (e.g., Lin et al., 2009). Along the west coast of North America in the eastern Pacific, significant negative anomalies appear in both phases of the QBO winters. Downstream to the east, positive and negative Z500 anomalies can be found in north Canada and the North Atlantic, respectively. These anomaly centers form a Rossby wave train from the North Pacific, across North America, to the North Atlantic.

The anomaly pattern intensifies in the North Atlantic sector in the second pentad, both in the WQBO and the EQBO winters, starting to look like a positive NAO (Fig. 2.1b and e). During the lagged 1 pentad in the EQBO winters, the positive anomalies over the Hudson Bay and northern Europe both move southward and intensify, while a negative anomaly develops over the Norwegian Sea which seems to result from a combination of the northward movement of the negative anomalies from both the North Atlantic and north Siberia (Fig. 2.1b). The geopotential height anomalies in the North Atlantic basin during the WQBO winters locally intensify and the two positive anomalies on both sides of the North Atlantic Ocean extend toward the central North Atlantic Ocean (Fig. 2.1e). Compared with the WQBO winters, the positive NAO signal appears weaker during the EQBO winters.

At lag=2 pentads, the signals in the North Pacific fade, but the positive NAO patterns are strengthened (Fig. 2.1c and f). The anomaly amplitude over the Atlantic basin in the EQBO winters (Fig. 2.1c) grows slightly. In the WQBO winters, on the other hand, the negative anomaly deepens and becomes more significant, so does the positive anomaly in the south (Fig. 2.1f). The positive anomalies on the two sides of the North Atlantic Ocean connect with each other covering the middle-latitude North Atlantic and extending into the Mediterranean Sea and North Africa. The pattern is highly similar with the positive NAO and the anomalies become more statistically significant.

For the MJO phase 7, the evolution of the extratropical circulation in the Northern Hemisphere in the EQBO years has some similarity with that of MJO phase 3 (Fig. 2.1a-c), but as expected, with opposite signs (Fig. 2.2a-c). However, although both the distribution of the anomalies and the projection indicate a negative NAO pattern in all 3 pentads, the Z500 anomalies over the Atlantic sector are not statistically significant. During the WQBO winters, the simultaneous composite map remains in a positive NAO pattern with a positive anomaly over the North Atlantic and Northern Europe, and a negative one sets in over Greenland (Fig. 2.2d). At the same time, there is also a negative anomaly over the tropical Atlantic and North Africa. The meridional structure of these three anomalies in the second pentad seems to be moving northward (Fig. 2.2e). The positive anomaly replaces the negative one over Greenland and partially extends into the polar region, while the negative one in the tropics also goes into the mid-latitudes, which initially forms a negative NAO pattern that is not yet very significant. During the third pentad, the west part of the dipole pattern continues moving northward slightly and the negative anomaly extends further west to cover the North Atlantic (Fig. 2.2f). The positive anomaly center locally intensifies and the negative anomaly in the Eastern Atlantic also deepens. The negative NAO forms and the anomaly centers become statistically significant, especially in the high latitudes over Greenland and Northern Europe. Comparing to the lag=2

Z500 anomaly of EQBO (Fig. 2.2c), the lagged teleconnection in the North Atlantic of WQBO is much stronger (Fig. 2.2f).

In summary, for both phases of the QBO, the evolution of the extratropical circulation anomalies over the Atlantic basin after the occurrence of the MJO phase 3 and 7 leads to the development of positive and the negative NAO respectively. This result generally agrees with previous studies (Cassou, 2008; Lin et al., 2009). However, the MJO associated NAO is stronger and more robust and significant during the WQBO winters than the EQBO winters.

In order to see if the result is sensitive to the length of defined season, we repeated the calculation for the DJF season as for the extended winter of NDJFMA. Qualitatively similar results are obtained, although the DJF season has a smaller sample size for the composite analysis and the difference between WQBO and EQBO is slightly less statistically significant for MJO phase 7 (not shown).

Compared with the lagged composites with respect to the OLR-based MJO index (OMI; Kiladis et al. 2014) which is regarded to present the convection feature of the MJO more directly, the similar result can be obtained (not shown). The main distribution of the geopotential height anomaly at 500 hPa are generally consistent with Figure 2.1 and Figure 2.2 but the amplitude is slightly weaker and thus the differences between EQBO and WQBO are also smaller. Hence, although the method of these two indices of the MJO contains different variables to describe the convection of the MJO with various aspects (Wheeler and Hendon, 2004; Kiladis et al., 2014), the results are qualitatively consistent.

2.3.2 SVD analysis

In order to identify the dominant extratropical teleconnection mode associated with tropical convection on the subseasonal time scale, we apply an SVD analysis between tropical

convection and the Northern Hemisphere circulation. Considering the fact that it takes about 10 days for the extratropical response to develop following a tropical forcing (e.g., Jin and Hoskins, 1995), the SVD analysis is performed between the pentad-averaged tropical OLR and the two-pentad lagged Northern Hemisphere Z500 anomaly fields. Such two-pentad lagged association between the extratropical circulation and tropical forcing is especially evident from the composite analysis of Z500 anomaly with respect to MJO phases 3 and 7, as discussed in the last section, as well as reported in previous studies (e.g., Lin et al., 2009). The SVD analysis is conducted separately for the EQBO and WQBO extended winters, with the objective of comparing the leading teleconnection patterns under these two different QBO phases.

Figure 2.3 presents the first mode from the SVD analysis of the covariance matrix of the tropical OLR anomaly and the two-pentad lagged 500-hPa geopotential height anomaly. The first SVD mode of OLR for EQBO (Fig. 2.3c) has a very similar distribution to that for the WQBO winters (Fig. 2.3d), which is characterized by a dipole structure of tropical convection with enhanced and suppressed convection in the Indian Ocean and western Pacific, respectively. This convection pattern is very similar to that of MJO phases 2-3 (Wheeler and Hendon, 2004). Looking at the leading SVD mode for Z500, clearly a positive NAO signal can be seen in the North Atlantic sector for both the WQBO and EQBO winters (Fig. 2.3a and Fig. 2.3b). The correlation reaches 0.73 between Figure 2.1c and Figure 2.3a and 0.72 between Figure 2.1f and Figure 2.3b. Therefore, the leading SVD mode represents an MJO phases 2-3 coupled with a two-pentad lagged teleconnection pattern of a positive NAO. The negative phase of this SVD mode indicates that MJO phases 6-7 are associated with a two-pentad lagged negative NAO. Compared with Figures 2.2 and 2.3, the correlation between Figure 2.2c and Figure 2.3a is -0.35 and -0.60 between Figure 2.2f and Figure 2.3b. This result is quite consistent with the composite analysis as discussed in the last section. The squared covariances explained by the first SVD mode under the two QBO phases are similar. Both the first SVD mode of the two

phases of QBO explain around 26% of the squared covariance and are clearly separated from the remaining modes.

Comparing carefully the OLR pattern of EQBO (Fig. 2.3c) with that of the WQBO winters (Fig. 2.3d), we see that the convection pattern over the Indian Ocean and the low latitude Southern Hemisphere is stronger in EQBO winters. The corresponding geopotential height anomaly pattern that lag the dipole OLR structure by two pentads in EQBO winters (Fig. 2.3a) has a stronger signal in the Northeast Pacific Ocean. This result agrees with Son et al. (2017) who found that stronger MJO convections during EQBO could lead to a stronger teleconnection over the North Pacific. In the North Atlantic sector, however, the Z500 anomaly as well as the NAO signal is stronger in WQBO (Fig 2.3b) than in EQBO (Fig. 2.3a).

Compared with the lagged composite analysis (Figs. 2.1 and 2.2), the SVD results display similar patterns over the North Atlantic basin. During the WQBO years (Fig. 2.3b), the NAO pattern extends to the continents on both two sides of the North Atlantic Ocean and the anomaly center over the south of Greenland is stronger than in the EQBO years, which agrees with the lagged composite analysis (Figs. 2.1f and 2.2f). On the other hand, the meridional dipole structure over the Atlantic basin during the EQBO years (Fig. 2.3a) appears confined to eastern North America and the west North Atlantic.

In summary, the SVD result indicates that the QBO modulates the MJO related teleconnection pattern in the extratropical Northern Hemisphere, especially the MJO-NAO connection. The teleconnection signal in the North Pacific is stronger in EQBO, whereas in the North Atlantic region the NAO teleconnection pattern in WQBO is stronger.

2.4 Possible mechanisms

One of the major mechanisms for the extratropical atmospheric response to tropical forcing is the two-dimensional Rossby wave propagation induced by upper tropospheric divergence of tropical convection (e.g., Karoly and Hoskins 1983). Many previous studies have illustrated the importance of the extratropical zonal westerly flow for Rossby wave propagation (e.g., Hoskins and Ambrizzi, 1993; Garfinkel and Hartmann, 2010; Lin and Brunet, 2018). Hence it is of interest to examine the mean state of the atmosphere in the two phases of the QBO to see if any difference between them could suggest an explanation as to why the MJO-NAO teleconnection differs between the two QBO phases.

The wintertime seasonal mean anomalies of the 500-hPa geopotential height for the two QBO phases are shown in Fig. 2.4. In the North Pacific, positive and negative seasonal mean Z500 anomalies are found in EQBO and WQBO respectively, which is consistent with Garfinkel and Hartmann (2010). Another difference between the two phases of QBO appears in the polar region, i.e., positive seasonal mean Z500 anomaly during EQBO while negative anomalies in WQBO.

The distribution of the DJF-mean zonal wind anomalies at 200 hPa for the two phases of the QBO is presented in Fig. 2.5. The distributions are quite similar including the strengthened (weakened) westerly wind in the subtropical North Pacific during WQBO (EQBO) but just slightly weaker when the temporal coverage is extended to the whole winter as November-April (not shown). Hence here the DJF-mean is presented in order to express the dominant features of the zonal wind field. In the subtropical central-eastern North Pacific Ocean near 30°N, there is a westerly (easterly) anomaly during DJF of the WQBO (EQBO), which is consistent with the Z500 anomaly as shown in Fig. 2.4. This represents a southward (northward)

shift of the westerly jet in the WQBO (EQBO) winters. The subtropical westerlies provide an environment for Rossby wave propagation, and changes in the westerly jet position and strength would lead to changes in the tropical-extratropical teleconnection behavior. Garfinkel and Hartmann (2010) showed that the QBO can modulate the North Pacific low and the jet using model simulations. The numerical experiments describe how the North Pacific responds to changes of the Pacific jet (Garfinkel and Hartmann, 2010). The stronger Pacific jet combined with the extension of the tropical easterly anomalies could lead to a stronger response of the North Pacific low. Through numerical experiments, Lin and Brunet (2018) illustrated that both the extended strong jet and the southward shifted subtropical westerly jet could provide a preferable environment for the stronger extratropical response associated with the MJO. Therefore, the enhanced and southward shifted westerlies in the subtropical North Pacific during WQBO are more favorable than EQBO for Rossby wave propagation and thus tropical-extratropical interactions.

Associated with the development of the extratropical circulation anomalies, the wave activity flux proposed by Takaya and Nakamura (2001), which illustrates a snapshot of the evolution of the wave packets, is calculated. Derived from the conservation of the wave-activity pseudomomentum, the wave activity flux vector's (**W)** horizontal component is defined as:

$$\boldsymbol{W} = \frac{1}{2|\mathbf{U}|}\begin{bmatrix} U(\psi'^2_x - \psi'\psi'_{xx}) + V(\psi'_x\psi'_y - \psi'\psi'_{xy}) \\ U(\psi'_x\psi'_y - \psi'\psi'_{xy}) + V(\psi'^2_y - \psi'\psi'_{yy}) \end{bmatrix},$$

where ψ' is the perturbation of the streamfunction and the subscripts are partial derivatives. **U** = (*U*,*V*) is the winter climatology of the zonal wind and the meridional wind at 200 hPa.

Figure 2.6 shows the wave flux activity calculated based on the lagged composites maps of the streamfunction anomalies at 200 hPa. The distribution of the stramfunction anomalies are generally consistent with the geopotential height anomalies of Fig. 2.1c, 2.1f, and Fig. 2.2c,

2.2f as an equivalent barotropic structure. The wave flux activities over North Atlantic basin with 2-pentad lag of the MJO phase 3 (Fig. 2.6a and 2.6b) also correspond to the seasonal mean of the anomalous zonal wind field at 200 hPa (Fig. 2.5). As Figure 2.5a, the anomalous easterly takes place over almost all the north pole area on the north higher than 60°N, the strong anomalous easterly seems hold back the wave flux from the further northward propagation from North Atlantic (Fig. 2.6a). The anomalous easterly in Figure 2.5b occupies the area covering the Arctic Archipelago and the southern part of Greenland with an anomalous westerly located over Canada and western Atlantic, which tends to be preferable for the wave flux propagating further north to Greenland, Norwegian Sea and North Europe (Fig. 2.6b). The wave flux activities (Fig. 2.6a and 2.6b) explain the more intensified negative pressure anomalies in the southern part of Green land and Norwegian Sea (Fig. 2.1f and Fig. 2.3b). After the occurrence of the MJO phase 7, the distribution of the streamfunction anomalies during the EQBO (Fig. 2.6c) indicates an inapparent NAO pattern with the lack of the positive anomaly over the North Atlantic basin compared with during the WQBO (Fig. 2.6d), which is consistent with the weaker eastward propagation of the wave flux along the west coast of North America (Fig. 2.6c). Compared with the WQBO, where the strongest gradient between the negative streamfunction anomaly center in North Pacific and the positive streamfunction anomaly center in Canada takes place corresponds to the strong and further east wave flux propagation (Fig. 2.6d). Liu et al. (2014) discovered that the stronger MJO-related eastward propagation of the wave flux over North Pacific when the MJO in its phase 7 and 8 in DJF of WQBO years may be connected with the stratospheric events. Besides, the differences of the main distribution of the wave flux activities after the occurrences of the MJO phase 3 and 7 might suggest the asymmetry of the mechanisms as well (Lin and Brunet 2018). Hence, the more detailed underlying mechanisms of how the MJO-NAO teleconnections form under the two phases of the QBO still need more investigations.

The vertical profile of the zonal mean of the zonal wind of each phase of the QBO is shown in Fig. 2.7 separately for the lower stratosphere and troposphere, which represents the seasonal mean anomaly of zonal wind at each level. The main phase of the QBO propagates downward from the stratosphere to the subtropical troposphere with a curved shaped path, which is consistent with the previous studies of the QBO (Crooks and Gray, 2005; Haigh et al., 2005; Pascoe et al., 2005). Figure 2.7 shows that the mean phase of the zonal wind in the tropical stratosphere is opposite to that in the troposphere. However, the main phase of the QBO modulates the mean zonal wind in the subtropics. Thus, a WQBO (EQBO) leads to an enhanced (reduced) westerly wind in the subtropical region near 30°N in the upper troposphere. As indicated in Fig. 2.5, this change in the subtropical westerlies mainly occurs in the North Pacific, where the MJO induced Rossby wave propagates.

In addition to the tropospheric horizontal Rossby wave propagation, the MJO may influence the NAO through a stratospheric pathway. The MJO convection may induce Rossby waves that propagate vertically into the stratosphere or the MJO teleconnection may produce preferential wave patterns that excite planetary-scale waves that in turn propagate into the polar stratosphere to modulate the stratospheric polar vortex (e.g., Garfinkel and Schwartz, 2017; Kang and Tziperman, 2017). The variability of stratosphere polar vortex then propagates downward to influence the tropospheric NAO / AO on a subseasonal time scale (e.g., Baldwin and Dunkerton, 2001). Another interesting feature shown in Fig. 2.7 is the enhanced (reduced) westerly wind in the high latitude upper troposphere in WQBO (EQBO) with its maximum between 100 and 400 hPa. Enhanced westerlies in WQBO winters in the high latitude upper troposphere would be favorable for the vertical propagation of planetary waves into the stratosphere. Previous studies have demonstrated that there is a QBO modulation of the polar night jet and polar vortex (Holton and Tang 1980, 1982). According to the investigation of Holton and Tang (1980), on the surface there is also an NAO signal associated with the QBO.

Further the QBO signal was shown to arrive at the extratropical surface through the Northern Annular Mode (NAM; Thompson and Wallace, 1998, 2000; Jiang et al., 2017) from the stratosphere downward to the troposphere (Coughlin and Tung, 2001). Jiang et al. (2017) also discovered that the MJO-provoked NAO events are significantly different from the non-MJO provoked NAO events in the stratosphere, and the life cycle of the MJO-provoked NAO events can last around 30 days. The study depicts the role of the stratospheric pathway for the MJO-NAO teleconnections. Thus, stratospheric processes and the interactions with the troposphere through the circulation patterns associated with the QBO provide another possible explanation for the QBO modulation of the MJO-NAO teleconnection.

Although previous studies indicate a stronger amplitude of the MJO during EQBO winters than WQBO winters (Son et al., 2017; Hendon and Abhik, 2018), whether or not the amplitude of the MJO would influence its teleconnections over the Atlantic basin remains unclear. Due to the small sample size of the observed WQBO and EQBO winters, the differences of the amplitude of each phase of the MJO are not significant between the two phases of the QBO. Thus, it is unclear if the varying convection patterns of the MJO under the two phases of the QBO could lead to the observed differences of the extratropical circulation anomalies. To further understand the underlying mechanisms of the MJO-NAO teleconnections associated with the MJO properties or the atmospheric circulation modulated by the QBO, a longer record of observational data and numerical experiments with a GCM of well-resolved stratosphere would be needed.

2.5 Conclusion

During the extended winter season from November to April, the extratropical circulation over the Atlantic which forms an NAO-like pattern after the occurrences of certain phases of the MJO is observed in both EQBO and WQBO winters. Under the WQBO, positive NAO patterns in the geopotential height at 500 hPa after the occurrence of the MJO phase 3 and negative NAO after the MJO phase 7 are stronger and more significant than under the EQBO. Here we applied the RMM index for the classification, while with respect to the OMI index the results are also qualitatively consistent. Moreover, the SVD analysis of the OLR and the geopotential height anomaly at 500 hPa with 2-pentad lag reveals different extratropical teleconnection patterns between the EQBO and the WQBO years. The extratropical pattern associated with the tropical dipole convective structure related to the MJO phase 3 and 7 under the WQBO is more confined in the Atlantic basin and more resembles the NAO. On the other hand, under the EQBO, the extratropical responses also contain a strong signal in the North Pacific, and the meridional dipole structure over the Atlantic basin is located in the east coast of North America. The results from the lagged composite analysis and the SVD show that the phases of the QBO modulate the MJO-NAO teleconnection. In an effort to identify the possible mechanisms behind the above results, the basic states for the two phases of the QBO were also compared. For the basic state of the zonal wind field at 200 hPa, the westerly anomaly under the WQBO in the subtropics corresponds to the location of the Asian jet, which is considered to provide a more preferable environment for the propagation of Rossby waves. Besides, the QBO-induced seasonal mean background change also leads the differences of the wave flux activities between the two phases of the QBO to form the teleconnections. Finally, the enhanced westerly zonal wind in WQBO winters in the high latitude upper troposphere would be favorable for the vertical propagation of planetary waves into the stratosphere, which also influences the NAO.

Further investigation of the dynamical interaction between the troposphere and the stratosphere through the observational data with a longer time coverage and numerical simulations may provide more information to better understand the dynamical processes of the QBO modulation of the MJO-NAO connection.

Acknowledgements

We would like to thank Prof. Jacques Derome and Prof. Timothy Merlis in McGill University for the helpful discussions during the process of this work and the useful suggestions to this manuscript. This study was supported by a Discovery Grant of the Natural Sciences and Engineering Research Council of Canada (NSERC). The source of data used in this study are https://www.esrl.noaa.gov/psd/data/gridded/data.ncep.reanalysis.html for the wind field and the geopotential height, https://www.esrl.noaa.gov/psd/data/gridded/data.interp_OLR.html for the outgoing longwave radiation, https://www.esrl.noaa.gov/psd/gcos_wgsp/Timeseries/Data/nino34.long.anom.data for the sea surface temperature, and http://www.bom.gov.au/climate/mjo/graphics/rmm.74toRealtime.txt for the RMM index.

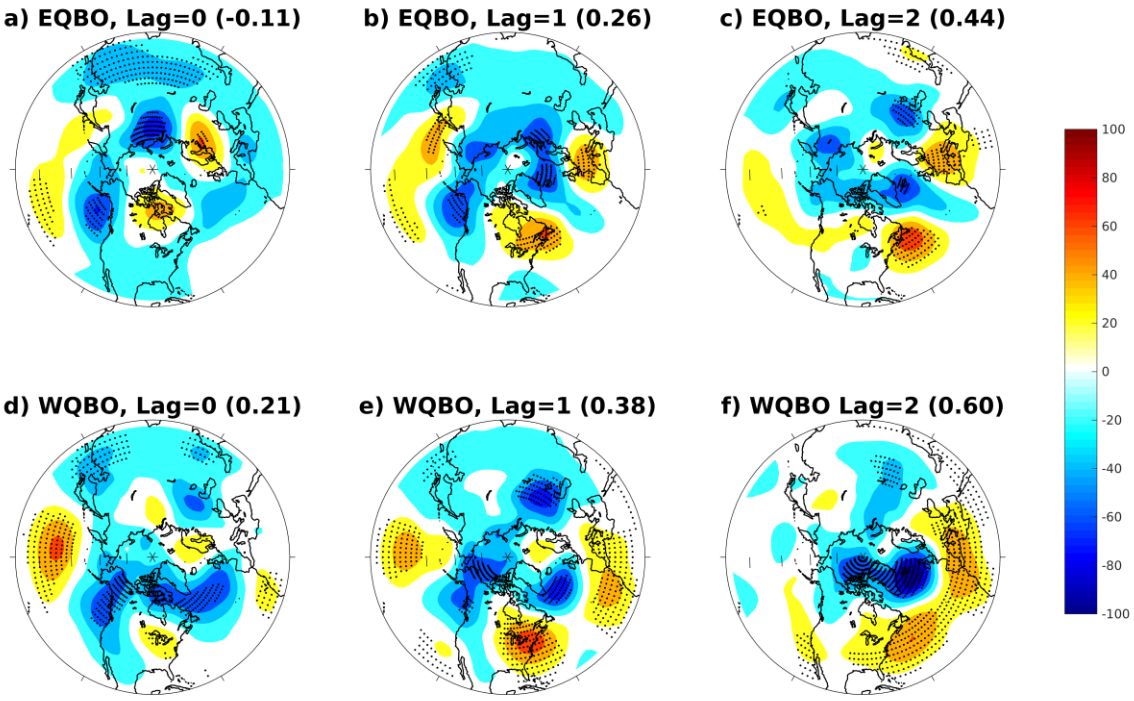

Figure 2.1 Lagged composites of 500-hPa geopotential height anomaly (m) for MJO phase 3 of EQBO events (a)-(c) and WQBO events (d)-(f). Stippled areas mean that the anomaly exceeds 0.05 significance level from zero by using Student-t test. The numbers in parenthesis are the composite NAO index.

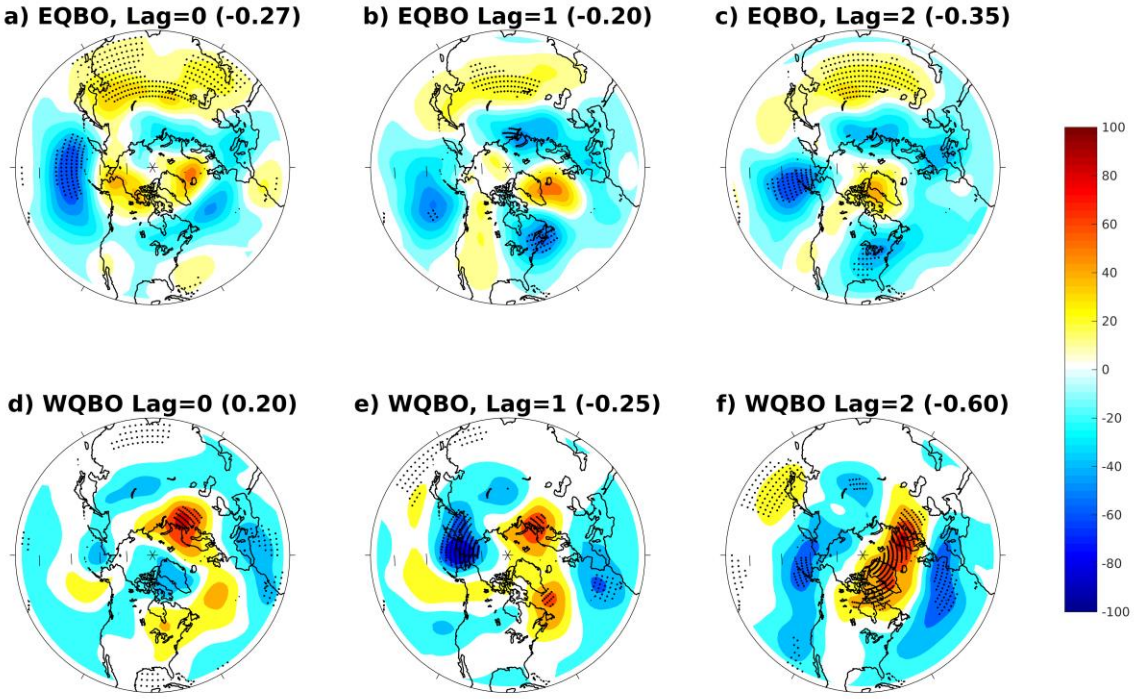

Figure 2.2 The same as Fig. 2.1 but for MJO phase 7.

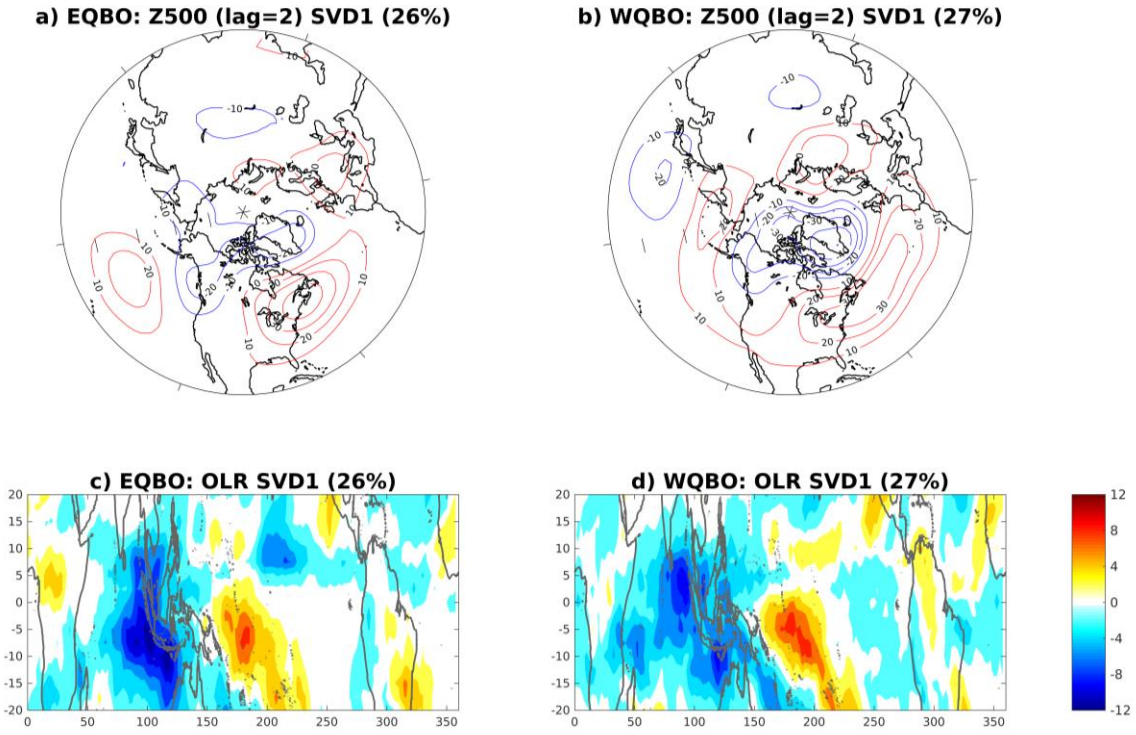

Figure 2.3 SVD1 of OLR ($W \cdot m^{-2}$) and 500-hPa geopotential height (m) with a lag of 2 pentads in EQBO winters (a, c) and WQBO winters (b, d). The anomaly fields are presented as heterogeneous regressions with the amplitude corresponding to one standard deviation of the principal component time series. The squared covariance explained by the SVD mode is shown in the parentheses.

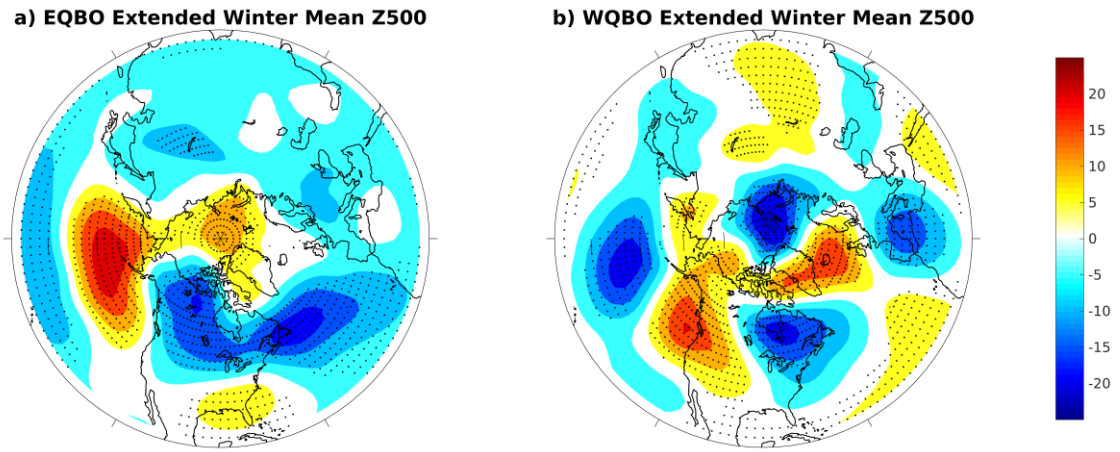

Figure 2.4 The distribution of geopotential height anomaly (m) at 500 hPa in EQBO winters (a) and WQBO winters (b). Stippled areas mean that the anomaly exceeds 0.05 significance level from zero by using student-t test.

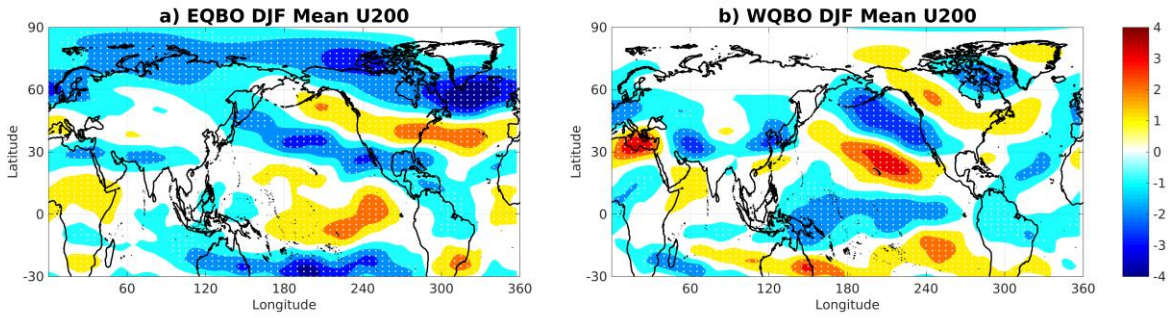

Figure 2.5 The distribution of zonal wind anomaly ($m \cdot s^{-1}$) in EQBO events (a) and WQBO events (b). Stippled areas mean that the anomaly exceeds 0.05 significance level from zero by using student-t test.

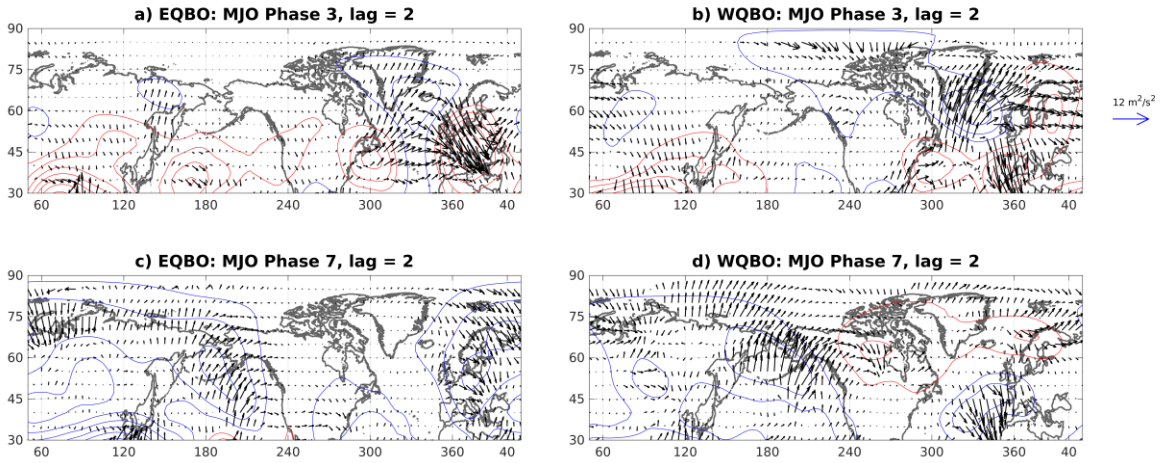

Figure 2.6 The wave activity flux at 200 hPa with respect to the MJO for lag of 2 pentads. The arrows are the W vectors on the x-y plane, and the scaling of the arrows is indicated as the blue one on the right side of (b). The contour lines are the streamfunction anomalies with the interval as $2 \times 10^6\ \mathrm{m^2 s^{-1}}$. The blue contours indicate negative value and the red ones are positive.

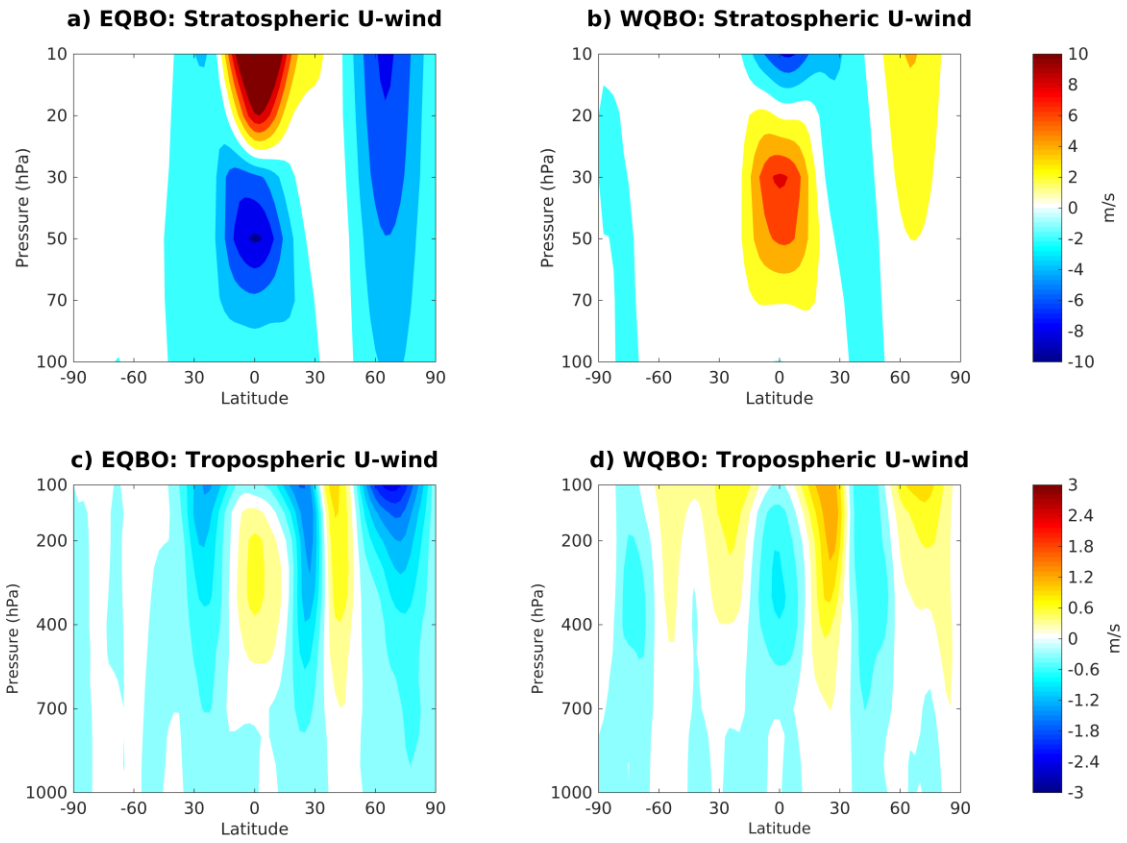

Figure 2.7 The zonal-mean zonal wind anomaly ($\mathrm{m \cdot s^{-1}}$) in stratosphere (a)-(b) and troposphere (c)-(d) in EQBO events and WQBO events. The contour interval is 2 $\mathrm{m \cdot s^{-1}}$ in the stratosphere (a)-(b) and 0.3 $\mathrm{m \cdot s^{-1}}$ in the troposphere (c)-(d).

QBO Phase	Winters (without strong ENSO events)
EQBO	79/80, 81/82, 84/85, 89/90, 96/97, 01/02, 03/04, 05/06, 12/13
WQBO	80/81, 85/86, 87/88, 90/91, 02/03, 04/05, 06/07, 08/09

Table 2.1 November-April identified as easterly phase (EQBO) and westerly phase (WQBO) of the QBO during 1979-2013.

EQBO								
phase	1	2	3	4	5	6	7	8
pentads	19	23	24	32	23	31	28	27
average amplitude	1.80	1.67	1.75	1.69	1.75	1.73	1.74	1.74
WQBO								
phase	1	2	3	4	5	6	7	8
pentads	13	25	23	19	23	24	27	24
average amplitude	1.66	1.77	2.06	1.99	1.62	1.55	1.58	1.84

Table 2.2 The number and the mean amplitude of active MJO events of each phase of MJO in the selected QBO years.

Chapter 3

Forecast Skill of the NAO in the Subseasonal-to-Seasonal Prediction Models

In the previous chapter, the modulation of the Madden-Julian Oscillation (MJO)-related teleconnections by the quasi-biennial oscillation (QBO) was investigated, and significantly stronger positive and negative North Atlantic Oscillation (NAO) after the occurrence of the MJO Phases 3 and 7 during winters of the westerly QBO than easterly QBO was found (Feng and Lin 2019). This chapter assesses the anomaly correlation skill and root-mean square error of the forecast NAO index in the operational models of the WCRP/WWRP Subseasonal-to-Seasonal (S2S) prediction project. In order to understand possible sources of skill, we analyze and compare the NAO forecast skills between forecasts initialized with 1) positive and negative phases of the NAO, forecasts 2) during easterly and westerly phases of the QBO, and 3) different MJO amplitudes and phases.

The manuscript which constitutes this chapter has been submitted to *Journal of Climate* and is in revision.

Abstract

The prediction skill of the North Atlantic Oscillation (NAO) in boreal winter is assessed in the operational models of the WCRP/WWRP Subseasonal-to-Seasonal (S2S) prediction project. Separate skill scores are computed for the two phases of the NAO, the two phases of the quasi-biennial oscillation (QBO), and for different phases of the Madden-Julian Oscillation (MJO). The reforecasts with the initial conditions having the negative phase of the NAO tend to have somewhat more skillful predictions than for the positive phase. Reforecasts made during the two phases of the QBO show no clear difference in skill. Among the eight phases of active MJO as the initial condition, phases 3-5 and phases 7-1 have better NAO forecast skills compared with the other phases and compared to initial conditions without an active MJO.

The S2S models can be divided into the high-top models, with relatively higher stratospheric vertical resolutions, and low-top models, with correspondingly lower stratospheric resolutions. Most high-top models are more sensitive to the selected initial conditions, and the prediction skill of the NAO is better than for the low-top models, though other aspects of the model differences may also be important.

3.1 Introduction

The North Atlantic Oscillation (NAO) is a dominant mode of atmospheric variability in the Northern Hemisphere, a mode with a profound influence on the weather and climate (e.g., Hurrell 1995, Hurrell et al. 2003), especially over Europe and eastern North America. With an equivalent barotropic vertical structure, the dipole pattern in sea level pressure (SLP) forms the NAO pattern that usually reaches its maximum amplitude during the boreal winter (e.g., Wallace and Gutzler 1981; Barnston and Livezey 1987). The positive phase of the NAO reflects a negative pressure anomaly center over southern Greenland and a positive anomaly along the middle-latitude North Atlantic. The negative phase has the same structure but with the opposite sign. The time scale of the NAO ranges from days to decades (e.g., Hurrell 1995). Given the important role of the NAO in shaping extratropical weather, it is of interest to assess the skill of operational models in predicting its evolution on the subseasonal time scale. In the present study, we analyze the NAO forecast skill of models in the World Climate Research Programme (WCRP) / World Weather Research Programme (WWRP) Subseasonal-to-Seasonal (S2S) prediction project. We look at the NAO forecast skill under different initial conditions: the phase of the NAO, the Madden-Julian Oscillation (MJO; Madden and Julian, 1971, 1972) phase and amplitude, and the phase of the quasi-biennial oscillation (QBO).

The MJO is the dominant mode of intraseasonal atmospheric variability in the tropics. The MJO associated convection activity tends to propagate eastward at a speed of about 5 m/s from the Indian Ocean, through the Maritime Continent to the western Pacific with a life cycle of 30-90-days (e.g., Zhang 2005). To describe quantitatively the amplitude and longitudinal location of the MJO convection, Wheeler and Hendon (2004) designed the Real-Time Multivariate MJO Index (RMM Index), an index that categorizes the MJO progression into eight different phases along the equator. Certain phases with an east-west dipole convective

structure in the equatorial Indian Ocean and western Pacific have been shown to lead the occurrences of the NAO (Lin et al. 2009). Phases 2-3 (6-7) of the MJO, reflecting an enhanced (suppressed) convection over the Indian Ocean and a suppressed (enhanced) one in the western Pacific, precede the occurrence of a positive (negative) NAO event by around 15 days (Lin et al. 2009). Because of its global influence, the MJO is regarded as a potential source of predictability on the subseasonal time scale (Lin et al., 2009; Vitart et al. 2017). Although the investigations of the MJO-related extratropical responses were often applied with the RMM index in the previous studies (e.g., Cassou 2008; Lin et al. 2009), the univariate OLR-based MJO index (OMI) derived by the OLR as the only variable is also commonly used to represent the convection feature of the MJO more directly than the RMM index (Kiladis et al. 2014). Thus, in this study the OMI index will be applied in order to determine if the definition of the MJO would lead to the different predictions of the NAO.

The leading mode of interannual variability in the tropical stratosphere is the QBO. The two phases of the QBO alternate over a period of around 28 months and are defined by the zonal-mean zonal wind direction: the easterly QBO (EQBO) and the westerly QBO (WQBO). In both phases, the zonal wind anomaly propagates downward to the tropospheric subtropics as a horseshoe pattern (Baldwin et al. 2001; Feng and Lin 2019). The stratospheric influence on tropospheric weather is a potentially important pathway for longer-than-synoptic timescale predictability. As the main stratospheric feature in the tropics, the QBO has long been investigated for its associations with the global circulations, inclusive of its impact on the tropospheric extratropics. The Holton-Tan effect (Holton and Tan 1980; 1982) refers to the influence of the QBO on the polar night jet and the extratropics. Watson and Gray (2014) reported on the link between the EQBO and a weaker stratospheric polar vortex. This weakened stratospheric polar vortex enhances the negative phase of both the stratospheric and tropospheric Northern Annular Mode (NAM) through a downward propagation (e.g., Baldwin

and Dunkerton 1999; Ruzmaikin et al. 2005). Baldwin and Dunkerton (1999) also discussed how the corresponding stratospheric sudden warming with the corresponding weaker polar vortex would cause the rapid change of the NAM into the negative phase, followed by a relatively slow return to the positive phase. The high correlation between the NAO and the NAM over the Atlantic basin would suggest a link between the QBO and the NAO as well.

The objective of the present study is to assess the NAO prediction skill represented as anomaly correlation between the forecast and observed NAO index and root mean square errors in a number of current S2S models. Previous studies found that in operational models it takes around 10-13 days for the NAO forecast skill, defined as the correlation between the observed and forecast NAO indices, to drop to 0.5 (Johansson 2007; Ferranti et al. 2015). Ferranti et al. (2015) further noted that the NAO forecast skill is flow dependent. In the negative NAO-initiated forecasts, it takes more time for the correlation to decrease to a specific value than in the positive NAO-initiated ones. Although the NAO forecast skill has been investigated in several operational models (Johansson 2007; Ferranti et al. 2015), how skillful the latest S2S models predict the NAO is not yet systematically assessed. Thus, the reforecasts of all the available models in the S2S prediction project (Vitart et al. 2017) are examined in this study.

This chapter is organized as follows. The data from the models and observations and the methods are introduced in section 3.2. The ensemble mean NAO skill over all the available forecasts in the hindcast period of the S2S models is presented in section 3.3. Section 3.4 discusses the skill dependence on the NAO phase and influence of the QBO and MJO. Some remarks on the model ensemble spread are presented in section 3.5. The summary is given in section 3.6.

3.2 Data and Methodology

3.2.1 S2S database

The S2S project, which aims to improve the forecast skill and understanding on the subseasonal to seasonal time scale (Vitart et al. 2017), was launched by WWRP and WCRP. The accessible data provided by the S2S project dataset include the real-time forecast and reforecast data from 11 operational centers. In this study, we use the reforecast data from 11 centers: the Australian Bureau of Meteorology (BoM), the China Meteorological Administration (CMA), the Institute of Atmospheric Science and Climate of the National Research Council (CNR-ISAC), Météo-France/Centre National de Recherches Météorologiques (CNRM), Environment and Climate Change Canada (ECCC), the European Centre for Medium Range Weather Forecasts (ECMWF), the Hydrometeorological Centre of Russia (HMCR), the Japan Meteorological Agency (JMA), Korea Meteorological Administration (KMA), the National Centers for Environmental Prediction (NCEP), and the UK Meteorological Office (UKMO).

Some information on the reforecasts from the S2S models used in the present study is provided in Table 3.1, including the period covered by the reforecasts and the ensemble size. As some centers run the hindcast on the fly for each realtime forecast, the reforecasts analyzed were conducted with a model version corresponding to the real-time forecast for the extended winter season from October 25, 2017 to March 1, 2018 since the NAO, the MJO and the QBO are more active and generally investigated during the boreal winter season. The years covered by each model are listed in Table 3.1. The length of the reforecasts varies from model to model. Although the frequency of the initialization of NCEP is daily, the reforecasts are selected twice a week to have a comparable sample size as other centers. More details on the models can be found in Vitart et al. (2017) and Lim et al. (2019). In order to assess the potential influence of stratosphere, one useful way to categorize the models is to divide them into two groups, those

with a high vertical stratospheric resolution and those with a low stratospheric resolution. Following Lim et al. (2019), the models with high stratospheric resolution with the model top at or higher than 1 hPa are defined as "high-top models": CMA, CNRM, ECMWF, JMA, KMA, NCEP, and UKMO. The low stratospheric resolution models, or "low-top models" are those from BoM, ISAC-CNR, ECCC, and HMCR. When the vertical resolution is also considered, Domeisen et al. (2020) grouped the models into the high-top models inclusive of CNRM, ECMWF, JMA, NCEP, and UKMO, and the low-top models inclusive of BoM, CMA, ISAC-CNR, ECCC, and HMCR.

According to previous studies, the predictability of the NAO from daily to subseasonal time scales could depend on the phase of the NAO itself (Ferranti et al. 2015; Lin 2020). The phases of the NAO are found to be associated with the occurrence of certain phases of the MJO (e.g., Lin et al. 2009) and the NAM that is likely related to the QBO through the stratospheric process (e.g., Baldwin and Dunkerton 1999; Ruzmaikin et al. 2005; Watson and Gray 2014). Thus, the initial conditions are classified into different groups for the comparisons, according to: (a) the phases of the QBO, (b) the phases of the NAO, and (c) the phases and amplitude of the MJO. The numbers of the selected cases are shown in Table 3.2. How the indices representing the different modes of variability are defined, and the threshold used for the case selection are described in the following subsections.

To calculate the forecast anomaly for a given year, the daily climatology is subtracted which is calculated as the mean of all the reforecasts initialized on the same date of all the other years, e.g., in a cross-validation framework. For instance, there are 20 reforecasts started on each January 1st from 1998 to 2017, with a length of 46 days in the ECMWF model. To calculate the forecast anomaly for the reforecast of January 1st, 2017, the daily climatology removed is the average of the 19 reforecasts initialized on January 1st from 1998 to 2016. By this way, the day-to-day variabilities are aimed to be removed. The climatology is lead time

dependent, thus the forecast anomaly for each lead time is obtained by subtracting the respective climatology. The method is applied to the ensemble mean, except when the spread among members is examined in section 3.5, where it is applied to individual ensemble members. Since the dates of reforecast vary from models to models, the observational data introduced in the following subsection is also calculated as the same method with the corresponding dates to each model.

3.2.2 Observations

The reforecasts will be compared to the reanalysis data from the National Centers for Environmental Prediction-National Center for Atmospheric Research (NCEP-NCAR) Reanalysis 1 (Kalnay et al., 1996). The data has a daily temporal resolution covering the period 1979-2017 and a global spatial resolution of 2.5-degree latitude by 2.5-degree longitude. The anomalies are calculated in the same way as for the S2S models. This study is part of the extension of Feng and Lin (2019) and thus the same observational dataset is applied with a prolonged temporal coverage. The investigations with the latest reanalysis data will be applied in the future.

3.2.3 The MJO index

The daily RMM index as the description of the MJO of Wheeler and Hendon (2004) is downloaded from http://www.bom.gov.au/climate/mjo/graphics/rmm.74toRealtime.txt. The RMM index comes from an empirical orthogonal function (EOF) analysis. The meridionally averaged zonal wind at 850 and 200 hPa, and the OLR anomalies between 15°S and 15°N are combined to perform the EOF calculation. RMM1 and RMM2 are the first two principal

components (PC). The amplitude of the MJO is defined as $\sqrt[2]{(RMM1)^2 + (RMM2)^2}$, and an active MJO event is defined when the amplitude exceeds unity.

The OMI Index (Kiladis et al. 2014) that is often applied as the direct description of the convection structure of the MJO is downloaded from https://psl.noaa.gov/mjo/mjoindex/omi.1x.txt. The OMI index is obtained from the first two PCs of the EOF analysis of 20–96-day filtered OLR between 20°S and 20°N. The amplitude of the MJO defined by the OMI index is also $\sqrt[2]{(OMI\ PC1)^2 + (OMI\ PC2)^2}$, and an active MJO event is defined when the amplitude exceeds unity as well. The phases of the MJO defined by the OMI index and the corresponding longitudinal locations are the same as defined by the RMM index of Wheeler and Hendon (2014) mentioned in the previous section.

3.2.4 The NAO index

The NAO index is calculated by projecting the Z500 anomaly onto the NAO spatial pattern defined as the second rotated EOF mode of monthly mean NCEP/NCAR reanalysis Z500 anomalies over the Northern Hemisphere (Figure 1 of Lin et al., 2009). In subsection 3.4.1, the initial condition of a positive NAO is selected with the NAO index larger than 0.5, and the initial condition of a negative NAO is selected with the NAO index smaller than -0.5.

3.2.5 The QBO index

The easterly and westerly phases of the QBO were classified based on the winter average (December to February, DJF) of the zonal wind between 10°S and 10°N at 50hPa of the reanalysis data. The temporal coverage is from 1979 to 2017, the same as other variables in the observations. Following Son et al. (2017), a winter average that is greater (less) than 0.5 (-0.5)

the temporal standard deviation is defined as a WQBO (EQBO) year. During this period, 12 EQBO years and 15 WQBO years are defined according to this method. After the removal of strong ENSO events, defined in the next subsection, 10 EQBO and 10 WQBO years remain.

3.2.6 The ENSO index

The El Niño-Southern Oscillation (ENSO) events are defined by the monthly Nino 3.4 index downloaded from the National Oceanic and Atmospheric Administration (NOAA; https://www.esrl.noaa.gov/psd/gcos_wgsp/Timeseries/Data/nino34.long.anom.data). Strong El Niño (La Nina) years are defined when the DJF mean Nino 3.4 index is greater (less) than 1 (−1) standard deviation.

3.3 The NAO Forecast Skill

The NAO correlation skill is defined as the correlation between the predicted and observed NAO indices for a given (lead) forecast time; the correlation is computed over the available forecasts for a given model. The root mean square error (RMSE) is computed in a similar fashion. For both the correlation and the RMSE, the model ensemble mean is used as the forecast.

Figure 3.1 shows the NAO correlation skill (Fig. 3.1a) and the RMSE (Fig. 3.1b) as a function of lead time obtained by using all the available start dates during the extended winter as clarified in Subsection 3.2.1 from Table 3.1. All the models are seen to have a correlation score above 0.5 for more than 10 days (Fig. 3.1a). The correlation of most high-top models remains above 0.5 for about 15 days or more, while that of the low-top models drops below 0.5

around day 12-14. After day 5, the correlation of most low-top models starts to decrease more quickly than that of the high-top models. After day 20, the correlation of all the models is lower than 0.4, and the differences between the high-top and low-top models are not apparent anymore.

The results for the RMSE, which, contrary to the correlation, includes a measure of the index amplitude error, are shown in Fig 3.1b. Not too surprisingly, the results are consistent with those of Fig 3.1a. In general, the high-top models have a lower RMSE than the low-top models indicating that the high-top models produce better NAO forecasts both in terms of pattern structure (the correlation) and amplitude (RMSE). The RMSE of the low-top models increases more quickly in the first few days, and for most models the errors approach saturation around day 15 with the amplitude less than around 0.2, and in some cases a little earlier.

Figure 3.2 shows the correlation skill of the averaged NAO index of day 11 to day 15 as the center of the boxes. The box/whisker plots provide an estimate of the confidence level in the correlations. The bootstrap resampling procedure is applied here to generate the 10 000 subsamples of the ensemble mean in order to measure the ensemble prediction skill. The top and bottom of the boxes represent the 25th and 75th percentile of the re-distribution from the 10 000 subsamples, and the whiskers are the 5th and 95th percentile. Except for the CMA which might be controversial as a high-top model for its stratospheric resolution (Domeisen et al. 2020), the models fall into two clearly separated groups: the low top models with lower correlations and the high-top models with higher correlations, better forecast skill. It is clear that, as far as predicting the NAO index is concerned, there is added value in having a higher stratospheric resolution.

3.4 Skill Dependence on the NAO Phase and Influence of the QBO and MJO

3.4.1 The skill dependence on the NAO phase

We first compare the NAO forecast skill when the forecasts are initiated with the two different phases of the NAO. The number of reforecasts then available for each model is shown in Table 3.2. Figure 3.3 shows the NAO correlation skill and the RMSE from the reforecasts initiated with the negative and positive NAO events. Overall the negative NAO events lead to a better correlation skill score than the positive NAO events in all the models, but at various degrees, before the correlation drops to 0.5. The NAO skill of the low-top models drops to 0.5 around day 10-12 for both initial conditions. For the high-top models, the NAO skill of forecasts initiated with a negative NAO remains above 0.5 for at least 15 days, while those initiated with a positive NAO drop to the value of 0.5 a little earlier. Thus, in general, for the S2S models, the negative NAO events are a little more predictable – as measured by the anomaly correlation score – than their positive counterparts. This result is in agreement with a previous study (Ferranti et al. 2015). Lin (2020) found that the negative NAOs tend to be more persistent in time than the positive ones, which could explain at least in part the difference in the skill scores seen above.

The RMSE results shown in Fig. 3.3 convey a rather different message. Contrary to the correlation forecast skill discussed above, for most models the forecast skill as measured by the RMSE is better for the positive NAOs than the negative ones, at least starting at about day 10. It would seem then that the amplitude of the negative NAOs is somewhat less predictable

than that of the positive NAOs, a difference that is more noticeable in the low-top than the high-top models.

Figure 3.4 shows the evolution of the composited NAO index corresponding to Fig. 3.3 with the shading area as (the case to case) one standard deviation. It should be remembered in reading this figure that while the indices are normalized by the standard deviations of the observations computed over all dates for which the index is either positive or negative, the subgroup of cases (dates) used for the forecasts can have a standard deviation different from unity. Similarly, as the subgroups of dates differ from model to model, the corresponding observations depicted in the figure can differ among models. First, we see from the figure that the average initial values and standard deviations of the negative NAO cases are generally somewhat larger than those of the positive NAO cases. This may explain, at least in part, why the RMSE of the negative NAO cases were found (Fig. 3.3) to be larger than those of the positive NAO cases.

3.4.2 Skill dependence on the QBO phase

It was found in previous studies that the QBO is correlated to the phases of the NAM (Coughlin and Tung 2001) and that the EQBO tends to coexist with negative NAOs in the troposphere during DJF more than is the case for the WQBO (Boer and Hamilton 2008). We assess here how the NAO forecast skill is modulated by the QBO and whether the high-top models perform better than the low-top models in capturing the QBO influence.

The NAO correlation skill scores for the EQBO and WQBO are presented in Fig. 3.5, in the same format as in Fig 3.3. For neither the correlation nor the RMSE skill score do we see a clear difference in the quality of the forecasts for the EQBO and WQBO periods, even in the high-top models. The HMCR and ISAC-CNR models show better correlation skill scores for

the EQBO than for the WQBO, but the reverse is true for the CNRM model. For the other models, the differences are minute. As for the RMSE scores, no convincing signal is apparent in any model for the first 15 days; after day 15, some differences appear in some models, but by then the correlations are so low that the forecast is unlikely to be useful for either the EQBO or the WQBO.

Lim et al. (2019) evaluated the QBO prediction skill of the S2S models and found that although most models were able to reproduce the alternation of the zonal wind at 50 hPa, the amplitude of the zonal wind in the low-top models was reduced significantly. Unfortunately, the better skill of the high-top models in predicting the QBO does not translate into a better NAO prediction skill as seen in Fig 3.5, as no systematic differences can be seen between the skills of the two classes of models.

3.4.3 Influence of the MJO

A number of studies have appeared on the MJO prediction skill in the S2S models (e.g., Vitart 2017; Lim et al. 2018; Lim et al. 2019). The prediction skill of the MJO was seen to extend to at least 12 days and to more than 25 days in the winter seasons in the S2S models. This opens the possibility that these S2S models may be able to draw on the predictability of the MJO and the known connection of the MJO to NAO (Lin et al., 2009) to show some improved NAO forecast skill when MJO is active. In this subsection, the NAO forecast skill will be examined in those cases when an MJO is present or absent in the initial conditions for each of eight different phases of the MJO.

Figure 3.6 compares the NAO forecast skill when the initial conditions contain inactive and active MJO events, regardless of the phase of the MJO – the possible influence of the phase of the MJO will be discussed later. In most low-top models (Fig. 3.6 I-a to I-d), the NAO

forecast skill of these two initial conditions remains very close up to the time when the correlation drops to 0.5. For these models the correlation skill score falls to 0.5 at about day 13 - 15 for both types of initial conditions. The high-top models, although in general have better correlation skill scores than the low-top models in a somewhat extended period (about two days) during which the correlation remains above 0.5, represent only slight differences of the correlation skill between the two initial conditions as the low-top models.

The RMSE scores shown in the lower part of Fig 3.6, shows negligible differences in the scores for the two types on initial conditions, indicating that predicting the amplitude (as opposed to the structure) of the NAO is not made easier by the presence of the MJO in the initial conditions, at least in the S2S models analyzed here, when the phase of the MJO is not taken into account.

When the OMI index which is more directly related to the representation of the convection features of the MJO is applied in Fig. 3.7, the correlation skill of all the models show very little difference before day 11-12 when the correlation drops to about 0.5. Afterwards, the difference of the prediction skill of the NAO becomes apparent in most models. The correlation skill does not seem sensitive to the existence of the MJO defined by RMM or OMI before the correlations drops to 0.5, the RMSE scores either.

In the observations, the MJO-associated NAO can be triggered by the wave activity through the stratosphere and have a longer persistence around 30 days than about 10 days of the NAO event without a preceding MJO event (Jiang et al. 2017). The investigation of Jiang et al. (2017) was applied with the RMM index, and the correlation skills applied with both the RMM (Fig. 3.6) and the OMI (Fig. 3.7) in many models represent the difference after day 10. The difference between the correlation skills of the existence of the MJO is larger when the OMI index is applied than the RMM index. As discussed by Kiladis et al. (2014), the representation of circulation defined by the RMM index includes the wind fields impacted by

both the tropics and extratropics and thus leads to the corresponding circulation patterns different from the OMI index. Hence, the existence of the MJO convection might possibly influence the prediction skills of the NAO after around 10 days when the OMI index that purely takes the OLR into consideration is applied.

Lin et al. (2009) have shown that the MJO is associated with the occurrence of the NAO after about two weeks, particularly when the MJO is in phase 3 (corresponding to enhanced convection over the Indian Ocean and reduced convection over the western tropical Pacific) and phase 7 (reversed convective anomalies). We now examine whether the S2S models are able to respond differently to MJO occurrences according to the location of the implied convection, i.e., according to the phase of the MJO. To that end, the active MJO events were classified according to the eight phases defined by Wheeler and Hendon (2004). Initiated with each phase of the MJO life cycle, the NAO correlation forecast skill is presented in Fig. 3.8 as a function of phase and lead time when the phase of the MJO is not taken into account. We see that in agreement with Fig. 3.6, the high-top models generally have relatively better skill. In most low-top models, the correlation falls to 0.5 by about day 15, while it lasts a little longer in the high-top models. For each model, the NAO skill also varies from phase to phase of the MJO as the initial condition. The differences in the correlation from phase to phase of the MJO in the low-top models are somewhat smaller than those of the high-top models.

For almost all models, the NAO correlation skill is higher when initialized with MJO phase 7 (Fig. 3.8), which, as mentioned earlier, corresponds to enhanced convection in the equatorial western Pacific and suppressed convection in the tropical Indian Ocean. MJO phases 3-4 also lead to relatively higher NAO skill for some models.

When the OMI index is applied for the MJO definition, the NAO correlation forecast skill as a function of phase and lead time is presented as Figure 3.9. Most models show the better skill of about 15-20 days from MJO phase 3 to phase 5, and the MJO phase 7 than other phases

(Fig. 3.9). Compared with Figure 3.8 where the forecast skill initiated with the MJO phase 7 that could reach 15 days and more before the correlation drops to 0.5 in most models, the forecast skill initiated with the MJO phase 7 lasts less than 15 days in most models before the correlation drops to 0.5, and only about 10 days in some models (Fig. 3.9) when the OMI index is used. Contrast to the MJO phase 7, the forecast skill initiated with the MJO phase 2 to phase 5 defined by the OMI index increases in most models when compared with the RMM index (Fig. 3.8). Although the MJO phase-initiated forecast skills differ from the definitions of RMM and OMI, the results from the S2S models are in general consistent with the observational MJO-NAO teleconnections of Lin et al. (2009) and the simulation of extratropical responses for the tropical heating (Lin et al. 2010).

3.5 Some remarks on the model ensembles spread

So far we have concentrated on the model ensemble means in determining the models' forecast skill. In this section, we use the "perfect model approach", an approach that will reveal some relevant information on the spread of the ensembles in the 11 models. So here, for each model, we consider any one member as a reference ("the truth") and compute the correlation skill score of the ensemble-mean of the remaining members when compared to the reference member. As is standard with this approach, we repeat the calculations, each time treating a different member as the reference. If the ensemble spread of a given model is similar to that of nature (natural variability), the observations would typically fall within the ensemble spread, and the forecast skill score of the perfect model approach would be similar (the same, except for sampling errors) to the one using the observations as the reference. If, on the other hand the spread of a model is smaller than that of natural variability, some observations would fall

outside the model spread, and the skill score of the perfect model approach can be expected to be better than that using observations as the reference. Finally, if the spread of a model is larger than that of natural variability, the observations would fall within the ensemble spread but the model member distribution would contain too many "outliers", and the perfect model scores can be expected to be worse than those using observations. The results of this section are based on all available forecasts listed as Table 3.2.

Figure 3.10 compares the correlation skill scores for the perfect model approach and the one using observations as the reference. The correlations of the ensemble members taken as the reference member with the ensemble mean of the remaining members are plotted for the spread. For most models, the perfect model scores are higher than those using observations, indicating ensemble spreads that are too small. Three models (ECCC, ECMWF, and JMA) have spreads that reproduce nature well.

3.6 Summary and conclusion

In this study the skill of the S2S models at predicting the NAO was investigated, in particular when the initial conditions included the two phases of the NAO, of the QBO, and the amplitude and eight phases of the MJO. The overall NAO correlation skill of all the selected available reforecasts indicates the current S2S models are able to represent the NAO with a correlation higher than 0.5 for about 10 days. Models characterized as "high-top models", with a relatively higher stratospheric resolution when compared to the other models, were found to maintain a correlation forecast skill above 0.5 a few days longer than the "low-top models". Consistent with the correlation skill, the RMSE of the high-top models was also seen to grow more slowly than that of the low-top models. Thus we conclude that for the prediction of the

NAO on a two-week time scale there is added value in using a model with relatively higher stratospheric resolution.

The analysis aimed at comparing the skill of forecasts done with positive NAO and negative NAOs yielded mixed results. When the forecast skill is measured by the correlation between the observed and predicted NAO indices, the negative NAOs were found to be better predicted, but the opposite was seen when the RMSE between the two indices is used. It would thus appear that the structure of the negative NAOs are better predicted than that of their positive counterparts, but the amplitude of the positive NAOs is better predicted. The difference of the NAO correlation skill between the two phases of the NAO is more apparent in the high-top models than the low-top models but not for the RMSE. The fact that the forecast RMSE of the negative NAO cases were found to be larger than those of the positive NAOs may be the reflection of the fact that the initial variance among the positive NAO cases is larger – a larger variance involving more cases with larger amplitudes and correspondingly higher chances of larger forecast errors.

When the potential influence of the phase of the QBO on the quality of the NAO forecasts was examined, no convincing evidence was found, both phases yielding similar skill scores. Even the high-top models showed no appreciable difference in skill scores between the two QBO phases. Thus the QBO influence on the NAO seen in observations (e.g., Coughlin and Tung 2001) was not captured by the S2S models in the present analysis. Similarly, the better simulation of the QBO amplitude by the high-top models than the low-top models reported by Lim et al. (2018) did not translate into better NAO forecasts by the former models.

A comparison of forecasts performed in the presence or absence of an MJO event in the initial conditions, regardless of its position, revealed close forecast correlation skill scores when the RMM index is applied. For the OMI-defined MJO events, the correlation skill with an inactive MJO as the initial condition drops much quicker than active MJO after about 10

days in most models, which agrees with the temporal length of the NAO without a preceding MJO event (Jiang et al. 2016). The difference in correlation skill scores is in general not apparent in the two groups of the S2S model regardless of the index. When it comes to comparing the forecast skill in the MJO present versus absent cases using the RSME score, the difference is not noticeable either, both sets of initial conditions leading to similar growths of the errors and no difference is seen between the high-top and low-top models.

An examination of the correlation skill scores as a function of the phase of the MJO showed that the S2S models are able to take advantage of the observed link between the NAO and the MJO in phases 3-4 or 7 in both cases with the RMM and OMI index applied. Indeed, the forecast correlation skill scores are best when the initial conditions contain an MJO in one of these two phases.

A short analysis based on the perfect model approach revealed that, with a few notable exceptions, the models tend to have smaller ensemble spreads than would be expected from natural variability. This is likely to lead to their having larger RMSE scores than if their spread better simulated nature's natural variability.

Finally, we note that there are differences beyond stratospheric resolution among the high-top and low-top models. Further analysis of the impact of other aspects of model formulation on NAO forecast skill, and its sensitivity to the initial atmospheric state, is warranted.

Acknowledgements

This research was made possible by an Natural Sciences and Engineering Research Council of Canada (NSERC) Discovery Grant to the second author.

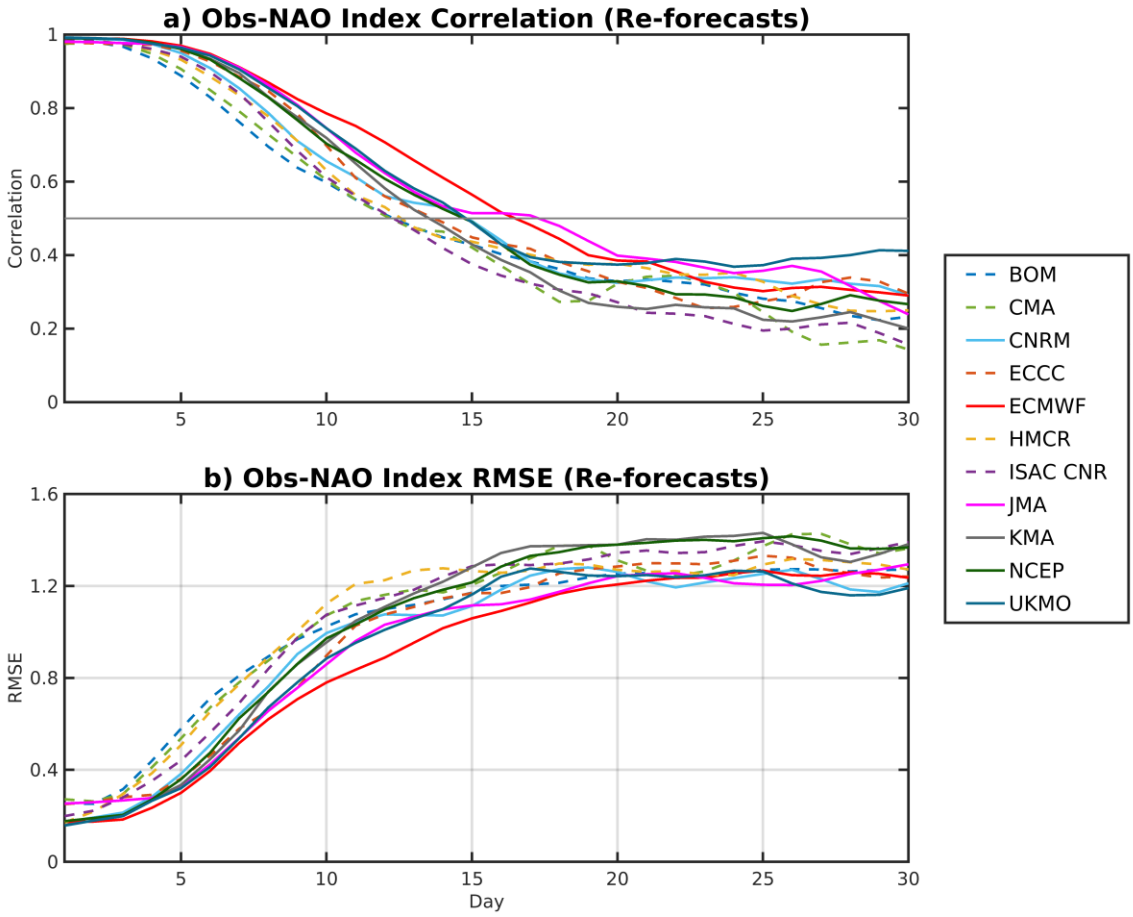

Figure 3.1 The correlation (a) and (b) RMSE between the model ensemble mean and observations as a function of lead time for the 10 S2S models. Low-top models are presented as dash lines, and the high-top models are presented as solid lines.

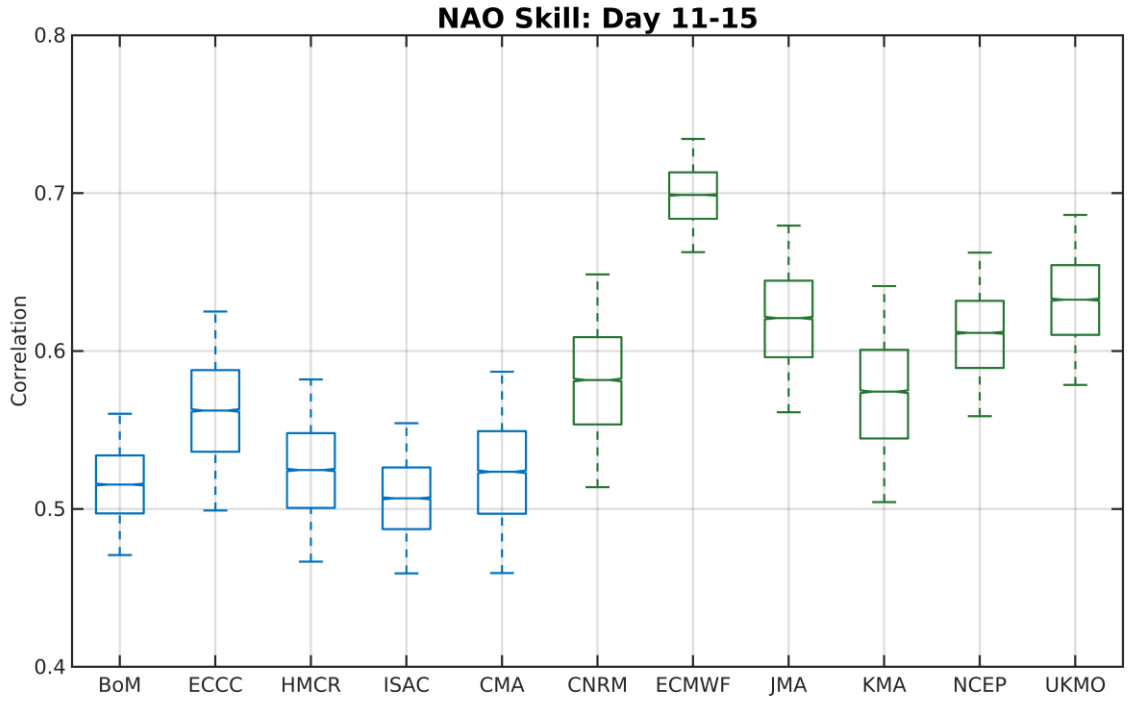

Figure 3.2 The correlation of the 10th-15th day average between the model ensemble means and observations as the median of the box and the whisker plot. The two sides of the box represent the 25th and 75th percentile of the distribution computed from a 10 000 bootstrap resampling procedure. The whiskers extend to the 5th and 95th percentile of the bootstrapped distribution.

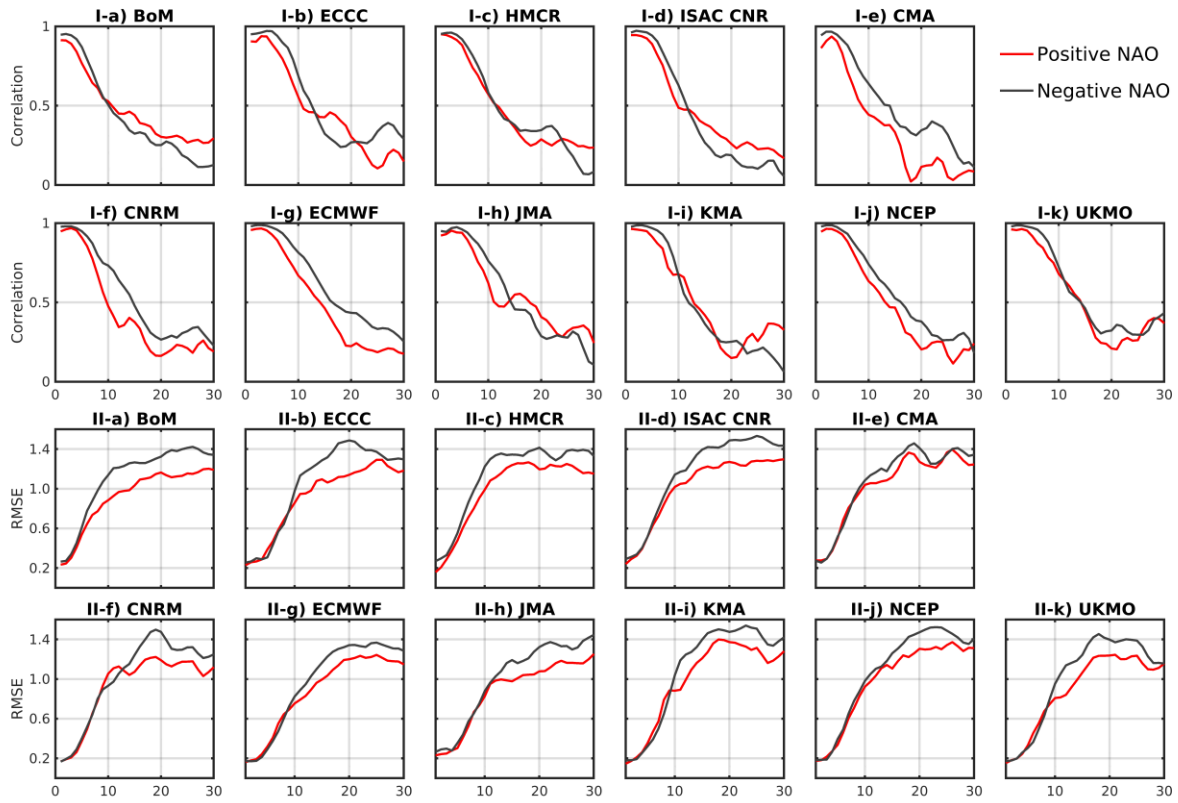

Figure 3.3 The correlation as the group I and root mean square error (RMSE) as group II between the model ensemble mean and observations as a function of lead time for the 11 S2S models with the initial condition under the two phases of NAO. Low-top models are represented as (a) – (d) and high-top models are (e) – (k) in alphabetical order.

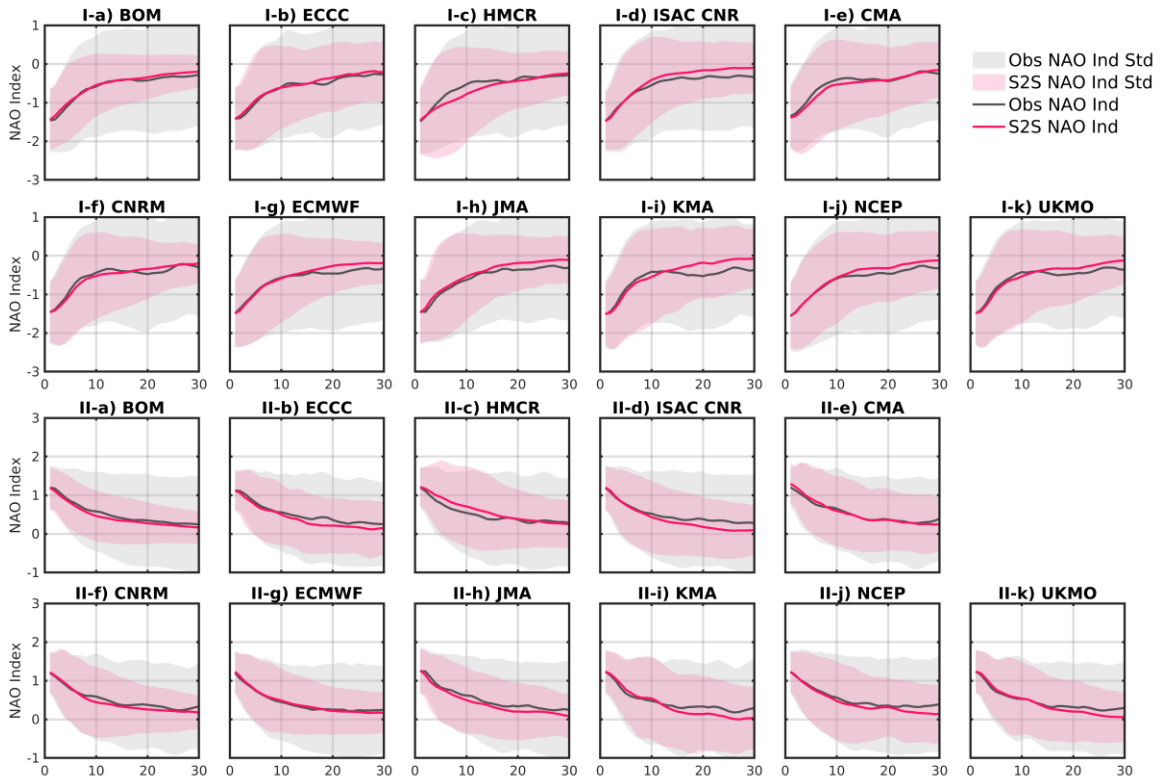

Figure 3.4 The composited negative NAO index as the group I and composited positive NAO index as group II between the model ensemble mean and observations as a function of lead time for the 11 S2S models. The shading area indicates 1 standard deviation. Low-top models are represented as (a) – (d) and high-top models are (e) – (k) in alphabetical order.

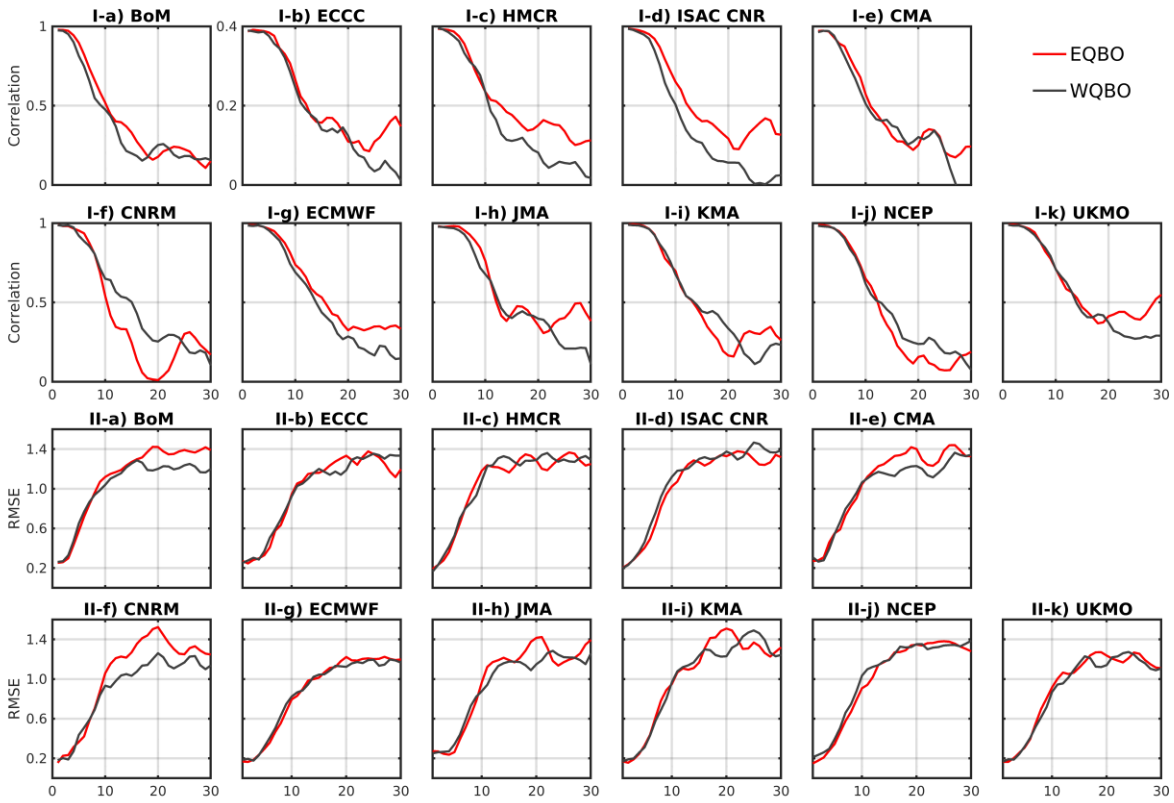

Figure 3.5 As Figure 3.3, but for the initial condition under the two phases of QBO.

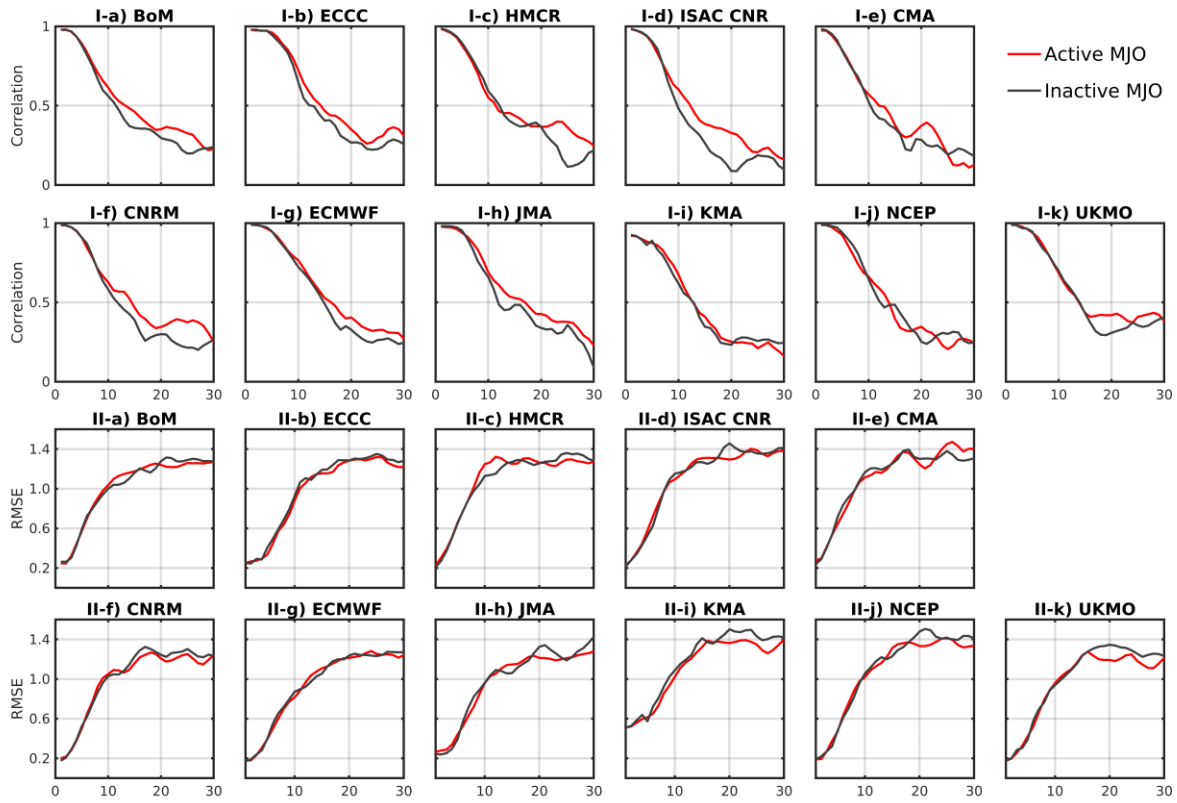

Figure 3.6 As Figure 3.3, but for the initial condition with active and inactive MJO events defined by RMM index.

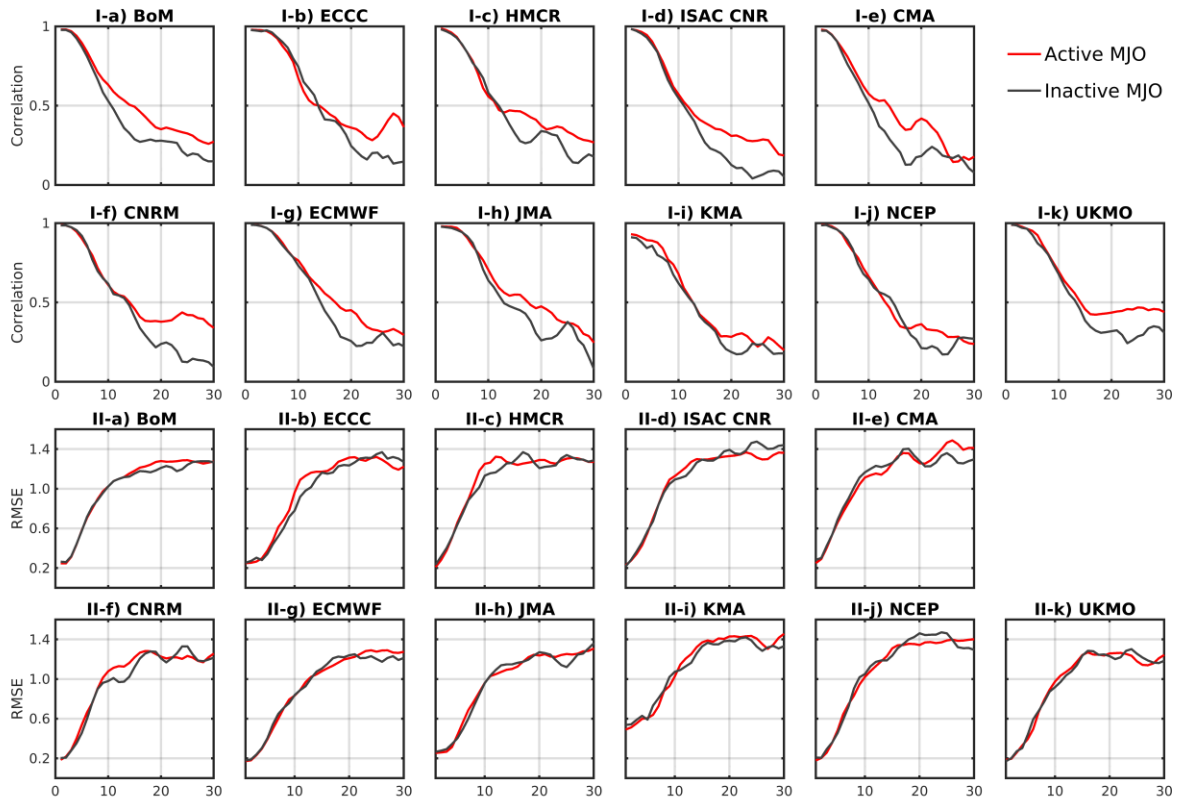

Figure 3.7. As Figure 3.3, but for the initial condition with active and inactive MJO events defined by OMI index.

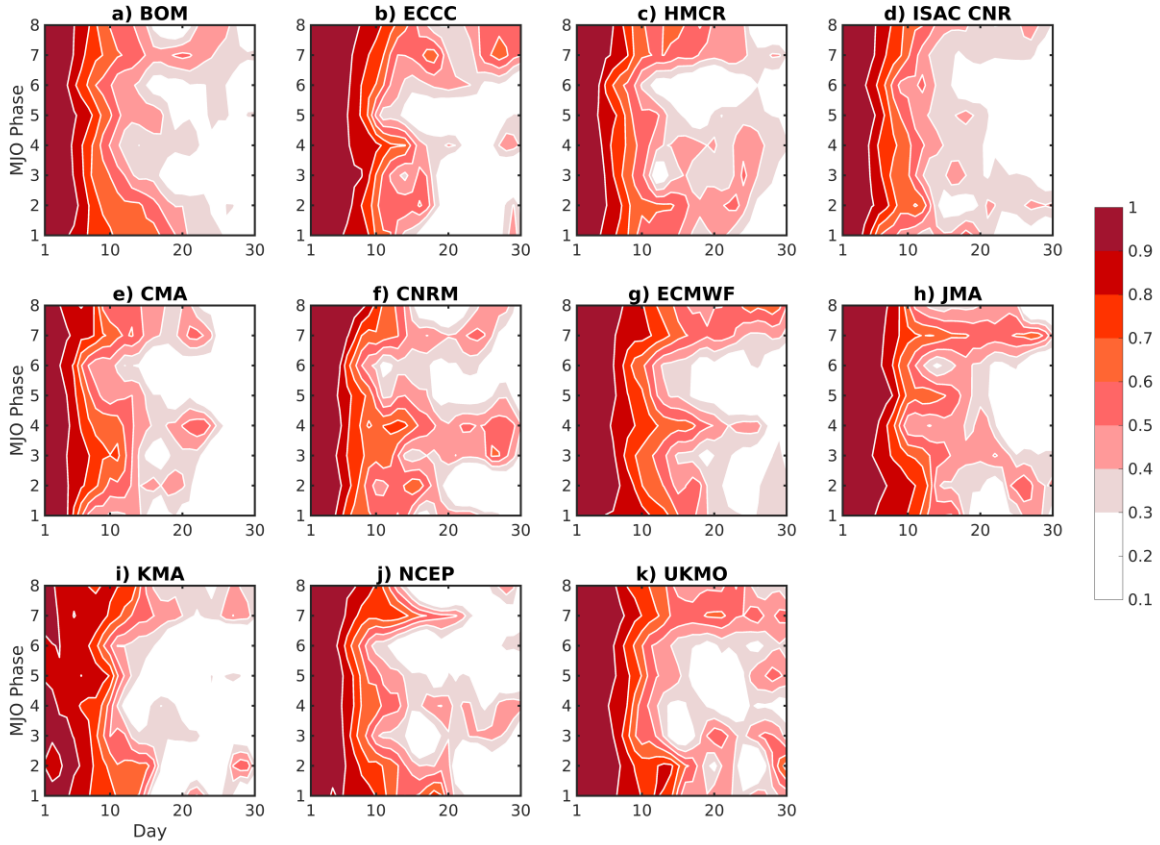

Figure 3.8 NAO skill as function of initial MJO phase defined by RMM index as y axis and lead time as x axis.

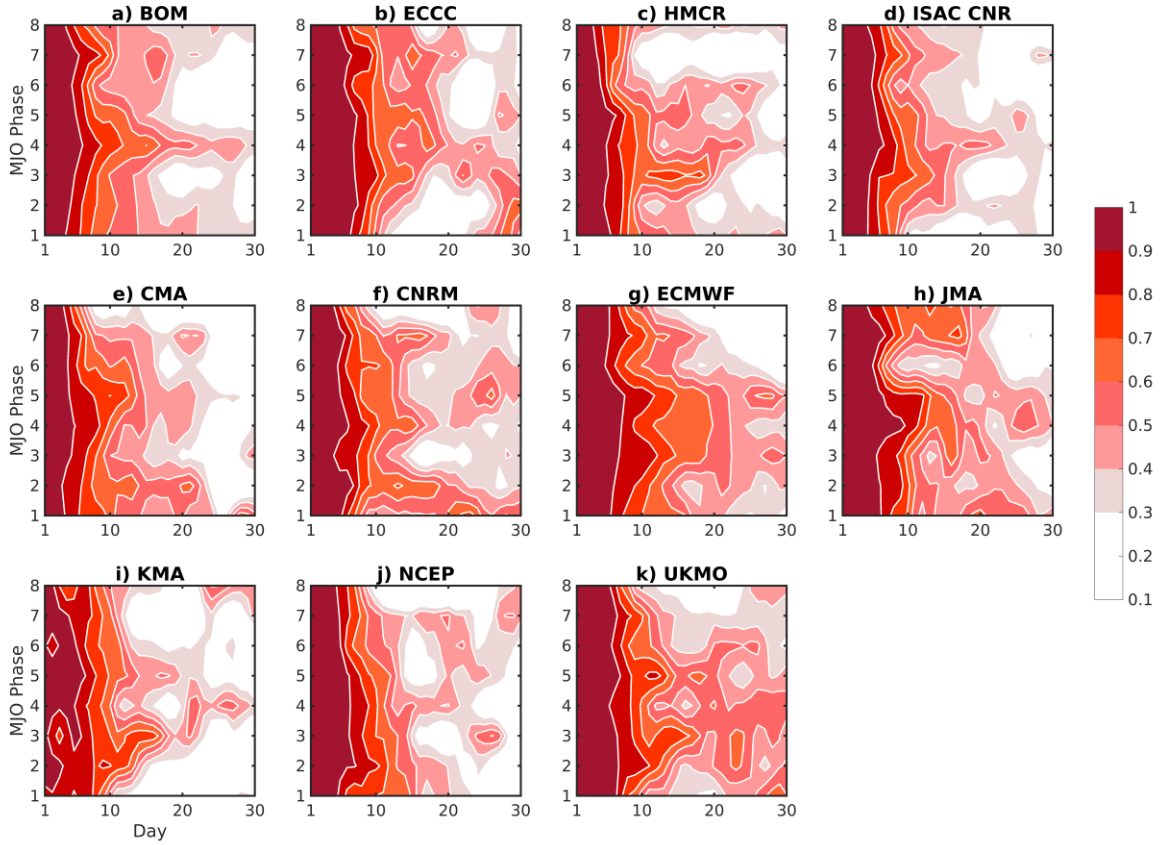

Figure 3.9. NAO skill as function of initial MJO phase defined by OMI index as y axis and lead time as x axis.

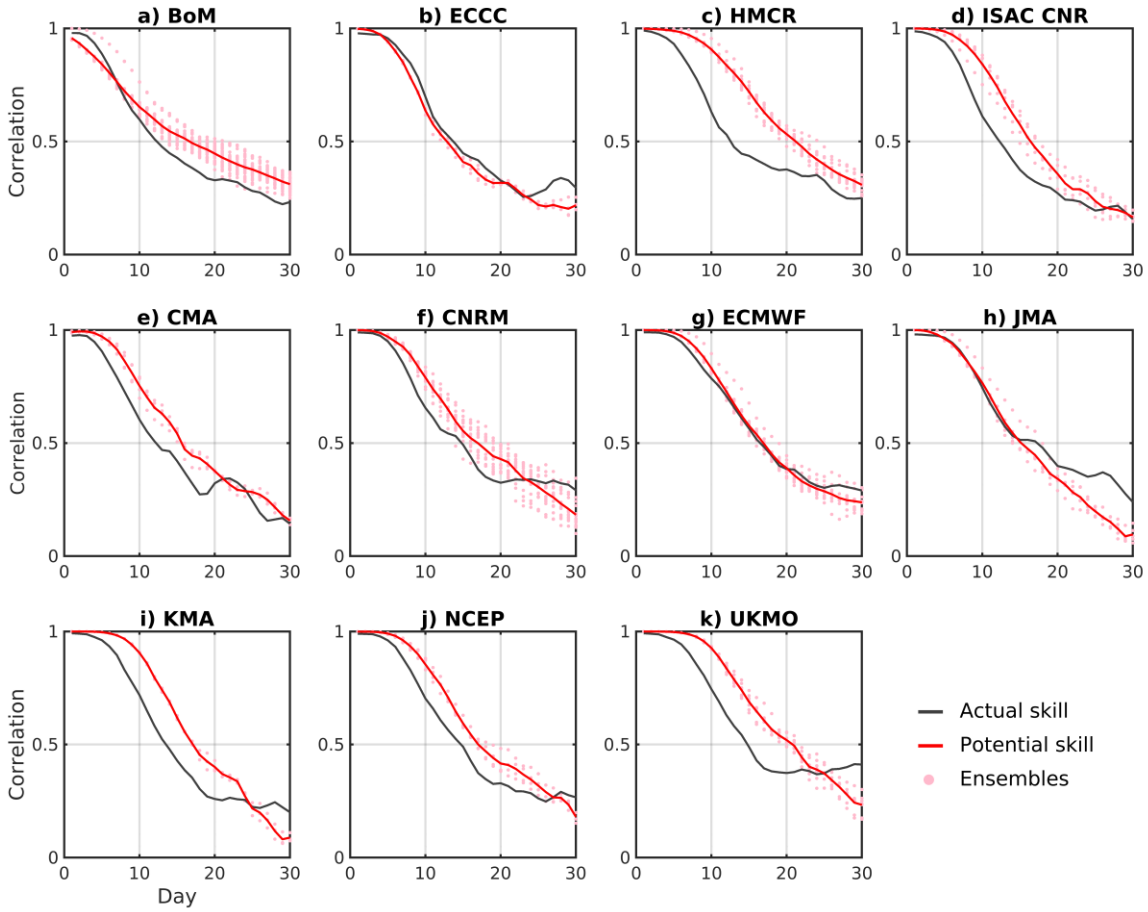

Figure 3.10 Actual (black curves) and an estimate of potential (red curves) skill for the S2S models. The dots indicate the correlations of the ensemble members taken as the reference member with the ensemble mean of the remaining members.

Model name	Reforecast period	Model frequency	Model resolution (Model top)	Ensemble size
BoM	1981-2013	6 times/month	T47 L17 (10 hPa)	33
CMA	1994-2014	Twice/week	T16 L40 (0.5 hPa)	4
ECCC	1995-2014	Weekly	0.45ºx0.45º L40 (2 hPa)	4
ECMWF	1997-2017	Twice/week	Tco639/ Tco319 L91 (0.01 hPa)	11
HMCR	1985-2010	Weekly	1.1ºx1.4º L28 (5 hPa)	10
ISAC-CNR	1981-2010	Every 5 days	0.8ºx0.56º L54 (roughly 6.8 hPa)	5
JMA	1981-2012	3 times/month	TL479/TL319 L100 (0.01 hPa)	5
KMA	1991-2010	4 times/month	0.83ºx0.56º L85 (85 km)	3
CNRM	1993-2014	4 times/month	TL255 L91 (0.01 hPa)	15
NCEP	1999-2010	Daily	T126 L64 (0.02 hPa)	4
UKMO	1993-2015	4 times/month	0.83ºx0.56º L85 (85 km)	7

Table 3.1 Description of the S2S models and the temporal coverage of the reforecasts taken in this study. The horizontal resolution of ECMWF is switched from Tco639 to Tco319 after the 15th day of the reforecast, and the horizontal resolution of JMA is switched from TL479 to TL319 after the 18th day of the reforecast.

	Total sample size	Positive NAO	Negative NAO	EQBO	WQBO	active MJO	inactive MJO
BoM	825	312	260	200	175	530/505	295/320
CMA	420	158	126	100	100	264/259	156/161
ECCC	360	140	113	90	90	234/222	126/138
ECMWF	700	254	210	175	210	458/417	242/283
HMCR	468	185	149	90	126	311/296	157/172
ISAC-CNR	720	270	219	168	168	467/448	253/272
JMA	384	145	128	84	84	261/237	123/147
KMA	340	129	109	68	68	223/206	117/134
Météo France (CNRM)	374	136	111	85	85	244/234	130/140
NCEP	432	157	126	108	144	277/276	155/156
UKMO	391	144	119	102	85	257/233	134/158

Table 3.2 The sample size of the selected initial conditions (RMM/OMI).

Chapter 4

Modulation of the MJO-Related Teleconnection by the QBO in Subseasonal-to-Seasonal Prediction Models

In Chapter 2, we investigated the modulation of the Madden-Julian Oscillation (MJO)-related teleconnection by the quasi-biennial oscillation (QBO) in observations. Then in Chapter 3, the MJO and QBO are taken as the possible sources of the NAO prediction skill and analyzed individually in Subseasonal-to-Seasonal (S2S) prediction project reforecasts. This chapter extends the analysis of the dataset of the WCRP/WWRP Subseasonal-to-Seasonal (S2S) prediction project. The objective is to assess the ability of the state-of the-art operational S2S models in capturing the QBO modulation of the MJO-related teleconnection.

This chapter is in preparation for submission to *Atmosphere-Ocean*.

Abstract

It was found in previous observational studies that the quasi-biennial oscillation (QBO) can modulate the Madden-Julian Oscillation (MJO)-related teleconnection over the Atlantic basin. In this study, we assess the modulation of the MJO-related teleconnection by the QBO in the operational models that participated in the subseasonal-to-seasonal prediction (S2S) project of World Climate Research Programme (WCRP) / World Weather Research Programme (WWRP). The enhancement of the positive NAO after the occurrence of the MJO phase 3, which corresponds to enhanced convection in the equatorial Indian Ocean and reduced convection in the tropical western Pacific, under the WQBO conditions is seen to be captured by most S2S models but, not unexpectedly, at different degrees of both the amplitude of the NAO pattern and index. In contrast, the enhancement of the NAO after the occurrence of the MJO phase 7, which has opposite signs of tropical convection anomalies as phase 3, under the WQBO conditions is not reproduced in most S2S models. Under the EQBO conditions, however, some S2S models can reproduce a significant negative NAO after the occurrence of the MJO phase 7, but not a positive NAO after the occurrence of the MJO phase 3. The results indicate that although the S2S models are able to predict a reasonable MJO up to around three weeks, representing the QBO impact on the extratropical teleconnection of the MJO remains challenging.

4.1 Introduction

The Madden-Julian Oscillation, the dominant mode of tropical atmospheric variability on the intraseasonal time scale, is a planetary-scale eastward propagating disturbance along the equatorial region (Madden and Julian 1971; 1972). From its onset in the western Indian Ocean, the MJO convection moves to the Maritime Continent at a speed of about 5 m/s and propagates faster across the rest of the equator with a period of approximately 30-90 days (e.g., Zhang 2005). Several theories have been proposed to explain the MJO. For example, four theories are summarized in Zhang et al. (2020). Based on its convective structure, Wheeler and Hendon (2004) designed the Real-Time Multivariate MJO Index (RMM Index) to describe the amplitude of the MJO and categorize its position along the equator into eight phases. The onset in the Indian Ocean is defined as phases 1 and 8. Phases 2 and 3 describe enhanced convection in the western Indian Ocean and suppressed convection in the western Pacific. When the convection is over the Maritime Continent, it is phases 4 and 5. Phases 6 and 7 have the same structure as phases 2 and 3 but with opposed signs.

The MJO has a global impact through teleconnections (e.g., Stan et al. 2017). A wide range of extratropical weather events are influenced by the MJO (e.g., Bond and Vecchi, 2003; Jones et al. 2004; Donald et al. 2006; Lin et al. 2009; Alvarez et al., 2016). Subseasonal variability of some major modes of variability have also been observed to be connected to the MJO, including the Pacific – North American pattern (PNA; e.g., Mori and Watanabe 2008) and the North Atlantic Oscillation (NAO; e.g., Lin et al. 2009). The NAO is a meridional dipole pattern in sea level pressure with an equivalent barotropic vertical structure over the North Atlantic basin and is known to be a prominent mode of climate variability in the Northern Hemisphere atmosphere (Wallace and Gutzler, 1981; Barnston and Livezey 1987; Hurell, 1995). The spatial structure of the NAO in the positive phase is composed of an anomalous

low pressure centred south of Greenland and a belt of anomalous high pressure to the south, across Eastern North America, the middle latitude North Atlantic Ocean and Europe. The negative phase of the NAO shares the same spatial structure as the positive NAO but with opposite signs. This seesaw pattern usually reaches a maximum amplitude during boreal winters. The time scale of the NAO spans a wide range, from the weekly to the interannual scales. Given its spatial and temporal extent, the NAO variability profoundly influences the weather and climate in the Northern Hemisphere, especially in northeastern North America and Europe (e.g., Hurrell, 1995, Hurrell et al. 2003). Lin et al. (2009) showed that the NAO has a preferred polarity after the occurrence of certain phases of the MJO. Among the eight phases of the MJO, phases 3 and 7 were found to be followed by a positive and negative NAO, respectively (Lin et al. 2009). A similar result was reported in Cassou (2008). The extratropical atmospheric response to the MJO was simulated in several numerical model experiments in which a tropical diabatic forcing associated with the MJO was specified (e.g., Lin et al. 2010, Seo and Son 2012). How the extratropical fluctuation of the geopotential height is induced by the dipole structure of the MJO convection was further illustrated in Lin and Brunet (2018). The MJO-NAO teleconnection usually takes around ten days to develop and reaches the maximum amplitude around 15 days. Thus, with this time scale, the MJO can be regarded as a potential source of predictability for the NAO on the subseasonal-to-seasonal (S2S) time scale.

The Quasi-biennial oscillation (QBO), the leading mode of the interannual variability in the tropical stratosphere, takes the form of a reversal of the mean-zonal wind direction, with a period of about 28 months. The wind direction reversal is observed to propagate downward to the tropospheric subtropics with a horseshoe pattern (e.g., Baldwin et al. 2001). The two phases (or wind directions) of the QBO are termed the easterly QBO (EQBO) and westerly QBO (WQBO). The possible associations of QBO with the extratropical atmospheric circulation has long been of interest. Holton and Tan (1980, 1982) showed that the QBO impacts the polar

vortex through the subtropical wind fields, a process now called the Holton Tang effect. Then, the QBO associations with the Northern Annual Mode (NAM) or the Arctic Oscillation (AO) was further investigated (e.g., Coughlin and Tung, 2001; Ruzmaikin et al. 2005; Marshall and Scaife, 2009). These studies clarified the underlying mechanisms of the modulation of the QBO on the extratropics and the polar region through the planetary wave activities (Ruzmaikin et al. 2005; Chen and Li, 2007; Garfinkel et al. 2012).

Recently, the QBO was found to modulate the MJO in the boreal winters, even more strongly than the El Niño-Southern Oscillation (ENSO; Yoo and Son 2016; Son et al. 2017). During the EQBO winters, the MJO generally occurs with greater amplitude, longer duration and with a farther eastward propagation than during WQBO winters (Son et al. 2017). Over the extratropical North Pacific, these authors also found a stronger MJO-associated teleconnection in the EQBO winters than the WQBO winters. They attributed this to the direct influence of the stronger MJO convection in the EQBO winters. However, the study of Garfinkel and Hartmann (2010) showed that the QBO modifies the teleconnections between tropics and extratropics through both direct and indirect (background flow related) processes. Subsequent studies examined the influence of the QBO on the MJO-NAO teleconnection (Feng and Lin 2019). During the extended winters, from November to April, after the occurrence of the MJO phases 3 and 7 the NAO in both phases was found to have a larger amplitude in the WQBO years than the EQBO years (Feng and Lin 2019; Song and Wu 2020). Although the underlying mechanisms remain to be elucidated, one possibility is that the subtropical wind field under the WQBO conditions may be more conducive to the propagation of Rossby waves, at the core of teleconnections (Feng and Lin 2019; Song and Wu 2020).

The S2S prediction ranging from about two weeks to a season aims to fill the gap between the mid-range weather forecasts and the seasonal-range forecasts (Vitart et al. 2015). As mentioned earlier, the MJO-associated teleconnection might serve as a potential source of

predictability on the subseasonal time scale. Vitart (2017) reported that most S2S models are to some extent able to represent the MJO-NAO teleconnection. It is of interest to examine if these models can also capture the modulation of the MJO-NAO teleconnections by the QBO as observed in Feng and Lin (2019).

The objective of this study is to assess the QBO modulation on the MJO-associated teleconnection over the North Atlantic basin in the S2S models. To that end composites of the extratropical teleconnection patterns predicted by the S2S models after the occurrence of the MJO will be examined and compared between the EQBO and WQBO winters. The reforecasts of all the available S2S models are used in this study.

The paper is organized as follows. The database of the S2S models, the observations and the methods of analysis are introduced in Section 4.2. Section 4.3 describes the 500 hPa geopotential height anomaly composites after the occurrence of the MJO during each of the two phases of the QBO and the composites are further compared in Section 4.4. Section 4.5 presents a discussion and the conclusions.

4.2 Data and Method

4.2.1 Observations

The National Centers for Environmental Prediction-National Center for Atmospheric Research (NCEP-NCAR) Reanalysis 1 (Kalnay et al., 1996) are taken as observations that covers the period of 1979-2017. Both the geopotential height and wind field data are with a daily temporal resolution and a spatial resolution of 2.5-degree latitude by 2.5-degree longitude on global grids.

To obtain the daily anomaly of each variable, the seasonal cycle at each grid point is first removed. We take the seasonal cycle here as the annual mean and the first three harmonics of the 38-year daily climatology. Then, to eliminate the interannual variability, we subtract the mean of each extended winter. The extended winter covers November 2 to March 31, inclusive of 150 days, and the leap years have 151 days.

The analysis is based on five-day averages (pentads) of the variables. The first pentad corresponds to 2-6 November and the last one as 26-30 March. February 29 is included in the 6-day average of the 24th pentad during the leap years.

In this study, the NAO index is calculated as the projection of the Z500 anomaly onto the NAO spatial pattern defined as in Feng and Lin (2019) which is the second rotated EOF mode of monthly mean Z500 anomaly over the Northern Hemisphere (Lin et al., 2009 Fig. 1).

The EQBO and WQBO years are defined according to the winter (December – February; DJF) average of the mean zonal wind between 10°S and 10°N at 50 hPa as previous studies (e.g., Yoo and Son 2016; Son et al. 2017). When the winter average is greater (less) than 0.5 (-0.5) standard deviation, it is defined as a WQBO (EQBO) year. From 1979 to 2019, there are 12 EQBO years and 15 WQBO years. After removing strong ENSO events (to be defined shortly), 10 EQBO and 10 WQBO winters remain, and all the selected years in Feng and Lin (2019) are included when computing the climatology. The list of the selected years is given in Table 4.1. The same results can be obtained if we extend the winter season from November to March.

To define the strong ENSO events, the sea surface temperature (SST) over the Nino 3.4 region (5°S-5°N and 170°-120°W) is used (https://www.esrl.noaa.gov/psd/data/climateindices/list/). A strong El Niño (La Nina) event is defined when the DJF anomaly is greater (less) than 1 (−1) standard deviation. The strong ENSO years are excluded from our analysis in order to minimize the influence of ENSO.

The daily RMM index was downloaded from the Australian Bureau of Meteorology website (http://www.bom.gov.au/climate/mjo/graphics/rmm.74toRealtime.txt), which was calculated from a combined empirical orthogonal function (EOF) analysis of the meridionally averaged zonal wind at 850 and 200 hPa, and the OLR anomalies between 15°S and 15°N (Wheeler and Hendon 2004). RMM1 and RMM2 are the first and second principal components, respectively. An active MJO event occurs when the amplitude, $\sqrt[2]{(RMM1)^2 + (RMM2)^2}$, exceeds one.

4.2.2 S2S models

The subseasonal-to-seasonal (S2S) prediction project (Vitart et al., 2017) was launched by the World Weather Research Programme (WWRP) and World Climate Research Programme (WCRP). Currently, the data from 11 research centres are accessible on the website of the European Centre for Medium-Range Weather Forecast (ECMWF). Here we use the reforecast data from the following centres: Australian Bureau of Meteorology (BoM), China Meteorological Administration (CMA), Institute of Atmospheric Science and Climate of the National Research Council (CNR-ISAC), Météo-France/Centre National de Recherches Météorologiques (CNRM), Environment and Climate Change Canada (ECCC), ECMWF, Hydrometeorological Centre of Russia (HMCR), Japan Meteorological Agency (JMA), National Centers for Environmental Prediction (NCEP), and Met Office (UKMO). The reforecasts of the Korea Meteorological Administration (KMA) were not used because the outgoing longwave radiation data was not available. The temporal coverage of reforecasts varies from model to model, which is presented in Table 4.2, including the period covered by

the reforecast and the ensemble size. A more detailed model description can be found in Vitart et al. (2017) and Lim et al. (2019).

To obtain the anomaly of a variable in the S2S model, the climatology as the mean of the reforecasts initiated on the same date of all the available years is removed in a cross-validation manner. For example, if there are 20 reforecasts initiated on January 1, the daily forecast anomaly of one year is obtained by removing the averaged January 1 reforecast of the other 19 years. This is done separately for each lead time. The daily 500 hPa geopotential height anomalies are averaged over consecutive five days to construct the pentad anomalies. The NAO index of the forecasts is then computed with the same method as for the observations. i.e., by projecting to the same NAO pattern.

As listed in Table 4.2, the reforecast period varies from model to model and contains various numbers of QBO years. Some models with a shorter reforecast period have less QBO years (Table 4.1). In order to have more events than those determined from just the initial condition, we use the first 20 days of each forecast to select the MJO cases, and the associated forecast Z500 anomalies are used for the composite calculation. During these 20 days, most models are able to produce a skillful MJO prediction with the bivariate correlation of RMM1 and RMM2 of the MJO remaining higher than 0.5 (e.g., Vitart 2017; Lim et al. 2018).

4.3 Modulation of the MJO-Related Teleconnection by the QBO

Cassou (2008) and Lin et al. (2009) showed that the amplitude of the NAO is enhanced following the occurrence of the MJO in certain phases, an effect that takes roughly 10 days to

maximize. The MJO-related teleconnection in the S2S models was assessed in Vitart (2017). Although the amplitude was shown to be underestimated in the forecasts when compared with the observations, all the S2S models were able to capture a realistic pattern over the Atlantic basin at 500 hPa (Vitart 2017).

The influence of the stratospheric QBO on the MJO and its related teleconnection is gaining increasing attention (e.g., Son et al. 2017). Feng and Lin (2019) found that the MJO-NAO teleconnection is modulated by the phase of the QBO. The MJO-related NAO was shown to be significantly stronger during the WQBO winters than during the EQBO winters (Feng and Lin 2019), for both the positive NAO after the occurrences of the MJO phase 3 and the negative NAO after the occurrences of the MJO phase 7.

4.3.1 MJO Phase 3

The 2-pentad lagged composites of the geopotential height anomaly at 500 hPa after the occurrence of the MJO phase 3 during EQBO extended winters in the Northern Hemisphere from 20° to 90° N are shown as Figure 4.1, for the observation and the ten S2S models. The numbers in the bracket are the composite NAO index, and the star sign on the upper right of the number indicates that the index is statistically significant at the 95% level according to a Student-t test.

The overall pattern of the composited observed anomaly (Fig. 4.1a) is very similar to Fig. 1 of Feng and Lin (2019) although one more EQBO year is added, and it projects to a positive NAO. For the S2S models (Figs. 4.1-b to k), the amplitude of anomalies over the Atlantic basin is weaker than in the observation, and the positive NAO pattern does not seem represented well in most models. Compared with the observation, some models tend to overestimate the positive 500 hPa geopotential height anomaly in the North Pacific (e.g., BOM, HMCR, ECMWF and

NCEP models), but almost all the S2S models underestimate the two positive anomaly centres over the eastern and western North Atlantic. However, we also notice that the amplitude of the extratropical responses over the Atlantic basin after the occurrence of the MJO in the S2S simulations are in general much weaker than in observations (Fig. 1– 4), and what might induce this underestimation of the anomalous geopotential height might need more investigations.

While half of the S2S models produce a positive NAO (Fig. 4.1), the amplitude is much weaker than in the observation Table 4.3 shows the evolution of the composited NAO index in the three pentads following the MJO events, and Table 4.4 lists the sample size for the composites. As mentioned in section 4.2, the active MJO events in the first 20 days of the reforecast are analyzed. Therefore, the model sample size is larger than the observation. The HMCR model produces a significant positive NAO in the first pentad and the third pentad. In the BoM model, although a negative NAO is generated, its amplitude decreases with time.

Figure 4.2 shows the 500 hPa geopotential anomaly at lag=2 pentads after the occurrence of the MJO phase 3 during the WQBO years. The positive NAO in the observation is strong and statistically significant, in agreement with that observed in Feng and Lin (2019). During the WQBO, most S2S models reproduce a significant positive NAO pattern as in the observation. Overall, the amplitude of the forecast anomalies over the Atlantic basin is weaker than in the observation except for ECCC, which produces an amplitude comparable to the observation. As summarized in Table 4.5, the positive NAO pattern after the occurrence of the MJO phase 3 during the WQBO condition have the most significant results.

Moreover, the temporal evolution of the composited NAO index (Table 4.3) also indicates the significance of the positive NAO in the three pentads after the occurrence of the MJO phase 3 in the forecasts of ECCC, ISAC-CNR, and CMA, ECMWF, JMA, and NCEP (in alphabetical order).

Compared to the EQBO winters (Fig. 4.1), the MJO teleconnection in the North Atlantic during the WQBO winters is stronger in most models (Fig. 4.2). During EQBO, only half of the S2S models produce a positive NAO, but the amplitude is less than half of the observation, and only one is statistically significant. In contrast, during WQBO associated with MJO phase 3, as shown in Fig. 4.2, eight models out of 10 are able to reproduce positive NAO and only one of them is not statistically significant. The composite NAO index shown in Table 4.3 indicates that under EQBO conditions, the observation and most S2S models tend to start with a negative NAO at the first pentad, and the value of the index increases with time. However, the temporal evolution of the composite NAO index under WQBO conditions is associated with a positive NAO in all the three pentads, which might be associated with the initial conditions related to the mean state of the NAO that corresponds to the preferable positive NAM/AO during WQBO (e.g., Baldwin and Dunkerton 1999; Watson and Gray 2014). Both the observation and most models start with a negative NAO index under the EQBO condition. Vitart (2017) investigated the MJO-NAO connection in the S2S models and suggested the possibility of sensitivity to horizontal resolution. The MJO teleconnection in the models with a low horizontal resolution (BoM, CMA, HMCR) is weaker than in the ones with a high horizontal resolution (JMA, ECCC, ECMWF; Vitart 2017). The impact of the horizontal resolution here under the EQBO condition does not seem very apparent, while under WQBO conditions, the models with a high horizontal resolution indeed reproduce a stronger positive NAO pattern than the low-resolution ones.

With regards to the stratospheric resolution, the S2S models with a higher stratospheric resolution were found to be able to better maintain the amplitude of the QBO than those with a coarser stratospheric resolution (Lim et al. 2019). Based on the vertical resolution, Lim et al. (2019) divided the S2S models into the high-top and low-top models. The high-top models with a relatively higher stratospheric resolution are the CMA, CNRM, ECMWF, JMA, NCEP,

and UKMO models, and the low-top models are those from BoM, ECCC, HMCR, and ISAC-CNR. In Figures 4.1 to 4, the low-top models are placed as (b)-(e) and high-top models as (f)-(k). In Figure 4.1 (EQBO winters) the influence of the stratospheric resolution is not apparent. In contrast, in Figure 4.2 (WQBO winters), the high-top models in general reproduce the positive NAO pattern with a larger amplitude.

4.3.2 MJO phase 7

Figure 4.3 shows the composites of 500-hPa geopotential height anomaly two pentads after the occurrence of the MJO phase 7 under EQBO conditions. For the observation, there is a negative NAO, as in previous studies (e.g., Lin et al. 2009) where the EQBO and WQBO winters were not separated. Compared to Feng and Lin (2019), the anomalies are generally enhanced when the winter season is defined as November to March and one more sample year added (this study), while the coverage of the area with the 95% significance level remains small over the Atlantic basin. As in the observation, all the models have a negative NAO except for HMCR that has an amplitude close to zero. The ECCC, ECMWF, and NCEP models show a comparable amplitude of negative NAO as the observation and with a composited NAO index that is statistically significant at the 5% level. The UKMO model also captures a significant negative NAO although the amplitude is weaker.

For the temporal evolution (Table 4.3), a negative NAO appears with the MJO phase 7 at lag=0 in the observation and all the S2S models. Then, the amplitude of negative NAO weakens with time in most models. In the ECCC and NCEP models, the composited NAO index becomes stronger with time and statistically significant from lag=1 pentad. For ECMWF and UKMO, the composited NAO index maintains a similar amplitude in all the three pentads. The negative NAO index is statistically significant in all three lags for ECMWF but only in lag=2 for UKMO.

Under the WQBO condition, the composites two pentads after the occurrence of the MJO phase 7 are presented as Figure 4.4. The amplitude of the observational anomaly also becomes stronger when the winter season is defined as November to March and two more sample years added (this study) compared to Feng and Lin (2019). Although the overall coverage of the significant areas reduces compared to Feng and Lin (2019), the composited NAO index remains significantly negative. Half of the S2S models show a positive NAO pattern instead of a negative one but none of the related NAO indices is statistically significant. Although the other half models show a negative NAO, only the JMA model has a significant signal with an NAO index of -0.34, weaker than the -0.51 of the observation (Table 4.5).

With the temporal evolution of the composited NAO index (Table 4.3), the result suggests that most S2S models could not well capture the trend of the growing negative NAO after the occurrence of the MJO phase 7 under WQBO conditions. Except for JMA, a negative NAO in the first pentad could not amplify, and the composited NAO index could not exceed -0.20, which indicates that those S2S models are unable to predict the NAO change in this case.

With regards to the model resolution, the models with higher horizontal resolution, i.e., UKMO, ECCC, and ECMWF, indeed better captures the negative NAO with a reasonable amplitude (Fig. 4.3) than the BoM, CMA, and HMCR models under the EQBO condition. However, the NCEP model with the strongest negative NAO actually has the third lowest horizontal resolution (Table 4.2). This indicates that the horizontal resolution is not the only factor determining the MJO-NAO connection. As for the case under the WQBO condition (Fig. 4.4), only JMA produces a significant negative NAO, and there is no clear indication if the horizontal resolution has any impact. With regards to the stratospheric resolution, under the EQBO conditions (Fig. 4.3), the high-top models tend to be associated with stronger geopotential anomalies in the North Pacific than the low-top models. Half of the high-top models could represent the significant negative NAO pattern, and among the low-top models,

only ECCC captures the MJO teleconnection. Under the WQBO condition (Fig. 4.4), the stratospheric resolution does not seem to have much effect either.

Figure 4.5 is a summary of the composited forecast NAO index two pentads after the occurrence of the MJO phases 3 and 7 under the two phases of the QBO compared with the observations. In general, for the positive NAO after the occurrence of the MJO phase 3, under the WQBO condition, the S2S models have a better agreement than under the EQBO condition (Fig. 4.5-a; 4.5-c), and the negative NAO after the occurrence of the MJO phase 7 appears to be opposite (Fig. 4.5-b; 4.5-d).

4.4 Discussion and Conclusion

This study examines the MJO-associated extratropical teleconnection over the North Atlantic basin 10 to 15 days after the occurrence of an MJO in 10 S2S models and compare the model results to observations. We focus on four different classes of forecasts, namely, those done following the occurrence of an MJO in phase 3 or in phase 7 during EQBO winters or during WQBO winters. The analysis is based on the ensemble means of the forecasts and on the average (composite) of forecasts done for the same MJO phase and the same type of winter (EQBO or WQBO). The results can be summarized as follows:

(i) Phase 3 MJO in WQBO winters

The observations show a statistically significant positive NAO as do seven of the 10 models.

(ii) Phase 3 MJO in EQBO winters

The observations show a positive NAO signal but not quite large enough to be statistically significant at the 5% level. Only one model shows a statistically significant positive NAO signal.

(iii) Phase 7 MJO in WQBO winters

The observations show a negative NAO that is significant at the 5% level. Only one model produces a significant negative NAO.

(iv) Phase 7 MJO in EQBO winters

The observations show a negative NAO signal that is not quite large enough to be significant at the 5% level. Four of the 10 models have a negative NAO signal that is significant at the 5% level. It may be noted that the observational signal, while not quite significant, is larger than that of the models with significant signal, which may be related to sample size and variance.

We can conclude from the above that, at least as far as the response to a phase 3 MJO is concerned, the type of winter, WQBO vs EQBO, has a noticeable influence, the WQBO winters leading to a stronger positive NAO in the observations and a much stronger signal in the models (Figure 4.5). The responses obtained for phase 7 MJOs are also of interest in that while the atmosphere produces stronger NAOs during WQBO winters than during EQBO winters, the models produce very mixed results, most of which are not statistically significant. In short, most models do not respond well to a phase 7 MJO, independently of the type of winter.

The QBO modulation of the MJO teleconnection in the S2S models appears to be sensitive to the model resolution. For the stratospheric resolution, the high-top models seem to better represent the MJO-NAO teleconnections after the MJO phase 7 under the EQBO conditions and after MJO phase 3 under the WQBO conditions than the low-top models. Vitart (2017) discussed the possible impact of horizontal resolution on the MJO teleconnections. Under

WQBO conditions, the S2S models with higher horizontal resolution tend to produce a stronger positive NAO pattern following MJO phase 3 than the lower ones. It is unclear how the air-sea coupling contributes to the MJO teleconnection as modulated by the QBO, as the uncoupled models, ECCC and JMA, can also capture the negative NAO with comparable amplitude as the observation following MJO phase 7.

Previous studies indicate that the S2S forecast skill might be affected by model biases (Lim et al. 2019; Lin 2020). It is likely that the MJO-NAO teleconnections are sensitive to the extratropical basic state. Therefore, model biases in the basic state would influence the MJO teleconnection and related NAO variability under the two phases of the QBO.

Acknowledgements

We would like to thank Prof. Jacques Derome and Prof. Timothy Merlis of McGill University for providing suggestions and helpful comments throughout this study. This research was supported by the Natural Sciences and Engineering Research Council of Canada (NSERC) Discovery Grant to the second author.

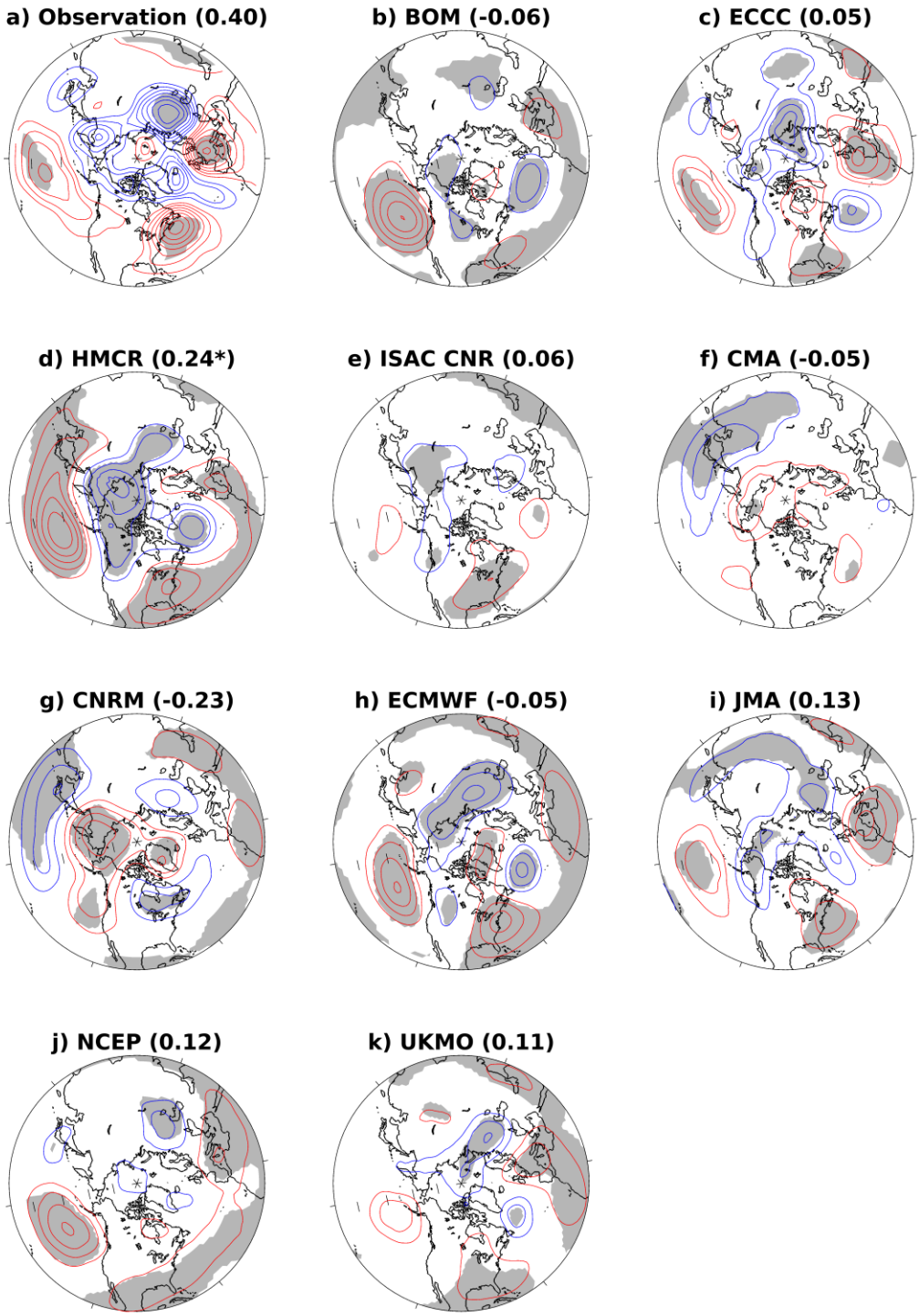

Figure 4.1 Lagged composites of 500-hPa geopotential height anomaly of the third pentad (11-15 days) for MJO phase 3 of EQBO events of observational data (a) and ten S2S simulations (b)-(k). Contours with negative values are blue, starting with -10 m. Contours with positive

values are red, starting with 10 m. The numbers in parenthesis are composited NAO index. Shaded area (star sign) means that the anomaly (composited NAO index) exceeds 95% significance level from zero by using Student-t test.

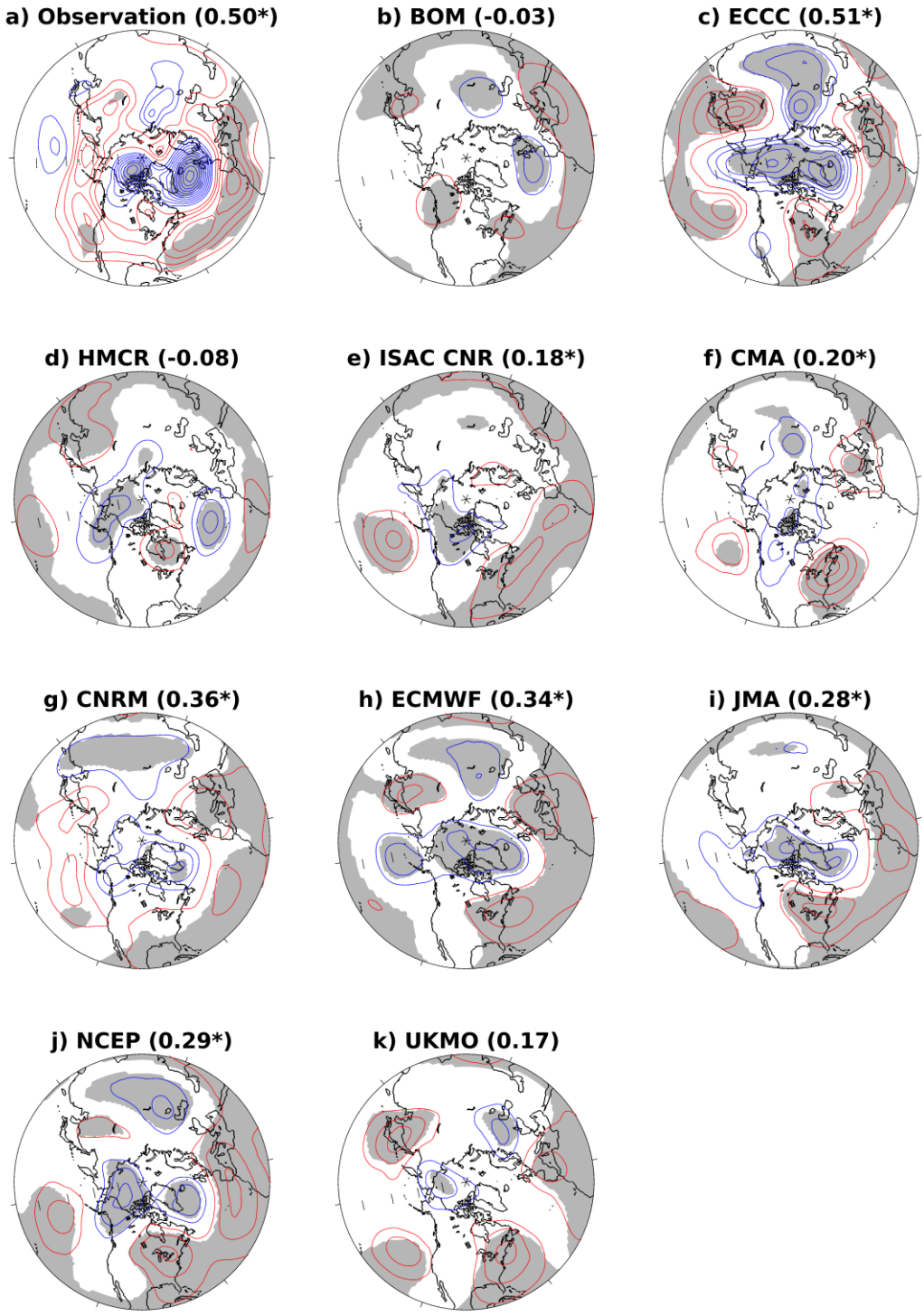

Figure 4.2 As Fig. 4.1 but for MJO phase 3 of WQBO events.

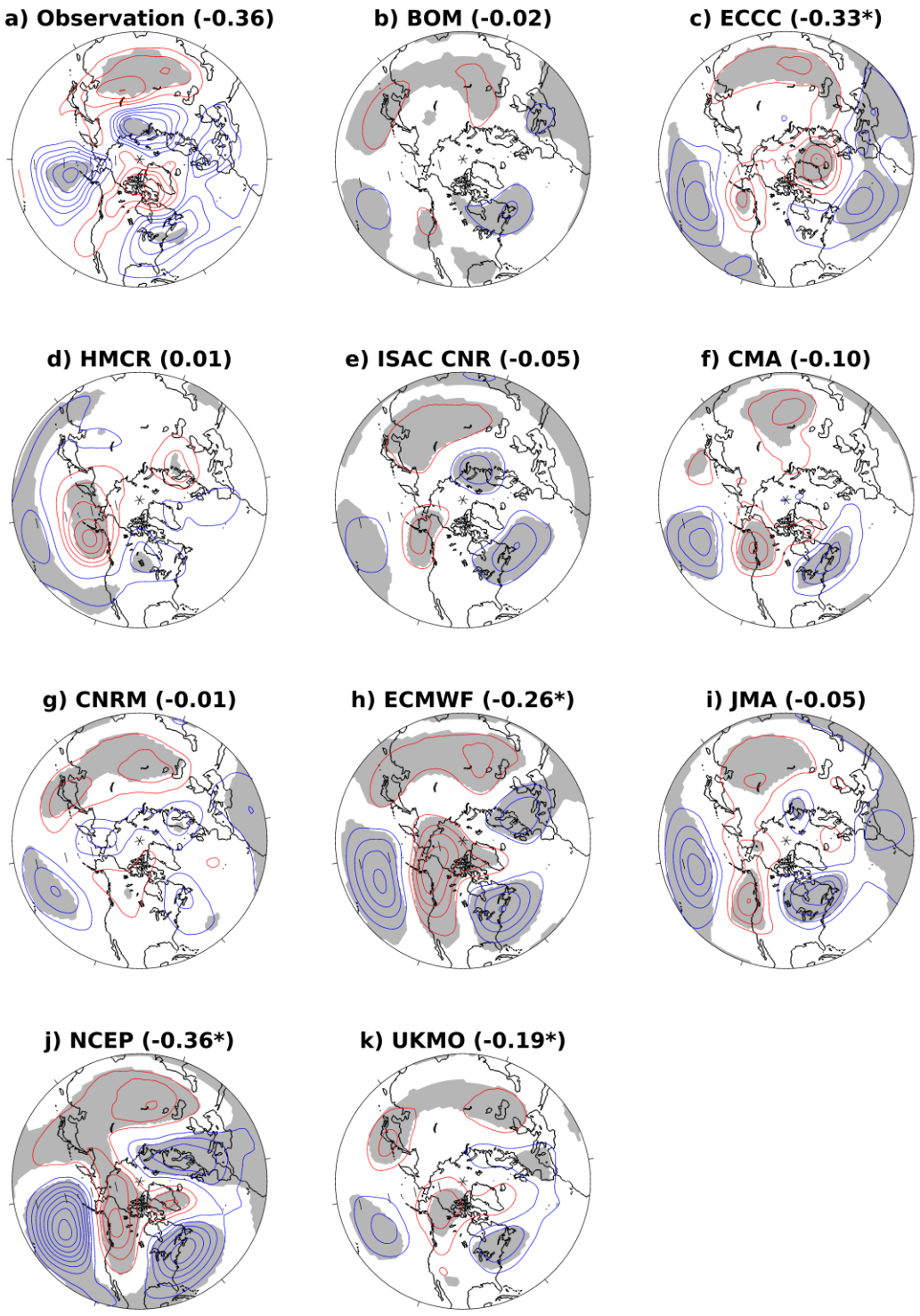

Figure 4.3 As Fig. 4.1 but for MJO phase 7 of EQBO events.

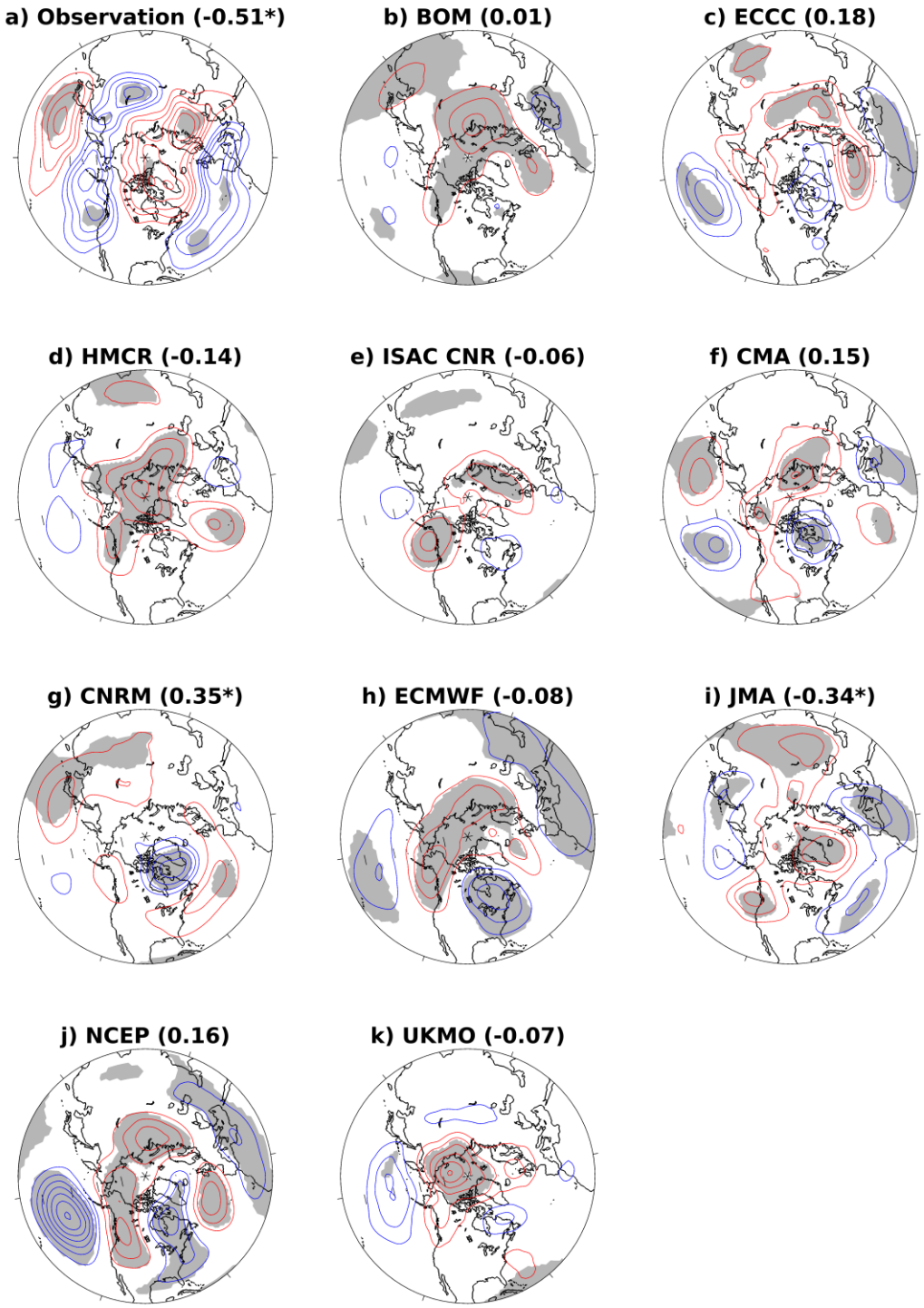

Figure 4.4 As Fig. 4.1 but for MJO phase 7 of WQBO events.

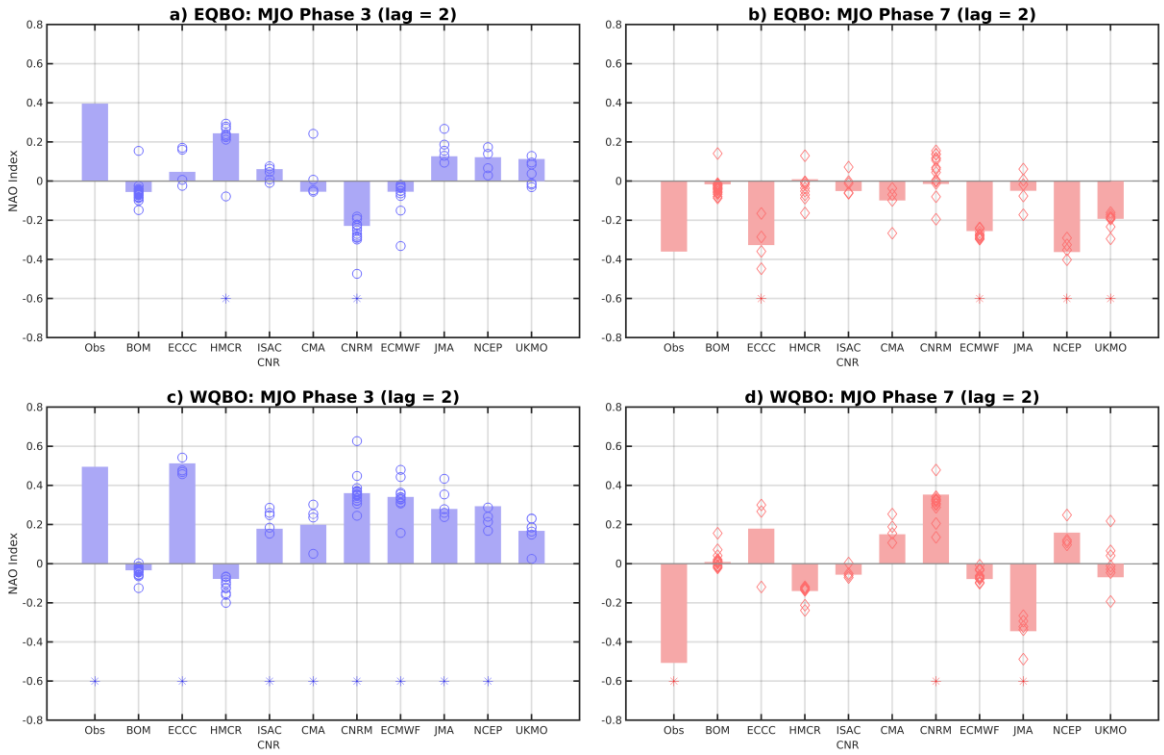

Figure 4.5 Composited NAO indices of the third pentad (11-15 days) for MJO phase 3 and 7 of the EQBO and the WQBO events of observational data and ten S2S simulations. Star signs are those passing the 95% significance level. The open circles and diamonds are the composited NAO index of individual ensemble members.

QBO Phase	Winters (without strong ENSO events)
EQBO	79/80, 81/82, 84/85, 89/90, 96/97, 01/02, 03/04, 05/06, 12/13, 14/15
WQBO	80/81, 85/86, 87/88, 90/91, 02/03, 04/05, 06/07, 08/09, 13/14, 16/17

Table 4.1 November-April identified as easterly phase (EQBO) and westerly phase (WQBO) of the QBO during 1979-2017.

Model name	Reforecast period	Model frequency	Model resolution (Model top)	Ensemble size
BoM	1981-2013	6 times/month	T47 L17 (10 hPa)	33
CMA	1994-2014	Twice/week	T16 L40 (0.5 hPa)	4
ECCC	1995-2014	Weekly	0.45ºx0.45º L40 (2 hPa)	4
ECMWF	1997-2017	Twice/week	Tco639/ Tco319 L91 (0.01 hPa)	11
HMCR	1985-2010	Weekly	1.1ºx1.4º L28 (5 hPa)	10
ISAC-CNR	1981-2010	Every 5 days	0.8ºx0.56º L54 (roughly 6.8 hPa)	5
JMA	1981-2012	3 times/month	TL479/TL319 L100 (0.01 hPa)	5
CNRM	1993-2014	4 times/month	TL255 L91 (0.01 hPa)	15
NCEP	1999-2010	Daily	T126 L64 (0.02 hPa)	4
UKMO	1993-2015	4 times/month	0.83ºx0.56º L85 (85 km)	7

Table 4.2 Temporal coverage of reforecasts used in this study.

		MJO phase 3				MJO phase 7		
		lag = 0	lag = 1	lag = 2		lag = 0	lag = 1	lag = 2
Obs	EQBO	-0.14	0.08	0.40	EQBO	-0.34	-0.32	-0.36
	WQBO	0.10	0.28	**0.50**	WQBO	0.02	-0.32	**-0.51**
BOM	EQBO	**-0.23**	-0.15	-0.06	EQBO	-0.08	-0.03	-0.02
	WQBO	-0.01	-0.02	-0.03	WQBO	-0.04	-0.06	0.01
ECCC	EQBO	-0.08	-0.10	0.05	EQBO	-0.24	**-0.30**	**-0.33**
	WQBO	**0.48**	**0.65**	**0.51**	WQBO	0.10	0.24	0.18
HMCR	EQBO	**0.33**	0.25	**0.24**	EQBO	-0.13	-0.07	0.01
	WQBO	0.00	0.00	-0.08	WQBO	-0.18	-0.09	-0.14
ISAC CNR	EQBO	0.11	0.12	0.06	EQBO	**-0.16**	-0.12	-0.05
	WQBO	**0.20**	**0.26**	**0.18**	WQBO	-0.13	-0.06	-0.06
CMA	EQBO	-0.13	-0.11	-0.05	EQBO	**-0.30**	-0.17	-0.10
	WQBO	**0.35**	**0.31**	**0.20**	WQBO	0.07	0.11	0.15
CNRM	EQBO	-0.13	-0.24	-0.23	EQBO	-0.32	-0.20	-0.01
	WQBO	0.26	0.29	**0.36**	WQBO	0.35	**0.45**	**0.35**
ECMWF	EQBO	-0.13	-0.08	-0.05	EQBO	**-0.27**	**-0.32**	**-0.26**
	WQBO	**0.28**	**0.38**	**0.34**	WQBO	-0.04	-0.05	-0.08
JMA	EQBO	-0.06	0.06	0.13	EQBO	-0.16	-0.11	-0.05
	WQBO	**0.25**	**0.27**	**0.28**	WQBO	**-0.34**	**-0.41**	**-0.34**
NCEP	EQBO	-0.15	0.03	0.12	EQBO	-0.16	**-0.34**	**-0.36**
	WQBO	**0.32**	**0.33**	**0.29**	WQBO	-0.09	0.04	0.16
UKMO	EQBO	-0.12	-0.11	0.11	EQBO	-0.19	-0.17	**-0.19**
	WQBO	**0.28**	0.23	0.17	WQBO	-0.19	-0.06	-0.07

Table 4.3 Lagged composites of the NAO index with respect to MJO phase 3 and 7 under the two phases of the QBO. Lag n is the number of pentad that NAO lags the MJO phase 3 or 7 by n pentads. Bolded numbers are statistically significant at the 95% level.

		MJO phase 3				MJO phase 7		
		lag = 0	lag = 1	lag = 2		lag = 0	lag = 1	lag = 2
Obs	EQBO	21	21	20	EQBO	26	25	24
	WQBO	26	24	23	WQBO	25	25	25
BOM	EQBO	95	95	95	EQBO	130	130	130
	WQBO	93	93	93	WQBO	81	81	81
ECCC	EQBO	31	31	30	EQBO	48	48	46
	WQBO	32	32	31	WQBO	41	41	39
HMCR	EQBO	53	53	53	EQBO	43	43	43
	WQBO	73	73	73	WQBO	57	57	57
ISAC CNR	EQBO	93	93	85	EQBO	138	138	123
	WQBO	105	105	91	WQBO	85	85	75
CMA	EQBO	52	52	52	EQBO	61	61	61
	WQBO	51	51	51	WQBO	58	58	58
CNRM	EQBO	30	30	30	EQBO	22	22	22
	WQBO	19	19	19	WQBO	27	27	27
ECMWF	EQBO	67	67	67	EQBO	105	105	105
	WQBO	82	82	82	WQBO	84	84	84
JMA	EQBO	43	43	40	EQBO	52	52	46
	WQBO	51	51	49	WQBO	38	38	37
NCEP	EQBO	61	61	61	EQBO	74	74	74
	WQBO	108	108	108	WQBO	84	84	84
UKMO	EQBO	48	48	48	EQBO	69	69	69
	WQBO	48	48	48	WQBO	40	40	40

Table 4.4 Sample size for the composite analysis shown in Table 4.3.

	EQBO	WQBO
MJO Phase 3	1 model	7 models and observation
MJO Phase 7	4 models	1 model and observation

Table 4.5 Summary table for the number of models which produce significant positive (negative) NAO after the occurrence of the MJO phase 3 (7) during the two phases of the QBO.

Chapter 5

Summary and Future Work

5.1 Summary and conclusion

This thesis has explored the evolution of the North Atlantic Oscillation (NAO) driven by the Madden-Julian Oscillation (MJO) under the modulation of the quasi-biennial oscillation (QBO) on the subseasonal time scale in both observations and model simulations and examined the prediction skill of the NAO in the WCRP/WWRP subseasonal-to-seasonal (S2S) prediction projects.

The westerly phase (WQBO) and easterly phase of the QBO (EQBO) occur with different patterns of the geopotential height fields and vertical wind profiles over the Northern Hemisphere, and the MJO-associated extratropical teleconnections are also observed to have different representations during the two phases of the QBO. The investigations of the evolution of the NAO after the occurrences of the MJO during the two phases of the QBO are presented in Chapter 2. Hence, how the MJO, QBO and even the NAO itself would influence the NAO prediction skills in the 11 state-of-art S2S models is assessed in Chapter 3. The representation of the modulation of the QBO on the MJO-related extratropical teleconnections of the S2S models is analyzed and compared with the observations in Chapter 4.

In Chapter 2, we found differences of the extratropical circulation over the Atlantic which forms an NAO-like pattern after the occurrences of certain phases of the MJO between EQBO and WQBO winters. Both the positive NAO after the occurrences of the MJO phase 3 and the

negative NAO after the occurrences of the MJO phase 7 during the WQBO extended winters from November to April are more significant and stronger than during the EQBO extended winters. This is confirmed by the different extratropical teleconnection patterns between the EQBO and the WQBO years from the singular value decomposition (SVD) analysis of the outgoing longwave radiation (OLR) and the geopotential height anomaly at 500 hPa with 2-pentad lag. During EQBO extended winters, the meridional dipole structure of the geopotential height anomalies is more confined in the east coast of North America compared with during WQBO. During WQBO extended winters, the negative OLR anomaly which could be regarded as the active convection over the Indian Ocean is weaker than during EQBO, however, the meridional dipole structure of the geopotential height anomalies covers the whole North Atlantic basin and more resembles the NAO pattern. In order to shed light on the possible underlying mechanism for these differences, the QBO modulation of the basic state was analyzed. The anomalous westerlies at 200 hPa during the WQBO in the subtropical North Pacific where the location corresponds to the Asian jet should be regarded as more preferable for the propagation of the Rossby wave induced by the convections of the MJO. Furthermore, the anomalous wind field in the polar region presents westerlies during WQBO and easterlies during EQBO. The enhanced westerly zonal wind in the high latitude upper troposphere would help the vertical propagation of planetary waves into the stratosphere as well.

Chapter 3 investigated the prediction skill of the NAO of the models of WCRP/WWRP subseasonal-to-seasonal (S2S) prediction projects. In particular, we compared the forecasts initiated with different phases of the NAO and the QBO, as well as the MJO conditions. The S2S models are able to forecast the NAO with a correlation skill higher than 0.5 up to around two weeks. From the analysis of the perfect model approach, most S2S models are found to have smaller ensemble spreads than from natural variability, and thus the perfect skill is better than the actual skill in most models.

When the forecasts are classified as positive and negative phases of the NAO in the initial conditions, the negative NAO is found to lead a better correlation skill than the positive NAO in most S2S models. The larger root-mean square error (RMSE) of the negative NAO-initiated forecasts than the positive NAO initiated ones might be due to the larger initial variance among the negative NAO cases that could have higher chances of larger simulation errors. However, the observed modulation of the QBO on the NAO (e.g., Coughlin and Tung 2001) does not seem captured by the S2S models in the present analysis. The forecasts initiated with the two phases of the QBO yield similar skills of both correlation and RMSE. For the MJO events, the active and inactive MJO-initiated forecasts represent the close correlation and RMSE prediction skills. The MJO in phases 3-4 or 7 lead the best NAO correlation skills among all the phases.

Furthermore, we also found that the S2S models with finer stratospheric resolutions referred to as high-top models in general produce higher NAO prediction skills of both correlation and RMSE than those with coarser stratospheric resolutions as low-top models. The higher prediction skills of the negative NAO initiated forecasts of most high-top models are found to be more apparent than in the low-top models. The NAO prediction skills with the MJO in phases 3-4 or 7 as the initial conditions of most high-top models also last longer than in the low-top models. However, in the QBO cases, the differences of the stratospheric resolution does not seem reflect on the prediction skills.

Following the previous chapters, the modulation of the QBO on the MJO-related extratropical teleconnections of the S2S models is assessed in Chapter 4. Under the WQBO conditions, seven of the 10 models represent a statistically significant positive NAO at the 5% level after the occurrences of the MJO phase 3 as the observations. While during the EQBO, the observations show a positive NAO signal after the occurrences of the MJO phase 3 as well but weaker than during the WQBO and not statistically significant, and only one model shows

a statistically significant positive NAO signal. After the occurrence of the MJO phase 7, although the negative NAO signal in the observations is not statistically significant at the 5% level, four of the 10 models have a statistically significant negative NAO during the EQBO. The observations show a statistically significant negative NAO at the 5% level after the occurrence of the MJO phase 7 under the WQBO conditions, however, only one model represents a statistically significant negative NAO signal in this case. The extratropical responses to the MJO phase 3 under the WQBO and EQBO conditions have a noticeable difference. During the WQBO, both the observations and most models lead to a stronger positive NAO than the EQBO. Nevertheless, the extratropical responses to the MJO phase 7 seem more arbitrary under the two phases of the QBO and the models represent mix results. The model properties are regarded as possible factors to influence the MJO-associated extratropical responses. The models with finer stratospheric resolutions seem better capture the NAO patterns after the occurrences of the MJO phase 3 and 7 than the models with coarser stratospheric resolutions. The horizontal resolution and air-sea coupling also may impact the simulated extratropical responses to the MJO, so more investigation is needed.

5.2 Future work

From the result of this thesis, we found the stronger MJO-associated extratropical responses over the Atlantic basin which forms the pattern like the NAO during the WQBO extended winters than the EQBO in the observations (Chapter 2). After the removal of the years with strong El Niño-Southern Oscillation (ENSO) events, 9 EQBO years and 8 WQBO years remain. We expect in the future there will be more cases for the further investigations of how the QBO modulates the MJO-NAO teleconnections. Furthermore, the stratospheric process needs more investigation. If the easterly and westerly phases of the QBO impact the

stratospheric circulation and the wave propagation and then modify the MJO-associated extratropical teleconnections might help the understanding the interactions of the climate variabilities in both the stratosphere and troposphere. Also, if the model simulation could help to clarify the possible underlying mechanisms is of interest.

The assessment of the S2S models for 1) the NAO prediction skill initiated with the NAO event, the QBO event, and the MJO events (Chapter 3), and 2) the representation of the QBO modulation on the MJO-NAO teleconnections (Chapter 4) are studied. As the S2S models are expected to improve the forecast of the scale spanning from subseasonal to seasonal and the S2S project is still running, there are possibilities for further investigations. In Chapter 3, we discover some differences of the NAO prediction skills between the high-top and low-top models which are defined by the stratospheric resolutions. However, the differences in model formulation beyond the stratospheric resolution may also play a role in the results found in Chapter 3 and Chapter 4. Following our analyses, the next step of assessing the reforecasts for the sensitivity to the initial conditions and the impact of the model formulations might be helpful to draw a more complete picture of the model ability for representing the evolution of the NAO. Moreover, the assessment of the influence of the stratosphere on the tropospheric teleconnections might also help to determine the importance of the stratosphere in the model predictions.

Bibliography

Alvarez, M. S., Vera, C. S., Kiladis, G. N., & Liebmann, B. (2016). Influence of the Madden Julian Oscillation on precipitation and surface air temperature in South America. *Climate Dynamics*, *46*(1), 245–262. https://doi.org/10.1007/s00382-015-2581-6

Ambaum, M. H. P., Hoskins, B. J., & Stephenson, D. B. (2001). Arctic Oscillation or North Atlantic Oscillation? *Journal of Climate*, *14*(16), 3495–3507. https://doi.org/10.1175/1520-0442(2001)014<3495:AOONAO>2.0.CO;2

American Meteorological Society, cited 2020: Teleconnection. *Glossary of Meteorology*. [Available online at http://glossary.ametsoc.org/wiki/Teleconnection.]

Bader, J., Mesquita, M. D. S., Hodges, K. I., Keenlyside, N., Østerhus, S., & Miles, M. (2011). A review on Northern Hemisphere sea-ice, storminess and the North Atlantic Oscillation: Observations and projected changes. *Atmospheric Research*, *101*(4), 809–834. https://doi.org/10.1016/j.atmosres.2011.04.007

Baldwin, M. P., Gray, L. J., Dunkerton, T. J., Hamilton, K., Haynes, P. H., Randel, W. J., Holton, J. R., Alexander, M. J., Hirota, I., Horinouchi, T., Jones, D. B. A., Kinnersley, J. S., Marquardt, C., Sato, K., & Takahashi, M. (2001). The quasi-biennial oscillation. *Reviews of Geophysics*, *39*(2), 179–229. https://doi.org/10.1029/1999RG000073

Baldwin, Mark P., & Dunkerton, T. J. (1999). Propagation of the Arctic Oscillation from the stratosphere to the troposphere. *Journal of Geophysical Research: Atmospheres*, *104*(D24), 30937–30946. https://doi.org/10.1029/1999JD900445

Baldwin, Mark P, & Dunkerton, T. J. (2001). Stratospheric harbingers of anomalous weather regimes. *Science*, *294*(5542), 581–584.

Barnes, E. A., & Hartmann, D. L. (2010). Dynamical Feedbacks and the Persistence of the NAO. *Journal of the Atmospheric Sciences*, *67*(3), 851–865. https://doi.org/10.1175/2009JAS3193.1

Barnston, A. G., & Livezey, R. E. (1987). Classification, Seasonality and Persistence of Low-Frequency Atmospheric Circulation Patterns. *Monthly Weather Review*, *115*(6), 1083–1126. https://doi.org/10.1175/1520-0493(1987)115<1083:CSAPOL>2.0.CO;2

Benedict, J. J., Lee, S., & Feldstein, S. B. (2004). Synoptic View of the North Atlantic Oscillation. *Journal of the Atmospheric Sciences*, *61*(2), 121–144. https://doi.org/10.1175/1520-0469(2004)061<0121:SVOTNA>2.0.CO;2

Boer, G. J., & Hamilton, K. (2008). QBO influence on extratropical predictive skill. *Climate Dynamics*, *31*(7), 987–1000. https://doi.org/10.1007/s00382-008-0379-5

Bond, N. A., & Vecchi, G. A. (2003). The Influence of the Madden–Julian Oscillation on Precipitation in Oregon and Washington. *Weather and Forecasting*, *18*(4), 600–613. https://doi.org/10.1175/1520-0434(2003)018<0600:TIOTMO>2.0.CO;2

Bretherton, C. S., Smith, C., & Wallace, J. M. (1992). *An intercomparison of methods for finding coupled patterns in climate data*. *5*(6), 541–560.

Cassou, C. (2008). Intraseasonal interaction between the Madden–Julian Oscillation and the North Atlantic Oscillation. *Nature*, *455*(7212), 523–527. https://doi.org/10.1038/nature07286

Chen, W., & Li, T. (2007). Modulation of northern hemisphere wintertime stationary planetary wave activity: East Asian climate relationships by the Quasi-Biennial Oscillation. *Journal of Geophysical Research: Atmospheres*, *112*(D20).

Coughlin, K., & Tung, K.-K. (2001). QBO signal found at the extratropical surface through northern annular modes. *Geophysical Research Letters*, *28*(24), 4563–4566. https://doi.org/10.1029/2001GL013565

Crooks, S. A., & Gray, L. J. (2005). Characterization of the 11-Year Solar Signal Using a Multiple Regression Analysis of the ERA-40 Dataset. *Journal of Climate*, *18*(7), 996–1015. https://doi.org/10.1175/JCLI-3308.1

Czaja, A., Robertson, A. W., & Huck, T. (2013). The Role of Atlantic Ocean-Atmosphere Coupling in Affecting North Atlantic Oscillation Variability. In *The North Atlantic Oscillation: Climatic Significance and Environmental Impact* (pp. 147–172). American Geophysical Union (AGU). https://doi.org/10.1029/134GM07

Densmore, C. R., Sanabia, E. R., & Barrett, B. S. (2019). QBO influence on MJO amplitude over the Maritime Continent: Physical mechanisms and seasonality. *Monthly Weather Review*, *147*(1), 389–406.

Domeisen, D. I. V. (2019). Estimating the Frequency of Sudden Stratospheric Warming Events From Surface Observations of the North Atlantic Oscillation. *Journal of Geophysical Research: Atmospheres*, *124*(6), 3180–3194. https://doi.org/10.1029/2018JD030077

Domeisen, D. I. V., Butler, A. H., Charlton-Perez, A. J., Ayarzagüena, B., Baldwin, M. P., Dunn-Sigouin, E., Furtado, J. C., Garfinkel, C. I., Hitchcock, P., Karpechko, A. Y., Kim, H., Knight, J., Lang, A. L., Lim, E.-P., Marshall, A., Roff, G., Schwartz, C., Simpson, I. R., Son, S.-W., & Taguchi, M. (2020a). The Role of the Stratosphere in Subseasonal to Seasonal Prediction: 1. Predictability of the Stratosphere. *Journal of Geophysical Research: Atmospheres*, *125*(2), e2019JD030920. https://doi.org/10.1029/2019JD030920

Domeisen, D. I. V., Butler, A. H., Charlton-Perez, A. J., Ayarzagüena, B., Baldwin, M. P., Dunn-Sigouin, E., Furtado, J. C., Garfinkel, C. I., Hitchcock, P., Karpechko, A. Y., Kim, H., Knight, J., Lang, A. L., Lim, E.-P., Marshall, A., Roff, G., Schwartz, C., Simpson, I. R., Son, S.-W., & Taguchi, M. (2020b). The Role of the Stratosphere in Subseasonal to Seasonal Prediction: 2. Predictability Arising From Stratosphere-Troposphere Coupling.

Journal of Geophysical Research: Atmospheres, *125*(2), e2019JD030923. https://doi.org/10.1029/2019JD030923

Donald, A., Meinke, H., Power, B., Maia, A. de H. N., Wheeler, M. C., White, N., Stone, R. C., & Ribbe, J. (2006). Near-global impact of the Madden-Julian Oscillation on rainfall. *Geophysical Research Letters*, *33*(9). https://doi.org/10.1029/2005GL025155

Feldstein, S. B. (2000). The Timescale, Power Spectra, and Climate Noise Properties of Teleconnection Patterns. *Journal of Climate*, *13*(24), 4430–4440. https://doi.org/10.1175/1520-0442(2000)013<4430:TTPSAC>2.0.CO;2

Feldstein, S. B. (2003). The dynamics of NAO teleconnection pattern growth and decay. *Quarterly Journal of the Royal Meteorological Society*, *129*(589), 901–924. https://doi.org/10.1256/qj.02.76

Feldstein, S. B., & Franzke, C. L. (2017). Atmospheric teleconnection patterns. *Nonlinear and Stochastic Climate Dynamics*, 54–104.

Feng, P.-N., & Lin, H. (2019). Modulation of the MJO-Related Teleconnections by the QBO. *Journal of Geophysical Research: Atmospheres*, *124*(22), 12022–12033. https://doi.org/10.1029/2019JD030878

Ferranti, L., Corti, S., & Janousek, M. (2015). Flow-dependent verification of the ECMWF ensemble over the Euro-Atlantic sector. *Quarterly Journal of the Royal Meteorological Society*, *141*(688), 916–924. https://doi.org/10.1002/qj.2411

Ferranti, L., Magnusson, L., Vitart, F., & Richardson, D. S. (2018). How far in advance can we predict changes in large-scale flow leading to severe cold conditions over Europe? *Quarterly Journal of the Royal Meteorological Society*, *144*(715), 1788–1802. https://doi.org/10.1002/qj.3341

Garfinkel, C. I., & Hartmann, D. (2010). Influence of the quasi-biennial oscillation on the North Pacific and El Niño teleconnections. *Journal of Geophysical Research: Atmospheres*, *115*(D20).

Garfinkel, C. I., Shaw, T. A., Hartmann, D. L., & Waugh, D. W. (2012). Does the Holton–Tan Mechanism Explain How the Quasi-Biennial Oscillation Modulates the Arctic Polar Vortex? *Journal of the Atmospheric Sciences*, *69*(5), 1713–1733. https://doi.org/10.1175/JAS-D-11-0209.1

Garfinkel, C., & Schwartz, C. (2017). MJO-related tropical convection anomalies lead to more accurate stratospheric vortex variability in subseasonal forecast models. *Geophysical Research Letters*, *44*(19), 10,054-10,062.

Haigh, J. D., Blackburn, M., & Day, R. (2005). The Response of Tropospheric Circulation to Perturbations in Lower-Stratospheric Temperature. *Journal of Climate*, *18*(17), 3672–3685. https://doi.org/10.1175/JCLI3472.1

Henderson, S. A., & Maloney, E. D. (2018). The Impact of the Madden–Julian Oscillation on High-Latitude Winter Blocking during El Niño–Southern Oscillation Events. *Journal of Climate*, *31*(13), 5293–5318. https://doi.org/10.1175/JCLI-D-17-0721.1

Hendon, H. H., & Abhik, S. (2018). Differences in Vertical Structure of the Madden-Julian Oscillation Associated With the Quasi-Biennial Oscillation. *Geophysical Research Letters*, *45*(9), 4419–4428.

Holton, J. R., & Lindzen, R. S. (1972). An Updated Theory for the Quasi-Biennial Cycle of the Tropical Stratosphere. *Journal of the Atmospheric Sciences*, *29*(6), 1076–1080. https://doi.org/10.1175/1520-0469(1972)029<1076:AUTFTQ>2.0.CO;2

Holton, J. R., & Tan, H.-C. (1980). The Influence of the Equatorial Quasi-Biennial Oscillation on the Global Circulation at 50 mb. *Journal of the Atmospheric Sciences*, *37*(10), 2200–2208. https://doi.org/10.1175/1520-0469(1980)037<2200:TIOTEQ>2.0.CO;2

Holton, J. R., & Tan, H.-C. (1982). The Quasi-Biennial Oscillation in the Northern Hemisphere Lower Stratosphere. *Journal of the Meteorological Society of Japan. Ser. II*, *60*(1), 140–148. https://doi.org/10.2151/jmsj1965.60.1_140

Hoskins, B. J., & Ambrizzi, T. (1993). Rossby Wave Propagation on a Realistic Longitudinally Varying Flow. *Journal of the Atmospheric Sciences*, *50*(12), 1661–1671. https://doi.org/10.1175/1520-0469(1993)050<1661:RWPOAR>2.0.CO;2

Hoskins, B. J., & Karoly, D. J. (1981). The Steady Linear Response of a Spherical Atmosphere to Thermal and Orographic Forcing. *Journal of the Atmospheric Sciences*, *38*(6), 1179–1196. https://doi.org/10.1175/1520-0469(1981)038<1179:TSLROA>2.0.CO;2

Houghton, J. T., Jenkins, G. J., & Ephraums, J. J. (1990). Climate change: The IPCC scientific assessment. *American Scientist; (United States)*, *80:6*. https://www.osti.gov/biblio/6819363

Hsu, H.-H. (1996). Global View of the intraseasonal Oscillation during Northern Winter. *Journal of Climate*, *9*(10), 2386–2406. https://doi.org/10.1175/1520-0442(1996)009<2386:GVOTIO>2.0.CO;2

Hurrell, J. W. (1995). Decadal Trends in the North Atlantic Oscillation: Regional Temperatures and Precipitation. *Science*, *269*(5224), 676. https://doi.org/10.1126/science.269.5224.676

Hurrell, J. W., Kushnir, Y., Ottersen, G., & Visbeck, M. (2003). An Overview of the North Atlantic Oscillation. In *The North Atlantic Oscillation: Climatic Significance and Environmental Impact* (pp. 1–35). American Geophysical Union (AGU). https://doi.org/10.1029/134GM01

Hurrell, J. W., & Van Loon, H. (1997). Decadal Variations in Climate Associated with the North Atlantic Oscillation. In H. F. Diaz, M. Beniston, & R. S. Bradley (Eds.), *Climatic Change*

at High Elevation Sites (pp. 69–94). Springer Netherlands. https://doi.org/10.1007/978-94-015-8905-5_4

Jiang, Z., Feldstein, S. B., & Lee, S. (2017). The relationship between the Madden–Julian Oscillation and the North Atlantic Oscillation. *Quarterly Journal of the Royal Meteorological Society*, *143*(702), 240–250.

Jin, F., & Hoskins, B. J. (1995). The Direct Response to Tropical Heating in a Baroclinic Atmosphere. *Journal of the Atmospheric Sciences*, *52*(3), 307–319. https://doi.org/10.1175/1520-0469(1995)052<0307:TDRTTH>2.0.CO;2

Johansson, Å. (2007). Prediction Skill of the NAO and PNA from Daily to Seasonal Time Scales. *Journal of Climate*, *20*(10), 1957–1975. https://doi.org/10.1175/JCLI4072.1

Jones, C., Waliser, D. E., Lau, K. M., & Stern, W. (2004). Global Occurrences of Extreme Precipitation and the Madden–Julian Oscillation: Observations and Predictability. *Journal of Climate*, *17*(23), 4575–4589. https://doi.org/10.1175/3238.1

Kalnay, E., Kanamitsu, M., Kistler, R., Collins, W., Deaven, D., Gandin, L., Iredell, M., Saha, S., White, G., Woollen, J., Zhu, Y., Chelliah, M., Ebisuzaki, W., Higgins, W., Janowiak, J., Mo, K. C., Ropelewski, C., Wang, J., Leetmaa, A., … Joseph, D. (1996). The NCEP/NCAR 40-Year Reanalysis Project. *Bulletin of the American Meteorological Society*, *77*(3), 437–472. https://doi.org/10.1175/1520-0477(1996)077<0437:TNYRP>2.0.CO;2

Kang, W., & Tziperman, E. (2017). More frequent sudden stratospheric warming events due to enhanced MJO forcing expected in a warmer climate. *Journal of Climate*, *30*(21), 8727–8743.

Karoly, D. J. (1983). Rossby wave propagation in a barotropic atmosphere. *Dynamics of Atmospheres and Oceans*, *7*(2), 111–125.

Karoly, D. J., & Hoskins, B. J. (1983). The steady, linear response of the stratosphere to tropospheric forcing. *Quarterly Journal of the Royal Meteorological Society*, *109*(461), 455–478.

Kiladis, G. N., Dias, J., Straub, K. H., Wheeler, M. C., Tulich, S. N., Kikuchi, K., Weickmann, K. M., & Ventrice, M. J. (2014). A comparison of OLR and circulation-based indices for tracking the MJO. *Monthly Weather Review*, *142*(5), 1697–1715.

Liebmann, B., & Hartmann, D. L. (1984). An Observational Study of Tropical–Midlatitude Interaction on Intraseasonal Time Scales during Winter. *Journal of the Atmospheric Sciences*, *41*(23), 3333–3350. https://doi.org/10.1175/1520-0469(1984)041<3333:AOSOTI>2.0.CO;2

Liebmann, B., & Smith, C. A. (1996). *Description of a complete (interpolated) outgoing longwave radiation dataset*. *77*(6), 1275–1277.

Lim, Y., Son, S.-W., & Kim, D. (2018). MJO Prediction Skill of the Subseasonal-to-Seasonal Prediction Models. *Journal of Climate*, *31*(10), 4075–4094. https://doi.org/10.1175/JCLI-D-17-0545.1

Lim, Y., Son, S.-W., Marshall, A. G., Hendon, H. H., & Seo, K.-H. (2019). Influence of the QBO on MJO prediction skill in the subseasonal-to-seasonal prediction models. *Climate Dynamics*, *53*(3), 1681–1695. https://doi.org/10.1007/s00382-019-04719-y

Lin, H. (2020). Subseasonal Forecast Skill over the Northern Polar Region in Boreal Winter. *Journal of Climate*, *33*(5), 1935–1951. https://doi.org/10.1175/JCLI-D-19-0408.1

Lin, H., & Brunet, G. (2018). Extratropical Response to the MJO: Nonlinearity and Sensitivity to the Initial State. *Journal of the Atmospheric Sciences*, *75*(1), 219–234. https://doi.org/10.1175/JAS-D-17-0189.1

Lin, H., Brunet, G., & Derome, J. (2009). An Observed Connection between the North Atlantic Oscillation and the Madden–Julian Oscillation. *Journal of Climate*, *22*(2), 364–380. https://doi.org/10.1175/2008JCLI2515.1

Lin, H., Brunet, G., & Mo, R. (2010). Impact of the Madden–Julian Oscillation on Wintertime Precipitation in Canada. *Monthly Weather Review*, *138*(10), 3822–3839. https://doi.org/10.1175/2010MWR3363.1

Lin, H., Frederiksen, J., Straus, D., & Stan, C. (2019). Chapter 7—Tropical-Extratropical Interactions and Teleconnections. In A. W. Robertson & F. Vitart (Eds.), *Sub-Seasonal to Seasonal Prediction* (pp. 143–164). Elsevier. https://doi.org/10.1016/B978-0-12-811714-9.00007-3

Lindzen, R. S., & Holton, J. R. (1968). A Theory of the Quasi-Biennial Oscillation. *Journal of the Atmospheric Sciences*, *25*(6), 1095–1107. https://doi.org/10.1175/1520-0469(1968)025<1095:ATOTQB>2.0.CO;2

Liu, C., Tian, B., Li, K., Manney, G. L., Livesey, N. J., Yung, Y. L., & Waliser, D. E. (2014). Northern Hemisphere mid-winter vortex-displacement and vortex-split stratospheric sudden warmings: Influence of the Madden-Julian Oscillation and Quasi-Biennial Oscillation. *Journal of Geophysical Research: Atmospheres*, *119*(22), 12,599-12,620.

Madden, R. A., & Julian, P. R. (1971). Detection of a 40–50 Day Oscillation in the Zonal Wind in the Tropical Pacific. *Journal of the Atmospheric Sciences*, *28*(5), 702–708. https://doi.org/10.1175/1520-0469(1971)028<0702:DOADOI>2.0.CO;2

Madden, R. A., & Julian, P. R. (1972). Description of Global-Scale Circulation Cells in the Tropics with a 40–50 Day Period. *Journal of the Atmospheric Sciences*, *29*(6), 1109–1123. https://doi.org/10.1175/1520-0469(1972)029<1109:DOGSCC>2.0.CO;2

Marshall, A. G., Hendon, H. H., Son, S.-W., & Lim, Y. (2017). Impact of the quasi-biennial oscillation on predictability of the Madden–Julian oscillation. *Climate Dynamics*, *49*(4), 1365–1377. https://doi.org/10.1007/s00382-016-3392-0

Marshall, A. G., & Scaife, A. A. (2009). Impact of the QBO on surface winter climate. *Journal of Geophysical Research: Atmospheres*, *114*(D18). https://doi.org/10.1029/2009JD011737

Mori, M., & Watanabe, M. (2008). The Growth and Triggering Mechanisms of the PNA: A MJO-PNA Coherence. *Journal of the Meteorological Society of Japan. Ser. II*, *86*(1), 213–236. https://doi.org/10.2151/jmsj.86.213

Naoe, H., & Shibata, K. (2010). Equatorial quasi-biennial oscillation influence on northern winter extratropical circulation. *Journal of Geophysical Research: Atmospheres*, *115*(D19). https://doi.org/10.1029/2009JD012952

Nishimoto, E., & Yoden, S. (2017). Influence of the Stratospheric Quasi-Biennial Oscillation on the Madden–Julian Oscillation during Austral Summer. *Journal of the Atmospheric Sciences*, *74*(4), 1105–1125. https://doi.org/10.1175/JAS-D-16-0205.1

O'Reilly, C. H., Weisheimer, A., Woollings, T., Gray, L. J., & MacLeod, D. (2019). The importance of stratospheric initial conditions for winter North Atlantic Oscillation predictability and implications for the signal-to-noise paradox. *Quarterly Journal of the Royal Meteorological Society*, *145*(718), 131–146. https://doi.org/10.1002/qj.3413

Pascoe, C. L., Gray, L. J., Crooks, S. A., Juckes, M. N., & Baldwin, M. P. (2005). The quasi-biennial oscillation: Analysis using ERA-40 data. *Journal of Geophysical Research: Atmospheres*, *110*(D8).

Rennert, K. J., & Wallace, J. M. (2009). Cross-Frequency Coupling, Skewness, and Blocking in the Northern Hemisphere Winter Circulation. *Journal of Climate*, *22*(21), 5650–5666. https://doi.org/10.1175/2009JCLI2669.1

Rodwell, M. J., Rowell, D. P., & Folland, C. K. (1999). Oceanic forcing of the wintertime North Atlantic Oscillation and European climate. *Nature*, *398*(6725), 320–323. https://doi.org/10.1038/18648

Roundy, P. E., MacRitchie, K., Asuma, J., & Melino, T. (2010). Modulation of the Global Atmospheric Circulation by Combined Activity in the Madden–Julian Oscillation and the El Niño–Southern Oscillation during Boreal Winter. *Journal of Climate*, *23*(15), 4045–4059. https://doi.org/10.1175/2010JCLI3446.1

Ruzmaikin, A., Feynman, J., Jiang, X., & Yung, Y. L. (2005). Extratropical signature of the quasi-biennial oscillation. *Journal of Geophysical Research: Atmospheres*, *110*(D11).

Scaife, A. A., Arribas, A., Blockley, E., Brookshaw, A., Clark, R. T., Dunstone, N., Eade, R., Fereday, D., Folland, C. K., Gordon, M., Hermanson, L., Knight, J. R., Lea, D. J., MacLachlan, C., Maidens, A., Martin, M., Peterson, A. K., Smith, D., Vellinga, M., … Williams, A. (2014). Skillful long-range prediction of European and North American winters. *Geophysical Research Letters*, *41*(7), 2514–2519. https://doi.org/10.1002/2014GL059637

Seo, K.-H., & Son, S.-W. (2012). The Global Atmospheric Circulation Response to Tropical Diabatic Heating Associated with the Madden–Julian Oscillation during Northern Winter. *Journal of the Atmospheric Sciences*, *69*(1), 79–96. https://doi.org/10.1175/2011JAS3686.1

Son, S.-W., Lim, Y., Yoo, C., Hendon, H. H., & Kim, J. (2017). Stratospheric Control of the Madden–Julian Oscillation. *Journal of Climate*, *30*(6), 1909–1922. https://doi.org/10.1175/JCLI-D-16-0620.1

Song, L., & Wu, R. (2020). Modulation of the Westerly and Easterly Quasi-Biennial Oscillation Phases on the Connection between the Madden–Julian Oscillation and the Arctic Oscillation. *Atmosphere*, *11*(2), 175. https://doi.org/10.3390/atmos11020175

Stan, C., Straus, D. M., Frederiksen, J. S., Lin, H., Maloney, E. D., & Schumacher, C. (2017). Review of Tropical-Extratropical Teleconnections on Intraseasonal Time Scales. *Reviews of Geophysics*, *55*(4), 902–937. https://doi.org/10.1002/2016RG000538

Takaya, K., & Nakamura, H. (2001). A Formulation of a Phase-Independent Wave-Activity Flux for Stationary and Migratory Quasigeostrophic Eddies on a Zonally Varying Basic Flow. *Journal of the Atmospheric Sciences*, *58*(6), 608–627. https://doi.org/10.1175/1520-0469(2001)058<0608:AFOAPI>2.0.CO;2

Thompson, D. W., & Wallace, J. M. %J J. of climate. (2000). *Annular modes in the extratropical circulation. Part I: Month-to-month variability*. *13*(5), 1000–1016.

Thompson, D. W., & Wallace, J. M. %J G. research letters. (1998). *The Arctic Oscillation signature in the wintertime geopotential height and temperature fields*. *25*(9), 1297–1300.

Vallis, G. K., Gerber, E. P., Kushner, P. J., & Cash, B. A. (2004). A Mechanism and Simple Dynamical Model of the North Atlantic Oscillation and Annular Modes. *Journal of the Atmospheric Sciences*, *61*(3), 264–280. https://doi.org/10.1175/1520-0469(2004)061<0264:AMASDM>2.0.CO;2

Vitart, F., Ardilouze, C., Bonet, A., Brookshaw, A., Chen, M., Codorean, C., Déqué, M., Ferranti, L., Fucile, E., Fuentes, M., Hendon, H., Hodgson, J., Kang, H.-S., Kumar, A., Lin, H., Liu, G., Liu, X., Malguzzi, P., Mallas, I., … Zhang, L. (2017). The Subseasonal to Seasonal (S2S) Prediction Project Database. *Bulletin of the American Meteorological Society*, *98*(1), 163–173. https://doi.org/10.1175/BAMS-D-16-0017.1

Vitart, Frédéric. (2017). Madden—Julian Oscillation prediction and teleconnections in the S2S database. *Quarterly Journal of the Royal Meteorological Society*, *143*(706), 2210–2220. https://doi.org/10.1002/qj.3079

Vitart, Frederic, Robertson, A., & Anderson, D. (2012). Subseasonal to Seasonal Prediction Project: Bridging the gap between weather and climate. *WMO Bulletin*, *61*.

Vitart, Frédéric, & Robertson, A. W. (2018). The sub-seasonal to seasonal prediction project (S2S) and the prediction of extreme events. *Climate and Atmospheric Science*, *1*(1), 1–7. https://doi.org/10.1038/s41612-018-0013-0

Walker, G. T., & Bliss, E. W. (1932). World Weather V. *Memories of the Royal Meteorological Society*, *4*, 53–84.

Wallace, J. M., & Gutzler, D. S. (1981). Teleconnections in the Geopotential Height Field during the Northern Hemisphere Winter. *Monthly Weather Review*, *109*(4), 784–812. https://doi.org/10.1175/1520-0493(1981)109<0784:TITGHF>2.0.CO;2

Wallace, J. M., Smith, C., & Bretherton, C. S. (1992). Singular value decomposition of wintertime sea surface temperature and 500-mb height anomalies. *Journal of Climate*, *5*(6), 561–576.

Wang, J., Kim, H., Chang, E. K., & Son, S. (2018). Modulation of the MJO and North Pacific storm track relationship by the QBO. *Journal of Geophysical Research: Atmospheres*, *123*(8), 3976–3992.

Wang, L., Ting, M., & Kushner, P. J. (2017). A robust empirical seasonal prediction of winter NAO and surface climate. *Scientific Reports*, *7*(1), 279. https://doi.org/10.1038/s41598-017-00353-y

Watson, P. A. G., & Gray, L. J. (2014). How Does the Quasi-Biennial Oscillation Affect the Stratospheric Polar Vortex? *Journal of the Atmospheric Sciences*, *71*(1), 391–409. https://doi.org/10.1175/JAS-D-13-096.1

Wheeler, M. C., & Hendon, H. H. (2004). An All-Season Real-Time Multivariate MJO Index: Development of an Index for Monitoring and Prediction. *Monthly Weather Review*, *132*(8), 1917–1932. https://doi.org/10.1175/1520-0493(2004)132<1917:AARMMI>2.0.CO;2

Woollings, T., Hoskins, B., Blackburn, M., & Berrisford, P. (2008). A New Rossby Wave–Breaking Interpretation of the North Atlantic Oscillation. *Journal of the Atmospheric Sciences*, *65*(2), 609–626. https://doi.org/10.1175/2007JAS2347.1

Yoo, C., & Son, S. (2016). Modulation of the boreal wintertime Madden-Julian oscillation by the stratospheric quasi-biennial oscillation. *Geophysical Research Letters*, *43*(3), 1392–1398.

Zhang, C., Adames, Á. F., Khouider, B., Wang, B., & Yang, D. (2020). Four Theories of the Madden-Julian Oscillation. *Reviews of Geophysics*, *58*(3), e2019RG000685. https://doi.org/10.1029/2019RG000685

Zhang, C. (2005). Madden-Julian Oscillation. *Reviews of Geophysics*, *43*(2). https://doi.org/10.1029/2004RG000158

Zhang, C., & Zhang, B. (2018). QBO-MJO Connection. *Journal of Geophysical Research: Atmospheres*, *123*(6), 2957–2967.